Cellulose (2021) 28:5169–5218
https://doi.org/10.1007/s10570-021-03881-z

REVIEW PAPER

High-performance nanostructured bio-based carbon electrodes for energy storage applications

Adel Al Rai · Meltem Yanilmaz

Received: 14 October 2020 / Accepted: 10 April 2021 / Published online: 18 April 2021

Abstract Polyacrylonitrile (PAN)-based carbon precursor is a well-established and researched material for electrodes in energy storage applications due to its good physical properties and excellent electrochemical performance. However, in the fight of preserving the environment and pioneering renewable energy sources, environmentally sustainable carbon precursors with superior electrochemical performance are needed. Therefore, bio-based materials are excellent candidates to replace PAN as a carbon precursor. Depending on the design requirement (e.g. carbon morphology, doping level, specific surface area, pore size and volume, and electrochemical performance), the appropriate selection of carbon precursors can be made from a variety of biomass and biowaste materials. This review provides a summary and discussion on the preparation and characterization of the emerging and recent bio-based carbon precursors that can be used as electrodes in energy storage applications. The review is outlined based on the morphology of nanostructures and the precursor's type. Furthermore, the review discusses and summarizes the excellent electrochemical performance of these recent carbon precursors in storage energy applications. Finally, a summary and outlook are also given. All this together portrays the promising role of bio-based carbon electrodes in energy storage applications.

A. Al Rai
Faculty of Aeronautics and Astronautics, Istanbul Technical University, Istanbul 34469, Turkey

M. Yanilmaz (✉)
Nano Science and Nano Engineering, Istanbul Technical University, Istanbul 34469, Turkey
e-mail: yanilmaz@itu.edu.tr

M. Yanilmaz
Textile Engineering, Istanbul Technical University, Istanbul 34469, Turkey

Graphic abstract

Keywords Biomass · Carbon · Physical properties · Electrochemical properties · Energy storage

Introduction

Although the year 2020 has witnessed a significant drop in CO_2 emission due to global lockdown measures against COVID-19 pandemic (Le Quéré et al. 2020; Liu et al. 2020e), tremendous efforts are needed to systematically tackle climate change. Depending more on renewable energy sources and shifting toward and relying more on environment friendly solutions, e.g. electric vehicles, is one of the measures toward a sustainable environment. With that, continuing to develop more efficient storage units is becoming the momentum to advance such sustainable technologies (Moriarty and Honnery 2016). Although substantial research and efforts have been made to enhance and develop energy storage units, energy storage is still a barrier against fully benefiting from renewable sources, and a significant increase in capacity is necessary to meet future demands (Leonard et al. 2020).

A conventional energy storage unit is composed of three functional parts: electrodes, liquid electrolyte, and separator. The working principle can be summarized by ions traveling from one electrode to the other passing through the separator during charging and discharging generating energy and power. In the recent literature, rechargeable batteries, such as

lithium-ion batteries (LIBs), and supercapacitors (SCs) are the most developed and researched energy storage devices (Mehtab et al. 2019). LIBs offer high energy density, while SCs offer high power density and having excellent cyclability and stability. In general, the advancement of such energy storage devices can be briefly summarized based on their functional parts as the following: The advancement of liquid electrolytes is mainly related to ionic conductivity and thermal and electrochemical stabilities (Liu and Yu 2019). While the advancement of separators is correlated with ionic resistivity and the overall safety of the unit (Muzaffar et al. 2019; Rai et al. 2021). The electrochemical performance and stability are related to the advance of the electrodes, which are the sole focus of this review.

In energy storage devices, carbon-based electrodes are extensively under research due to their excellent performance. The highly regarded performance is the result of miscellaneous and porous morphologies, ease of modification, and high electrochemical stability and specific capacitance (Endo et al. 2000; Ishikawa et al. 2006; Zhang and Zhao 2009). Carbon-based electrodes have been derived from a verity of petroleum chemicals such as poly(vinyl alcohol) (PVA) (Park et al. 2011), polyethylene oxide (PEO) (Lewandowski et al. 2001), pitch (Meng et al. 2017), polyvinylidene fluoride (PVDF) (Son et al. 2020), and polyacrylonytrile (PAN) (Stojanovska and Kilic 2019). Among them, PAN is the most commonly used precursor. PAN has shown to be an excellent carbon precursor due to its high carbon yield, high quality carbon structure, and formation of wide nanostructures and morphologies. Researchers have managed to synthesize and fabricate novel morphology of nanostructures such as flower particles (Chen et al. 2018b), hollow nanoparticles (Cao and Kruk 2015), ultrafine nanofibers (Lazzari et al. 2007), 2D-nanostrucuters (Zhong et al. 2014), and other novel nanostructures (Kopeć et al. 2019). Each of which possesses unique surface and physical properties making them ideal as electrodes in energy storage devices. For example, high energy density of 4.03 Wh kg^{-1} with excellent cycling stability over 1000 cycles were recorded for PAN-based cloth electrode in SC (Zheng et al. 2019). While using random PAN-based carbon nanostructures for an electrode in lithium-sulfur battery, 840 $mAhg^{-1}$ was recorded for the initial reversable capacity along with high cycling stability over 150 cycles (Zhang et al. 2019c).

Unfortunately, PAN and most of the other carbon precursors are petroleum chemicals, nonrenewable sources, and of toxic nature to the environment. Therefore, it is imperative to start depending on a new alternative (Fava et al. 2015). For any alternative to take over PAN's position as an excellent carbon precursor needs not only to sustain all its good advantages, but also needs to offer what PAN could not provide, hence, environmental sustainability, low-cost, and better electrochemical performance. This alternative is rather a collective of renewable and sustainable materials of bio-based origin. Bio-based carbon precursors are environmentally sustainable materials and of low-cost. In fact, the usage of biomass and biowaste materials as carbon electrodes in energy applications falls under the broad dentition of biorefinery (Fava et al. 2015), which one of its aims is converting bio-based resources into value-added products (Cherubini 2010).

To shed a light on the low-cost virtue, a survey on the available market prices of some of bio-based carbon precursors is composed in Table 1. It is clear that bio-bases sources offer a substantial economical advantage in the synthesis and production of carbon electrodes in energy applications. This advantage comes from the fact that most of biomass materials are the byproducts of agriculture (e.g. corn, rice, and wheat straws) or industries (e.g. lignin). Furthermore, most of biowaste food (e.g. rotten fish and shell of shrimps) and plants (e.g. flowers and phoenix tree leaves) are practically free of charge. It is worth noting that, in principle, the carbonization process of bio-based materials is more or less the same with that of PAN. As a result, the processing cost of PAN and bio-based precursors are comparable. Notable efforts to reduce the processing cost and time are evident. For example, increasing the production output of nanofibers using electrically-assisted solution blow spinning (Rai et al. 2020), and reducing carbonization process time by utilizing microwave assisted-hydrothermal (Naghdi et al. 2017) and microwave plasma pyrolysis (Islam et al. 2017) have been reported. As a consequence, bio-based materials are not only low-cost carbon precursors, but also can be processed at least at the same cost of PAN.

Electrochemical performance of biomass- and biowaste-based carbon electrodes is another critical

Table 1 Extraction and process cost of some bio-based and petroleum materials

Carbon precursor	Average cost ($/ton)	References
Corn straw	29	Edwards (2020)
Rice straw	19.3	Delivand et al. (2011)
Wheat straw	60.4	Littlewood et al. (2013)
Chitin (from seafood)	110	Yan and Chen (2015)
Kraft lignin	380	Ľudmila et al. (2015)
Organosolv lignin	400	Ľudmila et al. (2015)
High purity lignin	750	Ľudmila et al. (2015)
Cellulose (from sludge for nanofiber production)	113	Jonoobi et al. (2012)
Cellulose (dissolving cellulose for nanofiber production)	1648	Jonoobi et al. (2012)
PVA	2080*	Echemi (2020)
PAN (used for carbo fiber production)	4000*	Singh Gill et al. (2017)

*These prices may change significantly depending on the material grades, origin, and intended application

factor to define the feasibility of bio-based carbon precursors in energy storage applications. Generally, electrochemical performance of carbon-based electrode is correlated with the morphology, porosity and pore size, specific surface area, and doping level. Bio-based carbon electrodes possess unique nanostructures, high specific surface area, and high level of heteroatoms-doping. For some precursors, unique nanostructures are inherited from the biomass materials before carbonization (Wang et al. 2019b). Protein-based carbon (e.g. silk regenerated) and some other biomass-based, e.g. chitin, precursors retain a large amount of nitrogen, oxygen, and sometimes sulfur species after carbonization leading to self-doping (Chen et al. 2018a; Zhou et al. 2019). As a result of these superior physical and chemical features, high-performance electrodes in rechargeable batteries and SCs have been reported as is discussed and summarized in detail in "Bio-based nanostructured carbon materials for high-performance energy applications" section.

Environmentally sustainable biomass- and bio-wastes-based carbon electrodes are excellent options for high-performance energy storage applications. This review provides a summary and discussion on the preparation and characterization of the emerging and recent bio-based carbon precursors that can be used as electrodes in energy storage applications. The review is outlined based on the morphology of nanostructure and the precursor's type. For each section, preparation protocols and properties are thoroughly discussed. Furthermore, the review discusses and summarizes the excellent electrochemical performance of these emerging carbon precursors in storage energy applications. All this together portrays the promising role of bio-based carbon electrodes in storage energy applications.

Preparation and properties of nanostructured bio-based carbon materials

Particulate nanostructures (0D-nanostructures)

This category encompasses bio-based carbon powders with different morphologies such as nanoparticles, nanosheets, nanoplates, random geometrical nano-sized configurations, or nanoporous structure.

Lignin

Lignin, a complex amorphous biopolymer that acts as a binder to provide structural integrity in plants, is the most abundant natural material after cellulose (S. B. Lalvani 2000; Zakzeski et al. 2010). The synthesis of different lignin nanoparticles is an emerging interest (Gonzalez et al. 2017; Ago et al. 2017; Matsakas et al. 2018) but the scope of lignin-based carbon nanoparticles is still rather limited. The reason is that currently most of the synthesized lignin nanoparticles are in colloidal form, which impedes subsequent treatments such as carbonization and

activation. The most common configuration of lignin-based carbon nanoparticles is carbon dots forming colloidal suspension (Chen et al. 2016b; Rai et al. 2017; Si et al. 2018; Myint et al. 2018). The reported physical properties, e.g. specific surface area, of these carbon nanoparticles (Yiamsawas et al. 2017) are inferior to conventional activated polymeric-based carbon nanoparticles (Zhao et al. 2015b; Zhou et al. 2015). One report simultaneously managed to carbonize and activate lignin-based carbon nanoparticles with large surface area, 1100 m^2/g, however, the obtained nanoparticles showed signs of agglomeration and irregularity in their structure (Hu and Hsieh 2017). As a result of the difficulty of handling colloidal lignin-based carbon nanoparticles, a promising recent study featured the recovery of lignin nanoparticles in solvents using a two-step process (Matsakas et al. 2020); decreasing the solvent concentration and, subsequently, isolating the particles. The rate at which the solvent concentration evaporates was important to obtain good quality particles. In another study, freeze-drying method followed by subsequent stabilization and carbonization was used to overcome the isolation issue, however, the nanoparticles were of irregular shapes (Gonugunta et al. 2012).

Cellulose

Cellulose makes up a large portion of the plant's interior structure and is the most abundant natural material. Cellulose has been extracted from green plants, e.g. wood pulp. Due to the nature of cellulosic sources, their nanostructures are mainly fibrous and whiskery (see "Cellulose" section), while other particulate structures such as nanoparticles are difficult to obtain. Hence, in limited studies, randomly graphitic nanostructures are the only formation that can be found for limited applications, such as proton exchange membrane fuel cell (Guilminot et al. 2008; Sevilla and Fuertes 2010). This may not just indicate that the cellulose-based carbon nanofibrous is a more common structural configuration than its nanoparticulate counterparts, but maybe also easier to synthesize and apply in a variety of applications.

Chitin

Chitin, an abundant biopolymer with high nitrogen content due to the presence of N-acetyl groups, can be cheaply obtained as a by-product of seafood biowastes, for example, shells of crab, shrimp, and lobster (Yan and Chen 2015) and also can be extracted from insects (Zhou et al. 2017). Only a few reports have tackled the synthesis of carbon particulate nanostructures using chitin as a precursor. Elastic nitrogen-doped chitin-based CNFs microspheres were synthesized (Duan et al. 2016). Scanning Electron Microscopy (SEM) and Transmission Electron Microscopy (TEM) were used to capture the marvelous morphology as depicted in Fig. 1. Although the synthesis protocol is complicated and long, the inner structure of the nanofibrous microspheres is outstanding. The CNFs and sphere diameters were measured to be around 24 nm and 39 μm, respectively. The microspheres that were carbonized at 900 °C were partially graphitized and had very high specific surface area and pore volume of 1147 m^2/g and 2.12 cm^3/g, respectively.

Chitin-based carbon particulate nanostructures could be synthesized in different geometries demonstrating the capability of chitin to be a miscellaneous carbon resource. Another form of chitin carbon particulate nanostructure is carbon quantum dots. In one example, spherical diameters between 2 to 12 nm have been synthesized (Naghdi et al. 2017). Briefly, in a sealed vessel, a predetermined grammage of chitin nanofibers mixed with $CaCl_2$ ethanol solution was subjected to a temperature of 180 °C using one-pot microwave assisted-hydrothermal method. The change of color from colorless to dark was marked as evidence of the conversion to carbon quantum dots. Another example, chitin-based carbon nanosheets have also been synthesized by hydrophobization-induced interfacial-assembly method (You et al. 2017). First, the extracted chitin nanofibers from carb were dissolved in NaOH–urea before drop-wise addition of acrylonitrile that triggered hydrophobization reaction. The reported thickness of the resultant nanosheets was 27 nm and was reduced to around 3.8 nm with lateral size of 10 μm to form graphene-like structure after carbonization at 800 °C. The obtained chitin-based nanosheets carbon had high specific surface area and pore size range of 724 m^2/g and 1–40 nm, respectively.

Recent reports have demonstrated the activation with somewhat unconventional materials, e.g. $KMnO_4$ and Hydroxylapatite, that help in increasing specific surface area and nitrogen doping percentage as well

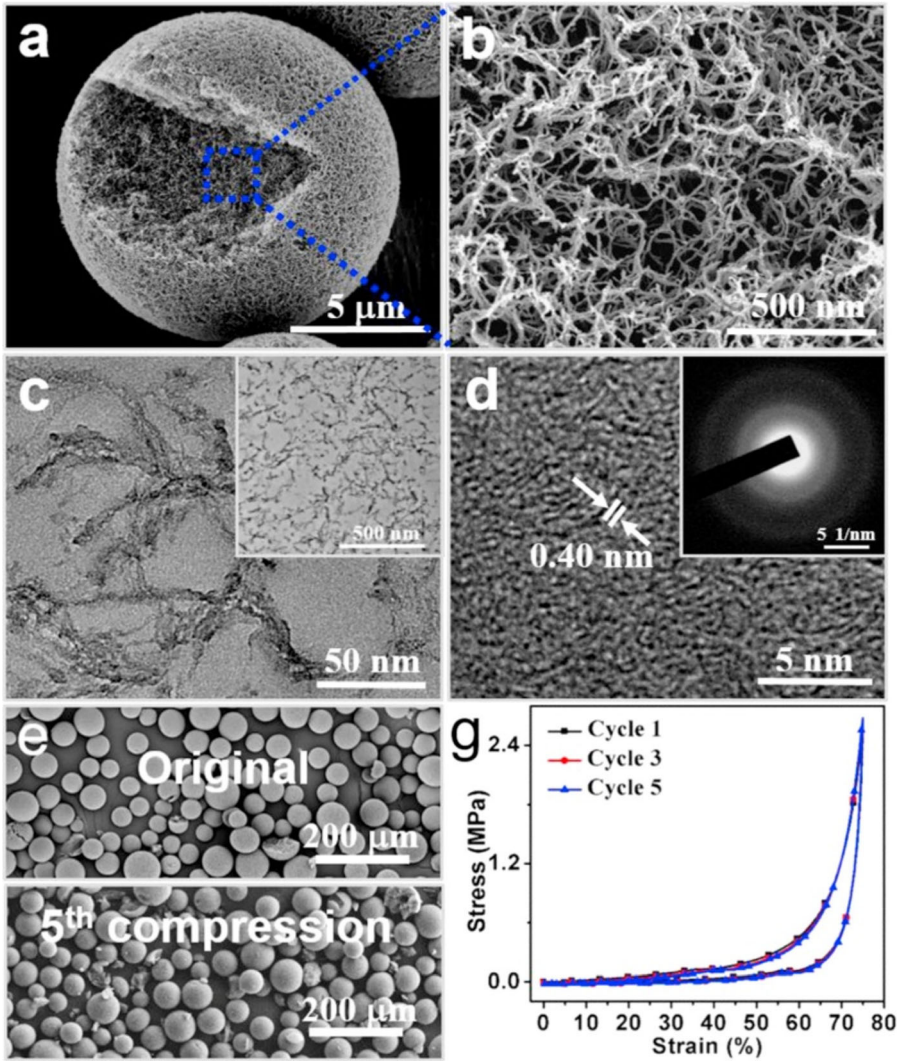

Fig. 1 **a**, **b** SEM images of elastic nitrogen-doped chitin-based CNFs microspheres, **c**, **d** corresponding TEM images and diffraction pattern, **e**, **g** SEM images before and after 5 cycles of compression and the corresponding stress–strain curve. Reprinted with permission from Duan et al. (2016). Copyright (2016) Elsevier

(Wang et al. 2020b; Chu et al. 2020). For instance, activation of chitin in hot $KMnO_4$ solution resulted in high specific surface area up to 1941 m^2/g at a relatively low carbonization temperature of 800 °C (Wang et al. 2020b). The large surface area was attributed to dismantling hydrogen bonds due to $KMnO_4$ reacting with chitin molecules before carbonization and the decomposition of by-products, e.g. K_2CO_3, during carbonization. Interestingly, $KMnO_4$ also acted as a template to form nanoporous structures during carbonization. Nonetheless, one of the drawback of chitin is its limited carbon yield, for instance, at a carbonization temperature of 800 °C carbon yield is only 10.5% (Wang et al. 2020b).

Protein.

Proteins are widely abundant bio-based materials and rich of nitrogen species (Li et al. 2013; Demir et al. 2018). Due to the nature of extracting protein precursors, the conventional spherical nanoparticle structure is a rare configuration, while nanoporous powder and nanoplates are more common configurations (Demir et al. 2018). Carbonized protein-based nanoporous

carbon precursors possess excellent physical properties (Li et al. 2013). Some of the promising protein-based carbon precursors are egg, silk, fish, tofu, and some livestock feed such as Lemna minor, and enoki mushroom.

High sources of protein such as activated egg white and eggshell were carbonized and resulted in nanoporous carbon powders (Li et al. 2016a; Zhang et al. 2019b). The nanoporous powders of egg white and eggshell have high specific surface area of 2268 and 1572 m^2/g, respectively, and pore sizes smaller than 10 nm. Silk is another good candidate that serves as a protein source. Silk protein-based carbon nanoplates were synthesized from cocoons by, briefly, extracting silk fibroin from cocoons and dissolving it in lithium bromide and the mixture was casted to form a film (Yun et al. 2013). The as-casted film was treated with KOH and carbonized at a temperature of 800 °C to form nanoplates of lateral size around 5 µm and thickness of only a few nanometers. These nanoplates are physically similar to graphene and have similar Raman peaks ratio as well. The specific surface area of the activated nanoplates is substantial, 2557 m^2/g. Other protein-rich biowastes, e.g. fishes (Guo et al. 2017), have also been converted to nanoporous carbon materials. For example, a fish activated with $ZnCl_2$ and carbonized at 900 °C resulted in nanoporous carbon content with high specific surface area of 850 m^2/g and pore size of around 2.5 nm. Other promising protein-based carbon sources are tofu, livestock feed, e.g. Lemna minor, and enoki mushroom (Guo et al. 2015, 2016; Lee et al. 2017, 2018).

Others

Unconventional pristine and composite renewable bio-based, e.g. food and other bio-based wastes, have successfully been used as carbon precursors. Such materials possess high specific surface area and unique morphology that make them attractive carbon precursors for researchers to unravel their potential and find methods to process them. Food wastes, e.g. walnut and coconut shells, potatoes, and tea waste, are important classes of biowaste to obtain high quality carbon precursors (Sun et al. 2013; Long et al. 2015; Wu et al. 2015; Qu et al. 2015; Cao et al. 2019; Shang et al. 2020; Khan et al. 2020). Carbonized alkali-treated wheat flour and reduced MnO_2 nanowires-like composite has been simply synthesized in one-pot but with complex inner honeycomb-like nanoporous structure as illustrated in Fig. 2 (Wu et al. 2015). The unique interconnected honeycomb-like morphology was thought to be as a result of the synergetic role KOH played as a template and as an activation agent. Nitrogen-doped sulfur and gelatin-based carbon composite with ultrahigh surface area and total pore volume, 2893 m^2/g and 2.8 cm^3/g, respectively, were also synthesized by a series of chemical treatments (Qu et al. 2015). The nitrogen-doping was the result of the rich nitrogen species in gelatin while the high surface area and large pore volume were the results of physical activation using KOH. Also, impressively, activated carbonized porous walnut shells and tea waste with high specific surface areas of 3577 and 1610 m^2/g, respectively, were synthesized (Khan et al. 2020; Shang et al. 2020).

A variety of biomass sources, e.g. flowers, bagasse, have also been utilized as nanoparticulate carbon precursors (Chen et al. 2016a; Li et al. 2016b; Gao et al. 2017a; Liu et al. 2017a; Zhu et al. 2020b; Wan and Hu 2020). For example, seed-free willow catkin flower has been converted to nitrogen-doped carbon by pyrolysis after being treated with KOH (Li et al. 2016b). The reported morphology consisted of graphene-like nanosheets with large surface area of 1533 m^2/g doped with heteroatoms nitrogen and sulfur. The carbonization of Perilla frutescens leaves, a common food plant in Southeast Asia, at 700 °C resulted in graphene-like nanosheets with high heteroatoms self-doping of oxygen and nitrogen at around 18.8 and 1.7%, respectively (Liu et al. 2017a). However, exhibited a somewhat moderate specific surface area of 655 m^2/g.

Nature biowastes, e.g. plant leaves, bamboo fiber, wheat straw, and dead ants, are yet another important class as nanoparticulate carbon precursors due to their abundance in nature (Du et al. 2019; Ji et al. 2020; He et al. 2020). The resultant activated graphene-like nanosheets of phoenix leaves, bamboo fiber, and wheat straw resulted in high specific surface area of 2208, 2561, and 2560 m^2/g, respectively (Du et al. 2019; Ji et al. 2020; He et al. 2020). Another interesting graphene-like nanosheets carbon doped with three heteroatoms, nitrogen, oxygen, and sulfur, was derived from dead ants (Zhao et al. 2018a). This ant-based carbon powder possessed ultrahigh specific surface area of 2650 m^2/g with mesopore size range between 2 to 6 nm.

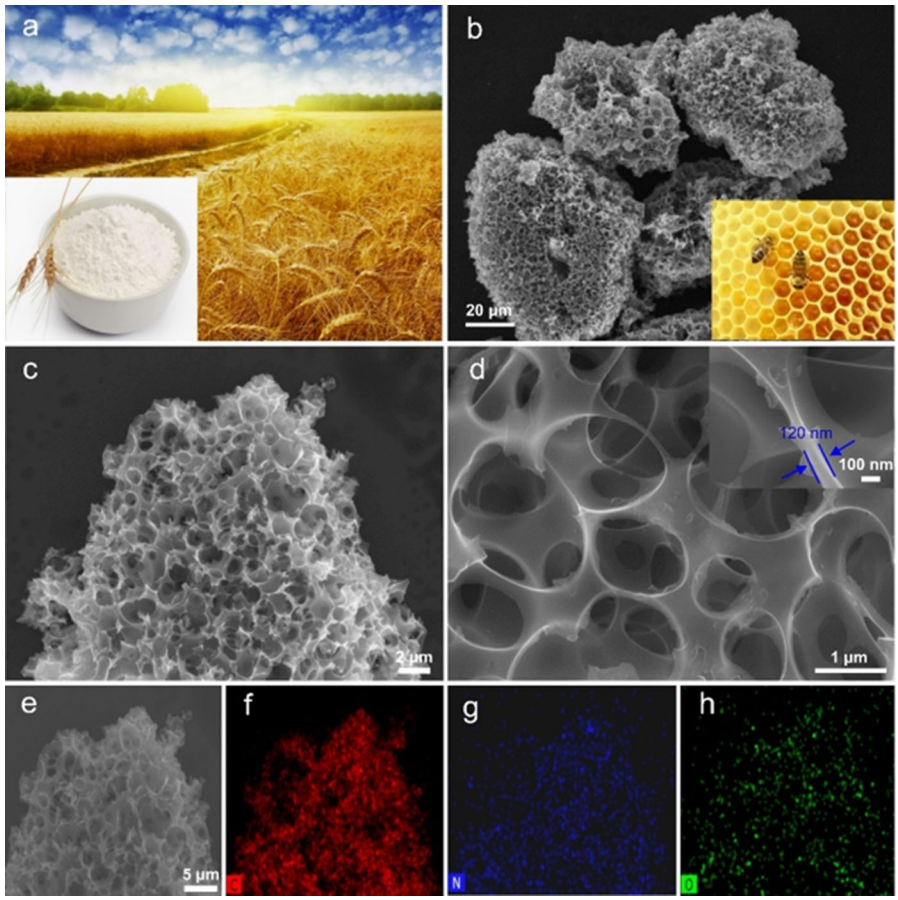

Fig. 2 **a** shows wheat flour, **b–e** SEM images of Carbonized alkali-treated wheat flour, and **f–h** elemental analysis of C, N, and O, respectively. Reprinted with permission from Wu et al. (2015). Copyright (2015) Elsevier

As summarized in Table 2, unconventional biomass and biowaste materials are showing to have high value as carbon precursors due to their distinct morphology and superior physical properties. The abundance of these renewable precursors for nanoparticulate carbon materials allows them to replace their conventional synthetic counterparts.

1D-nanostructure

This category is composed of bio-based materials that have large length-to-width ratio such as nanofibers, nanorods, nanoneedles, etc.

Lignin

Lignin-based carbon nanofibers (LCNFs) offer an important renewable alternative to PAN-based CNFs due to lignin's abundance and its relatively high carbon yield. There are two main approaches to obtain CNFs using lignin as a precursor, and both approaches involve electrospinning method. The first approach uses lignin as the only precursor to produce nanofibers, while the other approach, more common, uses lignin with other auxiliary polymers to form a spinnable blend. In the first approach, a high concentration of lignin is required (Lallave et al. 2007; Ruiz-Rosas et al. 2010). Usually, a high concentration solution is not considered as a proper solution in electrospinning due to the rapid solvent evaporation that eventually leads to clogging. Therefore, as a remedy to this issue, using a co-axial spinneret, allows for an extra amount of solvent to be supplemented to the polymer jet to compensate for the rapidly evaporating solvent. Co-axial electrospinning, thus, offers a solution to produce CNFs processed from pristine lignin sources.

Table 2 Comparison of physical properties of different biomass- and biowaste-based carbon particulate nanostructures

Carbon precursor	Additive/ activation agent	Doping conditions				I_D/I_G	$d_{(002)}$ (nm)	Specific surface area (m^2/g)	Total pore volume (cm^3/g)	Pore size (nm)	References
		Doping mechanism	N (%)	O (%)	S (%)						
Kraft lignin	–/–	None	–	8	–	–	–	552	0.3	14.8	Yiamsawas et al. (2017)
Alkali lignin	–/KOH	None	–	–	–	1.2	–	483	0.3	0.6–1.4	Hu and Hsieh (2017)
Alkali lignin	–/NaOH	None	–	–	–	1.1	–	1847	1.1	0.6–1.4	Hu and Hsieh (2017)
Chitin (Cicada slough)	–/KOH	Self-doping	1.5	33.8	–	–	–	2097	1.09	1.5	Zhou et al. (2017)
Chitin	–/$KMnO_4$	Self-doping	1.4	10.6	–	$\sim$ 0.9	–	1488	1.29	3.5	Wang et al. (2020b)
Chitin (N-acetylglucosamin)	–/Hydroxylapatite	Self-doping	High	–	–	0.86	–	756	2.34	0.7–2.1	Chu et al. (2020)
Protein (Eggshell)	–/KOH	Self-doping	7.5	7.6	0.7	Small	Small	1572	–	1–3	Zhang et al. (2019b)
Protein (Tofu)	–/KOH	None	–	–	–	–	–	2960	1.47	2.0	Lee et al. (2017)
Walnut shells	–/KOH	None	–	–	–	1.19	–	3577	2.19	3–7	Shang et al. (2020)
Tea waste	–/KOH	None	–	–	–	0.92	–	1610	–	6.0	Khan et al. (2020)
Bagasse	–/KOH	Self- and external-doping	–	15.9	6.1	1.03	–	326	0.42	–	Wan and Hu (2020)
Leaves (Phoenix)	K_2FeO_4/K_2FeO_4	Self- and external-doping	0.8	6.7	–	0.93	–	2208	1.27	2.3	He et al. (2020)
Bamboo fiber	$K_3Fe(CN)_6$/KOH &thiourea	Self- and artificial-doping	3.2	6.1	2.2	2.08	–	2561	1.34	< 10	Ji et al. (2020)

However, coaxial electrospinning lacks simplicity and requires extreme care to balance the flow rate of both spinnerets during electrospinning. It is worth noting that conventional electrospinning, one spinneret model, has been reported for the production of nanofibers of pristine lignin solution followed by conversion to LCNFs (Lallave et al. 2007; Ruiz-Rosas et al. 2010; García-Mateos et al. 2018). However, other researchers have failed to reproduce similar results (Dallmeyer et al. 2010, 2014) and have concluded that the system is impractical for the production of LCNFs. One group attempted spinning different technical lignins, namely softwood kraft lignin, hardwood kraft lignin, and sulfonated kraft lignin, using one-spinneret electrospinning but failed to produce any fibers regardless of the solution concentration (Dallmeyer et al. 2010). They only managed to produce beaded fibers at a concentration higher than 50% which would not be suitable for long production process due to eventual clogging.

The second approach uses traditional electrospinning by mixing lignin with some auxiliary polymers to form a blend solution that is easily spinnable compared with the poorly spinnable pristine lignin solution. It is important to note, however, that the use of synthetic polymers defeats the purpose of using lignin as a friendly environmental precursor to produce CNFs. This issue has been tackled by minimizing the amount of percentage of the auxiliary polymeric (Ding et al. 2016), e.g. using lignin in higher percentages compared to the auxiliary polymer, or by using water soluble polymers, somewhat friendlier options, e.g. PVP and PVA. As a result, blending has become a much common approach to produce LCNF using conventional electrospinning rather than using the complex coaxial electrospinning setup.

Table 3 summarizes the most common auxiliary blends, solvents, additives and enhancers, and carbonization conditions used to prepare LCNFs using electrospinning method. Lignin has been blended with a variety of polymers in order to enhance the spinnability of lignin to produce nanofibers and subsequently convert them into LCNFs. PAN is the most common auxiliary polymer thanks to its high carbon yield and mechanical properties (Ding et al. 2016). Besides PAN (Ruiz-Rosas et al. 2010; Choi et al. 2013; Xu et al. 2013, 2014; Ding et al. 2016; Dalton et al. 2019; Jayawickramage et al. 2019; Demiroğlu Mustafov et al. 2019; Dai et al. 2019; Zhang et al. 2020b; Du et al. 2020a), many other polymers have also been used as auxiliary polymers to enhance lignin spinnability, such as PVP (Ma et al. 2018; Cao et al. 2020), PVA (Ago et al. 2012; Lai et al. 2014; Ma et al. 2016, 2019; Zhao et al. 2018b; Jayawickramage and Ferraris 2019; Roman et al. 2019), PEO (Dallmeyer et al. 2010; Hu and Hsieh 2013; Cho et al. 2019; Du et al. 2020b), TPU (Culebras et al. 2019), and PLA (Culebras et al. 2019). Worth reporting that, to some less extent instead of blending, direct synthesize of lignin and PAN copolymer has been reported as a precursor of LCNFs for energy applications (Youe et al. 2016, 2018).

To further enhance the lignin/polymer blend spinnability in electrospinning, the literature demonstrates a wide variety of materials as potential blend enhancers. Interestingly, nanocrystalline cellulose as an additive has been used to enhance the spinnability of lignin/PEO blend by controlling the molecular orientation of lignin during electrospinning (Cho et al. 2018, 2019). Non-precious metals have been used as a catalyst to increase the lignin yield but also showed notable enhancement in the spinnability of lignin. For instance, the addition of 10 wt.% of Ni ions to organosolv lignin blend increased the light lignin fragments yield to 87%, and enhanced the solution spinnability during electrospinning (Du et al. 2020b). As summarized in Table 3, other enhancers reported are platinum acetylacetonate, methylene diphenyl diisocyanate, graphene nanosheets, and butyric anhydride (Ruiz-Rosas et al. 2010; Ding et al. 2016; Culebras et al. 2019; Dai et al. 2019).

Depending on the starting materials, it seems that lignin/polymer blend tends to have higher carbon yield than the pristine polymers. Though PAN has the highest carbon yield among synthetic polymers, pristine lignin and lignin/PAN blend results in even higher LCNFs yield (Xu et al. 2014; Ding et al. 2016). The final stabilization and carbonization temperatures are more crucial than heating rate and holding time to determine the final carbon yield. A recent study showed that the final stabilization temperature of lignin-based nanofibers has a much more effect on carbon yield compared with heating rate and holding time combined (Cho et al. 2019). They showed that after stabilization at 200, 230, 250, and 280 °C the yield decreased to around 87, 82, 78, and 65%, respectively. After carbonization at 1000 °C the corresponding carbon yield stood at 38.4, 44.4, 47.9,

Table 3 Process conditions and protocol of lignin derived CNFs using electrospinning

Carbon precursor	Materials processing conditions						Carbon conversion conditions		Final carbon yield (%)	References
	Catalyst/active material/ enhancer	Solvent	Auxiliary polymer	Lignin/ polymer ratio	Blend concentration (wt.%)	Viscosity (Pa.s)	Stabilization	Carbonization		
Alkali lignin	KOH	Water	–	–	20	–	Nitrogen @105 °C @10 °C/min for 0.5 h	Nitrogen @900 °C for 0.5 h	18.2	Hu and Hsieh (2017)
Alcell lignin	–	Ethanol	–	–	50	0.35–0.45	Atmosphere @200 °C @0.25 °C/min for 24 h	Nitrogen @900 °C @10 °C/min	31.6	Lallave et al. (2007)
Alcell lignin	–	Ethanol	–	–	50	–	Atmosphere @200 °C @0.05 °C/min for 36 h	Nitrogen @900 °C @10 °C/min	39	Ruiz-Rosas et al. (2010)
Alcell lignin	Platinum acetylacetonate	Ethanol	–	–	50	–	Atmosphere @200 °C @0.05 °C/min for 36 h	Nitrogen @900 °C	38.7	Ruiz-Rosas et al. (2010)
Organosolv lignin	Ni ions	DMF	PEO	95/5	25	–	Atmosphere @250 °C @1 °C/min for 1 h	Nitrogen @900 °C @5 °C/min for 1 h	–	Du et al. (2020b)
Alcell lignin	Nitrogen doping	DMF	PEO	90/10	~ 20	–	Atmosphere @200 °C @1 °C/min for 2 h	Nitrogen @900 °C @10 °C/min for 2 h	–	Wang et al. (2013)
Low sulfonate alkali lignin	NaOH and KOH	Water	PEO	90/10	10	–	Atmosphere @105 °C @10 °C/min for 0.5 h	Nitrogen @850 °C for 0.5 h	–	Hu and Hsieh (2013)
Softwood kraft lignin	NCC	DMF	PEO	27wt.%/ 1wt.%	28	–	Atmosphere @230 °C @5 °C/min for 0.5 h	Nitrogen @1000 °C @10 °C/min for 1 h	44.4	Cho et al. (2019)
Softwood kraft lignin	NCC	DMF	PEO	27wt.%/ 1wt.%	28	–	Atmosphere @230 °C @5 °C/min for 0.5 h	Nitrogen @1000 °C @10 °C/min for 1 h	47.9	Cho et al. (2019)
Softwood kraft lignin	NCC	DMF	PEO	27wt.%/ 1wt.%	28	–	Atmosphere @230 °C @5 °C/min for 0.5 h	Nitrogen @1000 °C @10 °C/min for 1 h	49.1	Cho et al. (2019)

Table 3 continued

Carbon precursor	Materials processing conditions						Carbon conversion conditions		Final carbon yield (%)	References
	Catalyst/active material/ enhancer	Solvent	Auxiliary polymer	Lignin/ polymer ratio	Blend concentration (wt.%)	Viscosity (Pa.s)	Stabilization	Carbonization		
Ethanol-soluble lignin	–	DMF	PAN	85/15	20	0.144	Atmosphere @220 °C @0.2 °C/min for 6 h	Nitrogen @1000 °C @4 °C/min for 4 h	~ 51	Du et al. (2020a)
Tetrahydrofuran-soluble lignin	–	DMF	PAN	85/15	20	0.177	Atmosphere @220 °C @0.2 °C/min for 6 h	Nitrogen @1000 °C @4 °C/min for 4 h	~ 53	Du et al. (2020a)
N. Enzymatic hydrolysis lignin	–	DMF	PAN	60/40	12	–	Atmosphere @250 °C @1 °C/min	Nitrogen @800 °C @10 °C/min for 1 h	–	Zhang et al. (2020b)
Organosolv Lignin	–	DMF	PAN	70/30	15	–	Atmosphere @200 °C @0.1 °C/min for 12 h	Nitrogen @900or1100°C @5 °C/min for 1 h		Dalton et al. (2019)
Enzymatic hydrolysis	Graphene nanosheets	DMF	PAN	50/50	20	–	Atmosphere @260 °C @0.5 °C/min for 1.5 h	Nitrogen @1400 °C @5 °C/min for 1 h	–	Dai et al. (2019)
Organosolv lignin	–	DMF	PAN	50/50	20	~ 1.4	Atmosphere @200 °C @0.2 °C/min for 12 h	Nitrogen @1000 °C @5 °C/min for 0.5 h	39.4	Ding et al. (2016)
Organosolv lignin	Butyric anhydride	DMF	PAN	50/50	20	~ 2.2	Atmosphere @200 °C @0.2 °C/min for 12 h	Nitrogen @1000 °C @5 °C/min for 0.5 h	31.1	Ding et al. (2016)
Poplar sawdust lignin	PMMA	DMF	PVP	–	–	–	Atmosphere @300 °C @1 °C/min	Nitrogen @800 °C for 2 h	–	Cao et al. (2020)

Table 3 continued

Carbon precursor	Materials processing conditions						Carbon conversion conditions		Final carbon yield (%)	References
	Catalyst/active material/ enhancer	Solvent	Auxiliary polymer	Lignin/ polymer ratio	Blend concentration (wt.%)	Viscosity (Pa.s)	Stabilization	Carbonization		
Kraft lignin	–	Water	PVA	70/30	12	–	Atmosphere @100 °C @10 °C/min for 2 h, @180 °C @1 °C/ min for 16 h, and @220 °C @0.5 °C/ min for 8 h	Argon @1200 °C @5 °C/min for 1 h	–	Lai et al. (2014)
Alkali lignin	–	Water	PVA	80/20	24	0.48	Atmosphere @250 °C @2 °C/min for 1 h	Nitrogen @1000 °C @5 °C/min for 1 h	30–35	Jayawickramage and Ferraris (2019)
Alcell organosolv lignin	MDI	DMF	TPU	80/20	20	–	Atmosphere @150 °C @1 °C/min for 14 h, @200 °C for 1, and @250 °C for 1	Nitrogen @900 °C @10 °C/min for 0.5 h	47.5	Culebras et al. (2019)
Alcell organosolv lignin	MDI	THF/ DMF	PLA	80/20	20	–	Atmosphere@150 °C @1 °C/min for 14 h, @200 °C for 1, and @250 °C for 1	Nitrogen @900 °C @10 °C/min for 0.5 h	32.7	Culebras et al. (2019)

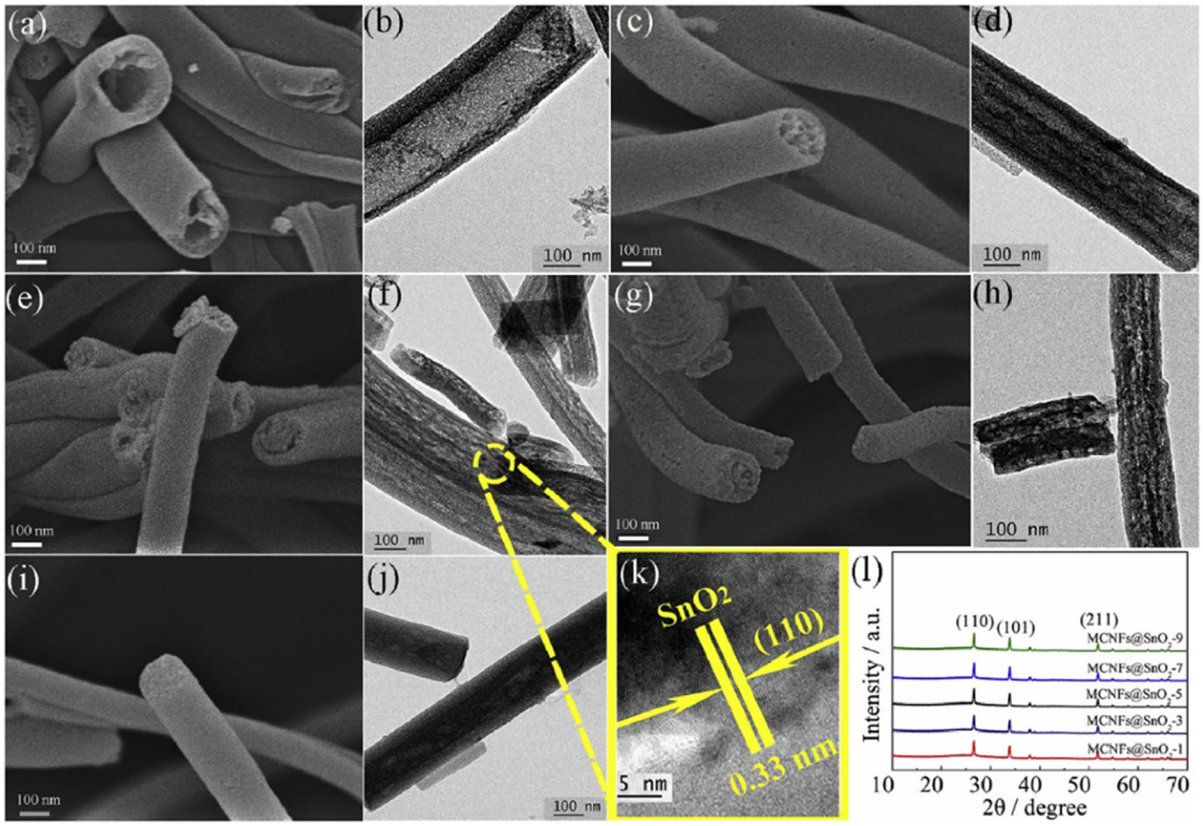

Fig. 3 SEM and TEM images of LCNF@SnO_2 with lignin and PMMA mixed at different mass ratios of **a**, **b** 1:9, **c**, **d** 3:7, **e**, **f** 5:5, **g**, **h** 7:3, and **i**, **j** 9:1, **k** HR-TEM image of when lignin PMMA ratio was 5:5, and l) XRD patterns of the samples. Reprinted with permission from Cao et al. (2020). Copyright (2020) Elsevier

nd 49.1%, respectively. Although this suggests that the higher the stabilization temperature the higher the carbon yield, when stabilization temperature reached 300 °C the carbon yield, at the same carbonization temperature (1000 °C), decreased to 44.8%. Therefore, the optimum stabilization temperature was around 280 °C. Stabilization process not only help increase carbon yield but also avoid fusion of the nanofibers (Cho et al. 2018; Roman et al. 2019), by cross-linking to increase the softening temperature of lignin nanofibers (Kadla et al. 2002; Luo et al. 2011; Chatterjee and Saito 2015). By monitoring the carbonization temperature, the final carbon yield could be controlled for pristine lignin-based and lignin/polymer blended LCNFs. For instance, pristine Alcell lignin nanofibers yielded LCNFs between 47.8 and 36.1% at carbonization temperatures of 600 to 1000 °C, respectively (Ruiz-Rosas et al. 2010), and alkali kraft lignin blended with PAN (1:1) yielded LCNFs between 51.2 and 39.8% at carbonization temperatures of 600 to 950 °C, respectively (Xu et al. 2014). It is worth noting that only a few studies reported carbon yield higher than 50% using ethanol-soluble and tetrahydrofuran-soluble lignins at high carbonization temperatures (Du et al. 2020a). According to Table 3, it could be concluded that carbon yield of lignin-based materials is in the range between 30 to 49%, and, strictly speaking, has a rough average yield of around 42%.

LCNFs, without post- or pre-treatments, already possess somewhat high specific surface area and pore volume (Wang et al. 2013; Ma et al. 2018). These are attributed to the removal of volatile substances during carbonization, such as oxygen which is present at high content on lignin fibers after stabilization (Brodin et al. 2010; Ruiz-Rosas et al. 2010; Baker et al. 2012; Yun et al. 2019). It is worth noting that lignin of lower molecular weight might play a crucial role in the

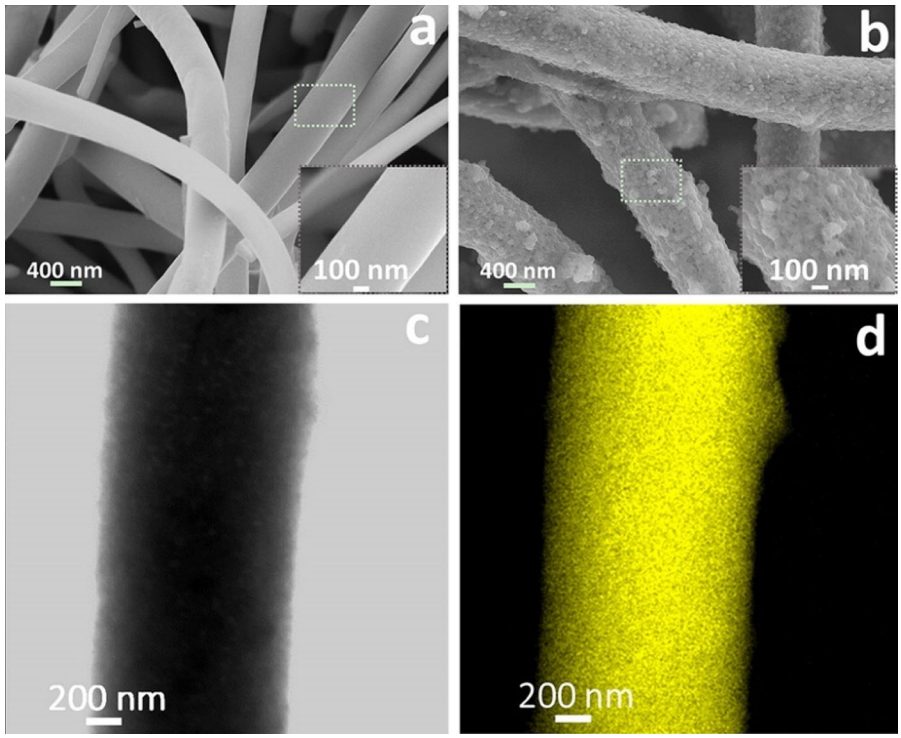

Fig. 4 SEM images of **a** pristine cellulose-based CNFs **b** polypyrrole-coated cellulose-based CNFs, **c** TEM image of polypyrrole-coated cellulose-based CNFs, and **d** EDS image showing nitrogen content on polypyrrole-coated cellulose-based CNFs. Reprinted with permission from Cai et al. (2015). Copyright (2015) American Chemical Society

formation of pores after carbonization (Jeon et al. 2015). Furthermore, specific surface area, pores size, and pore volume of traditional CNFs can be enhanced using chemical agents such as KOH, NaOH, H_3PO_4, K_2CO_3, Na_2CO_3, and $ZnCl_2$ (Jiang et al. 2002; Gryglewicz et al. 2005; Mitani et al. 2005; Kim et al. 2007; Im et al. 2009). Notably, KOH and NaOH are the common agents to treat LCNFs (Hu and Hsieh 2013; Li et al. 2014; Dai et al. 2019). Physical post-treatment methods, include air plasma, a mixture of CO_2 and N_2 gas, and N_2 gas, were also applied to increase surface area and porosity of LCNFs (Wang et al. 2013; Jayawickramage and Ferraris 2019; Zhang et al. 2020b). On the other hand, pre-treatment methods include the incorporation of porogen in the spinning solution (Ma et al. 2018). Surface treatment and activation of LCNF incorporated with graphene nanosheets were carried out by dispersing the CNFs into KOH solution using ultrasonic treatment (Dai et al. 2019). Graphene nanosheets played an agent role to induce heteroatoms of N and S in LCNF and increase surface area. Furthermore, lignin/polymer blend section does not just affect the spinnability during electrospinning, but also affects the final morphology of LCNF. Depending on the chosen polymer, solution viscosity and electrical conductivity vary that in turn the nanofiber diameter could either increase or decrease. Moreover, if the selected polymer is miscible with lignin, e.g. TPU, the resulted LNCFs are smooth and of low pore volume, e.g. 0.01 cm^3g^{-1}, however; if the selected polymer is immiscible with lignin, e.g. PLA, the resulted LNCFs contain pores and have high pore volume, e.g. 0.31 cm^3g^{-1} (Culebras et al. 2019).

Complex carbon-based morphological nanostructures using lignin have been reported. A simple but interesting approach demonstrates the fabrication of a composite LCNF@SnO_2 as hollow multichannel nanofibrous powder using electrospinning method has been reported (Cao et al. 2020). First, at different mass ratios, 1:9, 3:7, 5:5, 7:3 and 9:1, lignin and PMMA were mixed in a DMF solution to which a predetermined amount of PVP and $SnCl_2.H_2O$ were added. The final mixture was used to prepare

nanofibers using electrospinning. After acid treatment and carbonization of the as-spun nanofibers, LCNF@SnO_2 composite as powder was prepared. The reason for obtaining the carbonized composite in powder from perhaps because of the brittleness of the resulted composite. PVA and PMMA were used as spinning auxiliary polymer and as a sacrificial phase material to create multichannel nanofibers, respectively. When the amount of lignin was the smallest (lignin to PMMA 1:9), the nanofibers formed almost a single hollow structure as shown in Fig. 3a, b. As the lignin amount was increased, smaller multiple hollow channels started to form up until solid nanofibers were formed (lignin to PMMA 9:1) shown in Fig. 3c–j. Specific surface area and total pore volume, 659 m^2/g and 0.56 cm^3/g, respectively, were the highest for multichannel nanofibers (lignin to PMMA 5:5). In addition, with the increase in the lignin amount, the nanofiber diameter decreased from 310 to 210 nm. Lignin offers an alternative green option to PAN to produce LCNFs with tunable morphology.

Cellulose

Self-assembly or bottom-up method of cellulose nanofibers is possible by a series of chemical pretreatments, controlling the initial cellulose concentration, and introducing freeze-drying (Han et al. 2013). The process, however, is long and somewhat complicated. Therefore, electrospinning, top-down method, is an attractive and simple method. Due to the poor spinnability of pristine cellulose, electrospun cellulose nanofibers are prepared using cellulose acetate (CA) dissolved in acetone, or a mixture of acetone/DMAc, or a mixture of acetone/DMF/trifluoroethylene. The as-spun membrane can be deacetylated by immersing CA nanofibers in alkaline solutions, i.e. NaOH at room temperature (Deng et al. 2013; Li et al. 2019b; Liu and Hsieh 2002, 2003; Lu and Hsieh 2010; Cai et al. 2015), or NaOH at elevated temperature (Ma et al. 2005), or NH_4OH, mixture of NH_4OH and NH_4Cl (Kuzmenko et al. 2014), or KOH (Son et al. 2004). The salts can be dissolved in ethanol, water, a mixture of ethanol and water, or a mixture of acetone and water. The deacetylated cellulose nanofibrous membranes tend to have a lower average fiber diameter, fiber distribution, and pore size compared with as-spun CA nanofibers (Deng et al. 2013). In addition, the deacetylation process conditions, i.e. salt concertation, mixture ratio, temperature, and immersing duration, affect the final morphology, surface area, surface roughness, and carbon yield of CNFs. For example, cellulose nanofibers immersed in low concentrated NaOH–ethanol or water solutions resulted in rather film-type structure after carbonization (Cai et al. 2015). While, cellulose nanofibers immersed in NaOH–low ethanol/water ratio solution, after carbonization, resulted in interbonded fused nanofibers due to diffusion inability of the mixture causing unhydrolyzed spots. Electrospun polypyrrole-coated cellulose-based CNFs deacetylated in 0.1 M NaOH-ethanol solution and carbonized at 850 °C resulted in nitrogen-doped interconnected network with a specific surface area of 501 m^2/g and pore size of 2.7 nm as shown in Fig. 4 (Cai et al. 2015). As Fig. 4 shows, polypyrrole-coated cellulose-based CNFs have rougher surface area than pristine cellulose-based CNFs. The rougher surface was the resultant of the high specific surface area, while nitrogen species were the results of the polypyrrole-coated layer. EDS results in Fig. 4d shows the nitrogen content on the coated nanofibers.

Carbon content in cellulose is around 44%, which is relatively low compared with other carbon precursors, and the final carbon yield after carbonization is only between 10–15%. This low-carbon yield issue was addressed in a two-decade old study by suggesting the impregnation of sulfuric acid to increase the yield (Kim et al. 2001). Sulfuric acid acted as dehydrating catalyst to remove oxygen atoms in form of water instead of CO and CO_2 gases that led to smaller loss of carbon atoms during carbonization. At optimum does of sulfuric acid, $\sim$ 6 wt.%, carbon yield reached 38%, which suggested loss of carbon atoms to be around 6% only. To further improve on this, a much recent study, improved the carbon yield simply by altering the composition of the deacetylated solution, NH_4OH, with the inclusion of NH_4Cl (Kuzmenko et al. 2014). Subsequently, without washing, the deacetylated cellulose nanofibers were carbonized. NH_4Cl offered thermal stability and increased carbon yield from 13 to 20%.

Cellulosic nanowhiskers are nanorod-like structure with a diameter between 10 to 30 nm, and unlike cellulosic nanofibers, they do not form interconnected nanofibrous structure. The art of production of cellulosic nanowhiskers (nanorod-like) and the effect of processing conditions can be found in a review that

provides a thorough comprehension on the topic (Eichhorn 2011). Briefly, depending on the initial cellulose source, nanowhiskers can be prepared using acid hydrolysis method. By controlling processing conditions, e.g. initial source, hydrolysis duration, temperature, and polydispersity, the final morphology and physical properties can be tuned (Eichhorn 2011; Haafiz et al. 2014). Moreover, cellulose-based carbon nanowhiskers, widely referred to as carbon nanoneedles, can be prepared by hydrolysis of microcrystalline cellulose using sulfuric acid at temperature of 45 °C for 3 h followed by thermal stabilization and carbonization at 240 °C and 1200 °C, respectively (Cho et al. 2015). Although some studies show the potential of manipulating the structure of cellulose-based carbon nanoneedle to develop nitrogen-enriched (Silva et al. 2012) and copper, nickel, or iron-doped carbon nanoneedles (Araujo et al. 2016) or form composite (Silva et al. 2015), there is a still more work to do to study and improve the current state of cellulosic-based carbon nanoneedles.

The cellulosic part of plants offers a solution to produce cellulose acetate nanofibers using electrospinning, while bacterial cellulose (BC), produced by bacterial fermentation, offers an alternative fast route without the need for electrospinning, due to its readily ultrafine nanofibers. BC nanofibers form 3D interconnected structure with a typical diameter of around 50 nm. Also, BC is distinguished against plant cellulose by its high chemical purity, crystallinity, mechanical property, degree of polymerization, and self-assembly (Shoda and Sugano 2005; Huang et al. 2014). Nonetheless, before carbonization, the network structure of bacterial cellulose pellicles needs to be preserved by subjecting it to freeze-drying (Lee et al. 2013; Yu et al. 2014; Jiang et al. 2016). Although the nanofibril is preserved after carbonization, the carbon yield is rather low, 2.3%. If freeze-drying is omitted as a pretreatment step, the carbon yield could be increased up to around 20%, however; the nanofibril structure will be completely destroyed after carbonization (Lee et al. 2013). To overcome this issue, freeze-dried BC as CNF precursor mixed with potassium citrate as carbon nanosheet precursor to act as a bridge between the nanofibers was carbonized at 850 °C (Jiang et al. 2016). The carbon yield was notably high, around 42%, which is probably due to the additional carbon content in potassium citrate. In addition, these nanosheet bridges enhanced the surface area and total pore volume, 1037 m^2/g and 1.03 cm^3/g, respectively, compared with pristine BC-based CNFs, 510 m^2/g and 0.74 cm^3/g, respectively.

In order to obtain a free-standing membrane, one group has demonstrated a strategy involving liquid nitrogen prior freeze-drying over a series of studies (Chen et al. 2013a, b). In addition, the same group has also suggested a cost-effective and industrially applicable method to prepare a free-standing nitrogen and phosphorus doped BC-based CNFs (Chen et al. 2014). In a typical procedure to obtain phosphorus-doped free-standing membrane, before freezing in liquid nitrogen, BC pellicle slices were immersed in $NH_4H_2PO_4$ aqueous solution at room temperature for 10 h. Subsequently, the samples were kept in liquid nitrogen, freeze-dried, and finally carbonized at 800 °C. The diameter range of BC-based CNFs was found to be 16 to 25 nm, while specific surface area and pore size were around 290 m^2/g and 2.2 nm, respectively.

Table 4 summarizes different process conditions and protocol of cellulose derived CNFs. It can be seen that each source of cellulose retains a unique preparation protocol providing suitable and applicable options for industrial scaling.

Chitin

Depending on the source of chitin, chitin nanofibers are extracted by a series of chemical and mechanical treatments with a diameter of around 20 nm. For example, using crab shells, chitin is extracted by treating the shells with NaOH and HCl for few days before being subjected to ethanol for few hours. Grinder treatment is followed to obtain non-aggregate nanofibers (Ifuku and Saimoto 2012). Due to the nanofibrous nature of chitin and its high nitrogen content, nitrogen-doped chitin-based CNFs (CCNFs) can be directly prepared from pure chitin without further subsequent activation. However, CCNFs do not sustain a free-standing membrane but rather nanofibrous powder.

Nitrogen-doped CCNFs have been prepared by thermal stabilization at 300 °C for 1.5 h followed by carbonization at 500, 600, 700, 800, and 900 °C (Hao et al. 2018b). Result demonstrated that as the temperature increased from 500 to 900 °C the specific surface area dropped from around 531 to 285 m^2/g, respectively. Nitrogen content decreased from around 10% down to 5%, respectively, while Raman spectra

recorded an increase in D-band to the G-band intensity ratio with the increase in carbonization temperature, which is an indication in increase in graphitization degree. Similar results, using pure chitin nanofibers, were reported in a separate study that showed as the carbonization temperature increased, from 500 to 900 °C, specific surface area decreased from around 458 to 263 m^2/g, with increase in pore size from 2.75 to 2.86 nm (Hao et al. 2018a). The results also showed graphitization degree increases with the increase of carbonization temperature. Heteroatoms doping, oxygen and nitrogen doping, of CCNFS was synthesized from an insect, namely cicada slough (Zhou et al. 2017). The chitin powder obtained from cicada slough was mixed with physical activation agent, KOH at different weight ratios, (KOH:chitin) 1:2, 1:1, 2:1, and 3:1, before carbonization at 800 °C. Results showed that oxygen amount increased as KOH content increased, and vice versa for the nitrogen amount. Although at weight ratio of 3:1, results showed that CCNFs possess high surface area and total pore volume of 2217 m^2/g and 1.02 cm^3/g, respectively, and the carbon yield was at 10.9%. It was also shown that as the weight ratio increased the carbon yield decreased, while specific surface area increased. At weight ratio of 1:2 the surface area and total pore volume were shown to be 1243 m^2/g and 0.57 cm^3/g, respectively, and carbon yield was at 38.2%. These results shed the light on the possibility of synthesizing oxygen- and nitrogen-doped CCNFs and controlling the surface area and carbon yield. CCNFs offer finer nanofibers compared with most synthetic-based CNFs but lack the ability to form stand-free membranes due to the nature of chitin extraction conditions.

Protein

Protein is an abundant source for CNFs but lacks the ability to form a stand-alone CNF membrane. To tackle this issue, one group suggested the incorporation of lignin into plant protein to form CNFs. Though the structure of the membrane was maintained, the average fiber diameter increased drastically from 540 to 2610 nm after lignin addition (Yang et al. 2018a).

Other proteins, such as prolamin, loss their fibril structure upon carbonization. Thus as a remedy solution, the addition of calcium salt, on one hand, enhanced the thermal stability and retained nanofibril structure, on the other hand, however, resulted in brittle CNFs (Yang et al. 2018b). To fabricate stable and flexible prolamin protein-based CNFs, the same previous group has suggested the utilization of transition metals, zinc, cobalt, and nickel (Wang et al. 2017b). They also followed a meticulous carbonization procedure after determining degradation temperature range of prolamin protein which was between 200 and 300 °C. First, the sample was heated to 200 °C at a rate of 5 °C/min and maintained for 2 h. Second, at lower heating rate of 1 °C/min the temperature was increased to 300 °C and maintained for 4 h. Finally, at heating rate of 1 °C/min the temperature was increased to 800 °C and maintained for 2 h before it was allowed to cool down to room temperature. The notable issues of protein-based CNFs are brittleness and free-standing capability that are yet to be addressed thoroughly.

Others

Biowaste-based nanofibrous and 1d-structures are rather limited compared with 0d-strcuture. For instance, carbonized kiwi fruits have shown to yield only partial carbonized nanofibrous structure along with nanosheet structure (Cheng et al. 2020). With a more distinct hollow nanofibrous structure, hexagonia apiaria, a type of fungus, has shown capability to preserve this distinct hollow nanofibrous structure after activation with KOH and carbonization at 800 °C for 2 h (Deng et al. 2017). The fiber diameter of hexagonia apiaria decreased from 2 μm to 620 nm after carbonization and was reported to have high specific surface area of 1280 m^2/g. A group of researchers managed to synthesize magnetic nanofiborus carbon composite as sawdust as the carbon precursor (Liu et al. 2014). Briefly, purified sawdust waste, was mixed in Fe precursor, $FeCl_3$ solution, at elevated temperature, and the resultant dried material was carbonized. The nanofibers growth was thought to be as a combination of the high temperature and the role of catalyst played by Fe species mimicking chemical vapor deposition method. The specific surface area of the fibers was recorded to be around 360 m^2/g.

The use of electrospinning to prepare nonconventional biomass and biowaste-based carbon nanofibers is rather limited because the process strongly depends on the spinnability of the biomass precursor, which is usually poor. Depending on the nature of the starting

Table 4 Process conditions and protocol of cellulose derived CNFs

Carbon precursor	Materials processing conditions						Carbon conversion conditions		Carbon yield (%)	Ref
	Assembly method	Auxiliary/ starting substance	Solvent/ Extraction medium	Concentration (wt.%)	Regeneration/ Purification agent	Aid process	Stabilization	Carbonization		
Cellulose acetate	Electrospinning	–	Acetone and DMAc	20	0.05 M NaOH	–	Atmosphere@240 °C @3 °C/min for 1 h	Argon @800up to2200°C @10 °C/ min for 2.5 h	–	Deng et al. (2013)
Cellulose acetate	Electrospinning	–	Acetone and DMAc	20	0.05 M NaOH	–	Atmosphere@240 °C @5 °C/min for 1 h	Argon @900 @10 °C/ min for 0.5 h	–	Li et al. (2019b)
Cellulose acetate	Electrospinning		Acetone and DMAc	–	NaOH or NH_4OH	–	–	Nitrogen @800 @5 °C/min for 2 h	20	Kuzmenko et al. (2014)
Cellulose acetate	Electrospinning	–	–	–	0.1 M NaOH	–	–	Nitrogen @850 for 2 h	–	Cai et al. (2015)
Cellulose acetate	Electrospinning	PAN	DMF	~ 12	–	–	Atmosphere@240 °C for 2 h	Argon @800 for 2 h	–	Li et al. (2019a)
Cellulose nanowhiskers	Self-assembly (Hydrolysis process)	Microcrystalline cellulose	H_2SO_4	–	–	Centrifugation & freeze-drying	@240 °C @3 °C/min for 1 h	@800or1200 @10 °C/ min for 2.5 h	–	Cho et al. (2015)
Cellulose nanowhiskers	Self-assembly (Hydrolysis process)	Cotton	65% H_2SO_4	–	–	Centrifugation	–	Nitrogen @800or1200	–	Araujo et al. (2016)
Bacterial cellulose	Self-assembly (Gelation process)	Nata-de-Coco	Deionized water	–	0.1 M NaOH	Freeze-drying	–	@950or1200 @5 °C/ min for 0.5 h	2.3	Lee et al. (2013)
Bacterial cellulose	Self-assembly (Gelation process)	BC pellicles	–	–	Deionized water	Freeze-drying	Nitrogen@350 °C @1.5 °C/min for 1 h	Nitrogen@800 for 1 h		Yu et al. (2014)
Bacterial cellulose	Self-assembly (Gelation process)	BC pellicles	–	–	Deionized water	Liquid nitrogen and freeze-drying	–	Nitrogen@850 @3 °C/min for 1 h	~ 42	Jiang et al. (2016)
Bacterial cellulose	Self-assembly (Gelation process)	BC pellicles	–	–	Deionized water	Liquid nitrogen and freeze-drying	–	Argon@1300 for 6 h	–	Yang et al. (2019)

material, spinnability simply could be improved by blending with an auxiliary polymer. For example, by employing electrospinning using a mixture of PEO and sodium alginate followed by a treatment in ionic cobalt solution, alginate nanofibers decorated with cobalt nanoparticles were fabricated (Li et al. 2015a). The electrospun nanofibers were carbonized in ammonia atmosphere before immersion in acid treatment. The resultant carbonized alginate nanofibers had distinct half-sphere mesopores between 10 to 40 nm and a diameter of around 100 nm as shown in Fig. 5. It was argued that during acid treatment, cobalt nanoparticles were removed leaving behind the mesopores, and that the ammonia environment was a key role to aid in graphitization process and forming desirable defects sites that enhance electrochemical properties. Another method features using electrospinning and liquefied walnut shell followed by carbonization to synthesize walnut shell-based nanofibers has been reported (Tao et al. 2017). The calculated average diameter was around 175 nm and had a specific surface area of around 408 m^2/g. Since electrospinning offers great control on the morphology of the nanofibers, more efforts are needed to prepare tailored unconventional biomass and biowaste-based carbon nanofibers by means of developing spinnable biomass and biowaste materials.

To summarize, lignin, cellulose, chitin, and other biomass materials can be considered as the modern precursors for CNFs. Such materials not only provide us a renewable and sustainable option but also can be easily manipulated to obtain a tailored nanostructure with substantial physical properties suitable for energy applications. Table 5 summarizes the physical properties of different biomass- and biowaste-based CNFs.

It is worth to emphasize the different methodologies of KOH activation treatment due to their impact on the physical properties of carbon electrodes as is evident in Tables 2, 3, and 5, and throughout the reviews. The application of the KOH treatments differs depending on the adopted protocol. The most conventional method involves activation by soaking pre-carbonized materials into KOH solution or with a mixture of KOH and other activation agents. Solution concentration, mixture ratio, activation time, and activation temperature are the effective parameters that control the final physical properties of the carbon electrodes (He et al. 2016; Shehnaz et al. 2018; Zubbri et al. 2021). Others have utilized less common approach to active their samples using KOH as the activation agent. For example, one group utilized

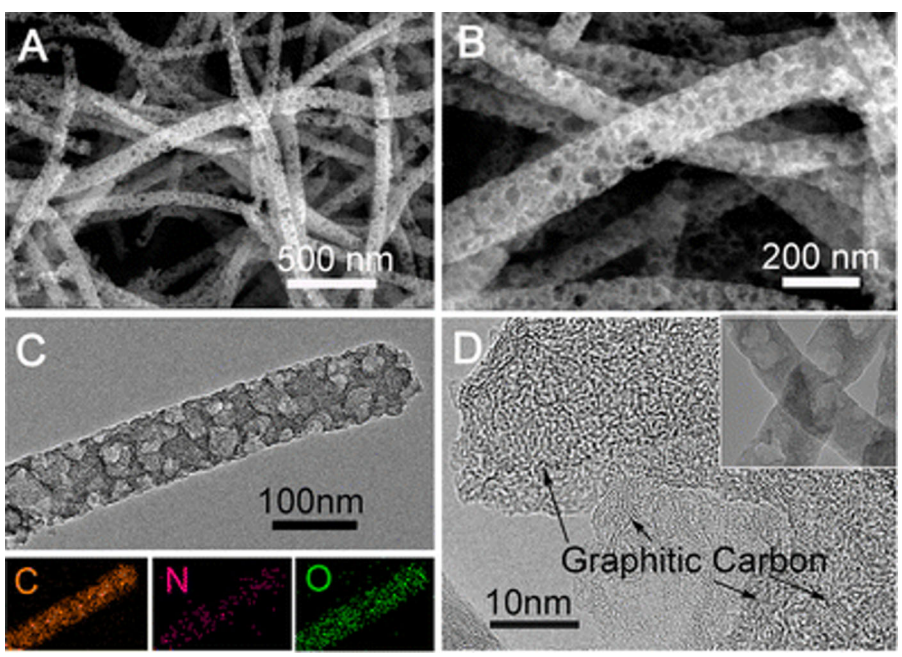

Fig. 5 **a**, **b** SEM and **c**, **d** TEM images of half-sphere mesopores alginate nanofibers carbonized at 600 °C. Reprinted with permission from Li et al. (2015a). Copyright (2015) American Chemical Society

Table 5 Comparison of physical properties of different biomass- and biowaste-based CNFs

Carbon precursor	Additive/ activation agent	Doping conditions				I_D/I_G	$d_{(002)}$ (nm)	Specific surface area (m^2/g)	Total pore volume (cm^3/g)	Pore size (nm)	References
		Doping mechanism	N (%)	O (%)	Others (%)						
Organosolv lignin	Graphene nanosheets/ KOH	Self-doping	12	–	0.7 (S)	0.88	0.34	2439	1.29	2–100	Dai et al. (2019)
Alkali lignin	MgO/–	None	–	–	–	–	–	1140	0.627	2–100	Ma et al. (2018)
Alkali lignin	Mixture of CO_2 and N_2	None	–	–	–	0.98	–	2170	0.987	2–4	Jayawickramage and Ferraris (2019)
Low sulfonate alkali lignin	NaOH	None	–	–	–	–	–	1444	0.91	0.7–1.5	Hu and Hsieh (2013)
Bacterial cellulose	Potassium citrate/–	None	–	–	–	0.89	–	1037	1.04	3.8–9.6	Jiang et al. (2016)
Bacterial cellulose	–/–	Self-doping	–	2.3	–	1.9	0.38	128	–	–	Yang et al. (2019)
Chitin	–/KOH	Self-doping	1.5	33.8	–	–	–	2217	1.09	1.5	Zhou et al. (2017)
Chitin	–/–	Self-doping	7.3	6.6	–	1.03	0.39	369	–	4.3	Hao et al. (2018b)
Protein(hordein &zein)-lignin	–/CO_2	Self-doping	1.3	4.3	–	1.01	0.38	1113	–	1.4	Yang et al. (2018a)
Plant protein	$Ca(OH)_2$/–	Self-doping	6.4	7.7	–	1.02	0.37	348	–	1.9–8.7	Yang et al. (2018b)
Fungus (hexagonia apiaria)	–/KOH	Self-doping	1.9	5	–	1.55	–	1280	–	2.2	Deng et al. (2017)

ultrasonic treatment to impregnate KOH on CNFs (Dai et al. 2019). Recent KOH activation methods involve assisted tool to minimize cost and time have also been reported. For instance, a group demonstrated that KOH treatment polysized in a microwave reactor can be effectively done within short time, 10 min (Feng et al. 2020). While another group showed that laser writing is also an effective method for KOH activation treatment since it's cost and time effective method (Liu et al. 2020b).

Most biomass and bio-based carbon precursors contain different chemical groups, thus making the KOH activation treatment differs from the activation treatment in carbon materials of petroleum nature. A recent study attempted to explore the role of KOH activation in biomass rich with oxygen groups (Chen et al. 2020b). They utilized Bamboo waste as their starting materials. As the result of abundant oxygen species, they found that activation with KOH can be effectively done at low impregnation ratios and low temperatures. Furthermore, activation can be further improved by allowing KOH to further react with carbon at slightly higher temperatures or higher impregnation ratios. It was argued that at low temperatures KOH reacted with the biomass and completely converted into K_2CO_3 accompanied with the release of byproducts such as phenols. As the temperature increased, K_2CO_3 was transformed to K_2O, and phenols release dropped. At the end of the activation process, stable oxygen groups were present and stable.

2D-nanostructure

This category is composed of bio-based carbonized thin films or papers with distinct nanocrystalline, and/or nanoporous structures.

Lignin

The potential of lignin-based carbon thin films in energy applications is still relatively new. The first characterization of a lignin-based carbon thin film is dated back to 2007 (Shen and Zhong 2007). The pore size and porosity of the film were found to be influenced by the amount of lignin (8–20 wt.%) that in turn influenced the UV adsorption and electric resistance properties of lignin-based carbon thin film. Recently, more complex lignin-based carbon thin film structures have been developed (Sun et al. 2019a; Luo et al. 2019). Interestingly, the addition of $NiCl_2$ as a catalyst and Na_2CO_3 as both a template and an activator to lignin solution had a pronounced effect on the physical properties of lignin-based carbon thin film (Sun et al. 2019a). Specific surface area of pristine lignin-based carbon thin film carbonized at 1000 °C was measured to be around 287 m^2g^{-1}, while lignin-based carbon thin film incorporated with Na_2CO_3 and treated with $NiCl_2$ carbonized at the same temperature was measured to be around 730 m^2g^{-1}. This increase of surface area was attributed to pores generated by the formation of Ni nanoparticles that helped form pores and channels, and to the decomposition of Na_2CO_3 into gases at different stages during carbonization that helped form more pores. Investigation of new activators and lignin's solvents, may prove vital for the development of lignin-based carbon thin films and the enhancement of their physical properties.

Cellulose

Pristine cellulosic-based and hierarchical composite nanostructured carbon films have attracted the attention of many research groups (Vuorema et al. 2010; Li et al. 2017a; Hwang et al. 2018; Meng et al. 2019). At a low-cost, a high degree of graphitization of pristine CNC film was fabricated at a carbonization temperature of 1000 °C (Zhu et al. 2017). Results illustrated surface area and pore sizes of 146 m^2/g and 1.7–30 nm, respectively. A simple and straightforward strategy was developed to prepare flexible film cellulose-based carbon nanofibers filled with activated carbon (Li et al. 2016c). First, cellulose and activated carbon were thoroughly mixed together and vacuum-filtered. Secondly, a flexible film, formed after freeze-drying, was carbonized at 800 °C for 2 h. The carbonized film preserved its integrity perhaps due to the available functional groups on cellulose nanofibers, e.g. hydroxyl group, that enhanced the interconnection between the two materials. The morphology of the film is depicted in Fig. 6. Results showed that the carbonized film had a large surface area of 1840 m^2/g which was due synergetic effect of the readily large surface area of the activated carbon and carbonized cellulose nanofibers. In a separate study, a combination of cellulose nanofibrils and cellulose nanocrystals (CNC) was prepared as nanostructured carbon film (Li et al. 2017b). But in order to avoid aggregation

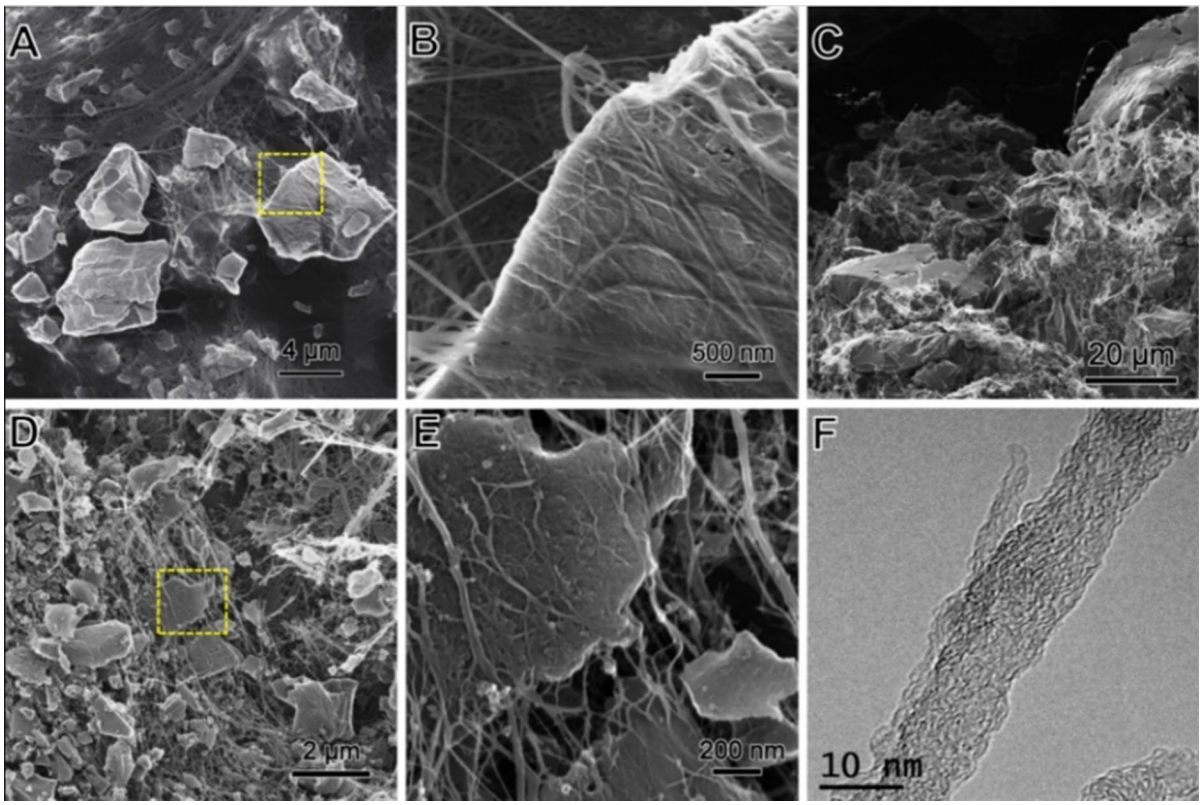

Fig. 6 SEM images at different magnifications of cellulose nanofibrils- and cellulose nanocrystals-based carbon film **A**, **B** before carbonization, **C**–**E** after carbonization, and **F** TEM image of single cellulosic carbon fiber. Reprinted with permission from Li et al. (2016c). Copyright (2016) Elsevier

between cellulose nanofibrils and CNCs, a sacrificial 5 nm thick layer of Al_2O_3 was deposited using atomic layer deposition on the uncarbonized cellulose nanofibrils/CNC film. The layer of Al_2O_3 was able to penetrate inside the sample through mesopores, thus, avoiding aggregation during carbonization which was carried out at 900 °C. The partially graphitized nanostructured carbonized film not only maintained nanofibrous and nanoporous structures but also exhibited large surface area, large total pore volume, and small pore size of around 1244 m^2/g, 2.2 cm^3/g, and 3.5 nm, respectively. Effort to fabricate a 2D-nanostructed composite film is noted too. A flexible 10 µm thick composite composed of carbonized cellulose paper and graphene/thin-graphite layer was fabricated in a one-step process using microwave plasma enhanced chemical vapor deposition (Ren et al. 2016). Edge oriented graphene sheets were grown on the paper, which was simultaneously carbonized during the process. The graphene growth and cellulose carbonization process were done in only 5 min. The carbon fibers are hollow filled with micro- and mesopores on their surfaces.

Chitin

Carbon nanoporous films have also been prepared from chitin derivatives. Using silica as a sacrificial material, chitin-based carbon film with high surface area and large pore volume was prepared (Nguyen et al. 2014). At the optimum silica concentration, surface area and pore volume were reported to be 1130 m^2/g and 1.0 cm^3/g, respectively, which were attributed to the space that was created by silica matrix during carbonization. In addition, silica content might have increased carbon yield too. Unique and scalable composite honeycomb-like chitin and reduced graphene film was also prepared (Wang et al. 2016). Before carbonization, the process consists of freezing and thawing cycles of a dispersion of chitin

and graphene oxide in NaOH-urea-water solution followed by coagulation using ethanol. Large pore interconnected structure, 1–3 μm, which is the result of phase separation, was attributed to the formation of honeycomb structure.

Others

There have been very few recent reports utilizing unconventional biomass and biowaste materials such as glucose, rice straw, and poly(furfuryl alcohol) as carbon precursors to develop nanostructured films (Hawes et al. 2019). The reported films were prepared by filtration method. Using infrared (IR) laser writing as the carbonization tool, carbonized poly(furfuryl alcohol) (PFA), a polymer that was derived from a biowaste, and reduced graphene composite (rGO) composite was prepared (Hawes et al. 2019). It was reported that the carbonization of PFA film using IR laser was not possible unless the medium contains some loads of graphene oxide (GO). In the composite, the laser intrigued the carbonization of PFA film and the reduction of GO to rGO sheets. The resultant morphology of the film was composed of PFA-based carbonized spheres with an average diameter of 670 nm with distributed rGO sheets that have lateral size ranging from 100 to 1400 nm. Another approach to prepare 2D-nanostructed carbon composite film using cotton fabrics as a substrate was also noted (Li et al. 2020). Nonetheless, binder-free 2D-nanostrcutured films and papers derived from biomass and biowaste materials are limited.

3D-nanostructure

This category is composed of bio-based 3D interconnected networks with distinct nanostructure features such as aerogel and foams.

Lignin

Aerogels are of low density and porous 3d-nanostructures. The preparation of lignin-based aerogels has been investigated by many groups. The main material parameters that go into the formation of lignin aerogels are (i) content of lignin and its molecular weight, (ii) auxiliary resins and their mass ratios, (iii) catalyst content, and (iv) extraction conditions, e.g. freeze-drying or CO_2 supercritical drying (Chen and Li 2010; Chen et al. 2011; Grishechko et al. 2013a). The initial amount of lignin and its molecular weight influence both gelation time and pore structure of the carbonized aerogel (Seo et al. 2014; Yang et al. 2017). The most notable auxiliary resin mixtures that have been studied are phenol–formaldehyde (Grishechko et al. 2013a), resorcinol–formaldehyde (Chen and Li 2010; Chen et al. 2011), and tannin–formaldehyde (Grishechko et al. 2013b), and NaOH and Na_2CO_3 are the most widely used catalysts among many others. These parameters have a pronounced effect on the final properties. For example, an interesting report showed that copper-doped lignin carbon aerogels resulted in higher porosity and specific surface area, 67% and 431 m^2g^{-1}, respectively, compared with pristine lignin-based carbon aerogel, 55% and 162 m^2g^{-1}, respectively (Xu et al. 2018a). In this example, copper played the role of the catalyst during sol–gel process, and the role of activator during carbonization. Table 6 summarizes some of these parameters and their corresponding physical properties for lignin-based and other biomass carbon aerogels.

The main advantage of lignin is that it has reactive sites, e.g. para carbon and ortho meta, that are available to react with formaldehyde as crosslinker, which lower the need to crosslinking in the presence of phenol or resorcinol (Grishechko et al. 2013a; Xu et al. 2015), unfriendly substances. Worth reporting that lignin-based carbon aerogels have shown to be fabricated without using phenol or resorcinol (Yang et al. 2017). Nonetheless, the main disadvantage of lignin-based aerogels is that they are brittle in nature which limits applications scope. To tackle brittleness of lignin aerogels, in one study, bacterial cellulose was incorporated to lignin to increase the elasticity of lignin-based carbon aerogels at a reversible strain of 20%, albeit with a low reported compressive strength of only 0.03 MPa (Xu et al. 2015).

Cellulose

Unlike lignin-based carbon aerogels, which typically involve resorcinol–formaldehyde as their main consentient, most of cellulose precursors, i.e. cellulose nanofibers, cellulose microcrystalline, and bacterial cellulose, could be used without auxiliary chemicals to fabricate carbon aerogels.

First, cellulose nanofibers have been used to form aerogels. For example, nitrogen doped cellulose-

Table 6 Material, preparation protocol, and physical properties of biomass- and biowaste-based carbon aerogels

Carbon precursor	Solvent/concertation (wt.%)	Catalyst	Auxiliary resin	Additive	Gel time temperature (°C)/time (hours)	Drying method	Density ($mgcm^{-3}$)	Porosity (%)	SSA* (m^2/g)	Total pore volume (cm^3/g)	Pore size (nm)	References
Organosolv lignin	Water/20	NaOH	Formaldehyde	–	85/2	Freeze-drying	0.005–1.0	> 0.45	19	0.007	1.5	Yang et al. (2017)
Kraft lignin	Water/20	NaOH	Formaldehyde	–	85/16	Freeze-drying	0.005–1.0	> 0.45	121	0.45	15	Yang et al. (2017)
Alkali lignin	Water/17	NaOH& Na_2CO_3	Resorcinol/formaldehyde	Bacterial cellulose	–	CO_2 supercritical liquid	2.6	–	199	–	17.8	Xu et al. (2015)
Enzymatic hydrolysis lignin	Water/–	Na_2CO_3	Resorcinol/formaldehyde	–	80/9	Ambient drying in acetic acid	–	60.4	779	0.48	9.4	Xu et al. (2018b)
Alkali lignin	Water/–	–	Resorcinol/formaldehyde	$CuCl_2{\cdot}6H_2O$	–/0.17	Freeze-drying	–	54.5	162	0.11	–	Xu et al. (2018a)
Alkali lignin	Water/–	–	Resorcinol/formaldehyde	CuCl2·6H2O	–/0.17	Freeze-drying	–	47.6	899	0.63	–	Xu et al. (2018a)
Fe_2O_3-bacterial cellulose	–	–	–	–	–	Freeze-drying	–	–	327	0.59	–	Huang et al. (2016)
N-doped bacterial cellulose	–	NH_3	–	–	–	Freeze-drying	–	–	875	0.78	3.0	Zhu et al. (2018a)
Chitin	phytic acid & hydrogen/8 & 3	–	–	–	110/6	Freeze-drying	–	–	586	–	< 2	Gao et al. (2019)
Shrimp shell chitin	NaOH-urea-H_2O/11:4:85 wt.%	–	–	–	50/2	Freeze-drying	–	–	521	0.3	< 2	Dassanayake et al. (2018)
Partially deacetylated chitin	Water/0.5–2.5	NaOH	–	NH3 & EtOH	–	Freeze-drying	–	–	1597	3.2	4.1	Ding et al. (2018)
Soy protein	Water/–	–	Cellulose	–	180/5.5	Freeze-drying	–	–	697	0.38	~ 5	Alatalo et al. (2016)
Agaric	–	NH_4Cl	–	–	–	Freeze-drying	–	–	2200	–	5–10	Zhang et al. (2019a)
Konjac glucomannan	Water	NaOH	SiO_2 nanofibers	–	–	Freeze-drying	0.14	99.99	–	–	–	Si et al. (2016)
Durian	–	–	–	–	–	Freeze-drying			618	0.43	> 5	Lee et al. (2020)
Jackfruit	–	–	–	–	–	Freeze-drying	–	–	511	0.28	> 5	Lee et al. (2020)

*SSA refers to specific surface area

nanofibers aerogels reinforced with GO was fabricated and carbonized to convert the cellulose-nanofibers to carbon and the graphene oxide to reduced graphene resulting in cellulose nanofibers-based reinforced rGO carbon aerogel (Zhang et al. 2018). Briefly, the nitrogen doping was possible by preparing a homogenous mixture of melamine, an organic material rich with nitrogen, and cellulose nanofibers in one pot. The resulted mixture was mixed with a predetermined amount of GO solution. The composite mixture was allowed to be dried in nitrogen liquid before initiating freeze-drying followed by carbonization at 600 °C. The carbonized aerogel resulted in a specific surface area of 487 cm^3/g, while its rich nitrogen content facilitated hydrophilicity, and the rGO allowed the aerogel to exhibit 40% recoverable volume change under compression loading. Another example illustrates hierarchical structure of cellulose-nanofibers composite aerogels decorated with $NiCo_2S_4$ nanocrystals (Liu et al. 2020a). The cellulose-nanofibers were freeze-dried to form aerogel then immersed in $NiCo_2S_4$ precursor before initiation of a hydrothermal reaction and carbonization at low temperature of 500 °C. It was found that the carbon aerogel composite has a relatively high specific surface area and large pore volume of 394 m^2/g and 0.9 cm^3/g, respectively.

Secondly, a recent study showed that another source of cellulose, namely cellulose microcrystalline, dried in a supercritical CO_2 was possible to produce carbon aerogels with large surface area and pore volume, 892 m^2/g and 1.80 cm^3/g respectively, which substantially further increased after CO_2 activation, 1873 m^2/g and 2.65 cm^3/g respectively (Zu et al. 2016). Moreover, by comparing specific surface area and total pore volume of the nonactivated carbonized (carbonized at the same temperature 800 °C) and freeze-dried carbon aerogel, 418 m^2/g and 0.75 cm^3/g respectively, with their supercritical dried counterparts, 892 m^2/g and 1.80 cm^3/g respectively, it seems that supercritical drying might be more effective. This was attributed to the inner structure difference where supercritically dried carbon aerogels are characterized as homogenous and its nanofibrous structure tending to aggregate less. Worth reporting that the process of making based carbon aerogels from cellulose microcrystalline is more complex than previous cellulosic nanofibers because it involves preparation of nanocellulose gels and regeneration before obtaining aerogel structure.

Thirdly, BCs have been carbonized to prepare carbon aerogels. The preparation of BC as carbon aerogel is a two-step process: freeze-drying of BC pellicles, to preserve nanofibril structure, and carbonization at high temperature to convert BC aerogels to low dense BC-based carbon aerogels (Wu et al. 2013; Huang et al. 2015). Other practices may involve freezing at -196 °C in liquid nitrogen prior to freeze-drying (Liang et al. 2012; Wang et al. 2014, 2020a) or freezing in supercritical CO_2 (Liebner et al. 2010). BC-based aerogels, filled with 3D nanofibrous structure with a diameter equal or less than 20 nm, are flexible and tend to be less dense, 0.004 to 0.008 cm^3/g (Liebner et al. 2010; Wu et al. 2013), than their traditional carbon counterparts, 0.15 to 0.75 cm^3/g (Fu et al. 2003; Wu et al. 2004). Depending on the initial size of BC pellicles and the fact that around 15% of the initial volume will be lost, carbonized BC aerogels size and volume can be tuned. In addition, BC aerogels can afford reduction in volume up to 90% when the carbon aerogels are under compression loads and return to their original shape after removal of loads (Wu et al. 2013). BC-based carbon aerogel hierarchical composites have also been developed (Wan et al. 2015; Huang et al. 2016; Zhuo et al. 2019; Wang et al. 2019a). For example, BC-based carbon aerogel decorated with iron oxide nanoparticles was developed with a specific surface area of 322 m^2/g (Wan et al. 2015). Briefly, after obtaining BC aerogels in liquid nitrogen, the as-prepared aerogels immersed in $Fe(NO_3)_3.9H2O$ solution for subsequent hydrothermal synthesis to obtain Fe_2O_3 nanoparticles. The resulted composite was freeze-dried and carbonized at 600 °C to obtain BC-based carbon aerogels decorated with Fe_2O_3 nanoparticles.

BC-based nitrogen-doped carbon aerogels can be prepared simply by thermally treating BC pellicles in ammonia environment followed by carbonization as illustrated in Fig. 7. Such treatment further enhances physical properties. For example, specific surface area and pore volume of BC-based nitrogen-doped carbon aerogels were found to be 875 m^2/g and 0.78 cm^3/g, respectively. While specific surface area and pore volume of pristine BC-based carbon aerogel were 585 m^2/g and 0.55 cm^3/g, respectively. Plus, nitrogen doping decreased graphitization degree by imparting defects (Zhu et al. 2018a). Nitrogen-doping has also been featured for BC-based carbon aerogels. Recent studies have demonstrated that nitrogen-doping in BC

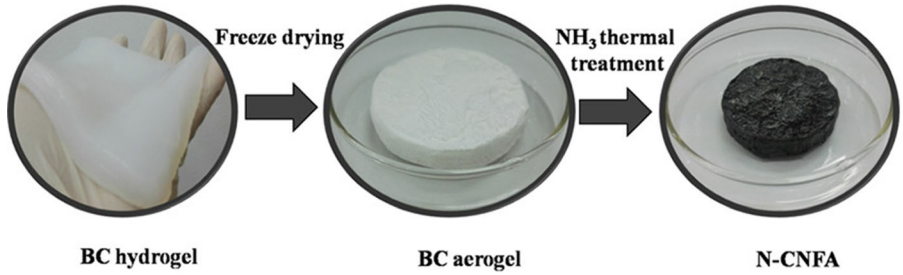

Fig. 7 Preparation of bacterial cellulose-based carbon aerogel. Reprinted with permission from Zhu et al. (2018a). Copyright (2018) Elsevier

could be obtained by incorporating the 3D structure with nitrogen-rich nanocrystals such as zeolitic imidazolate frameworks, e.g. ZIF-8 and ZIF-67, that contain 2-methylimidazole which is rich in nitrogen species (Fei et al. 2020; Chen et al. 2019). For example, using ZIF-8 nanocrystals, it was shown that the nitrogen content could reach up to 7% at a carbonization temperature of 900 °C (Chen et al. 2019).

Rapid microwave plasma pyrolysis as an alternative carbonization method has been reported to carbonize BC (Islam et al. 2017). The procedure was done in microwave plasma enhanced chemical vapor deposition system in methane and hydrogen environment under controlled pressure. The estimated temperature of carbonization was around 1200 °C. The entire plasma pyrolysis had lasted only for 15 min, and the pyrolyzed BC aerogel miniated its nanofibrous structure. The reported surface area, 57.5 m^2/g, however, is inferior to traditionally carbonized BC aerogels. Overall, cellulosic carbon aerogels prepared from BC not only are easy to prepare compared with other cellulosic precursors, but also show high quality porous inner nanostructure.

Chitin

Depending on chitin source and preparation protocols, chitin-based carbon aerogels have successfully been developed with distinct inner structures. Usually, chitin aerogels have nanofibrous inner structure with a fine diameter of 10 nm (Nogi et al. 2010). Unlike cellulose- and lignin-based carbon aerogels, chitin-based carbon aerogels already contain high amount of nitrogen atoms depending on carbonization conditions, for example, at 600 and 900 °C the nitrogen content is around 8% and 6%, respectively (Nogi et al. 2010; Li et al. 2015c). Moreover, self-doping of heteroatoms, nitrogen and oxygen atoms, is possible too. For example, nitrogen- and oxygen-rich chitin-based nanosheets carbon aerogels with high surface area of 586 m^2/g and average pore size less than 2 nm have been developed (Gao et al. 2019). The protocol starts by dispersing chitin powder in phytic acid and hydrogen peroxide solution before placing the mixture in autoclave environment at elevated temperature of 110 °C for 6 h. Subsequently, after rinsing with water, the mixture was freeze-dried before carbonization. The attributed large surface area was thought to be related to the decomposition of nitrogen and oxygen content during carbonization.

Depending on the starting chitin, different preparation methods have been reported. One approach involves the use of sol–gel method (Ding et al. 2012; Dassanayake et al. 2018). First, chitin powder was dispersed in NaOH-urea-water solution at low temperature, − 20 °C, before thawing (Dassanayake et al. 2018). Freezing and thawing cycles were repeated more than once for the solution before subjecting the obtained transparent solution to gelation process at elevated temperature, 50 °C. After washing with water, the hydrogel was freeze-dried at − 105 °C. The chitin aerogel was carbonized at 800 °C and resulted in high specific surface area. Another different approach illustrated in Fig. 8 involves using deacetylated chitins nanofibers dispersed in NaOH solution after weak acid treatment (Ding et al. 2018). Next, a hydrogel process was initiated by ammonia and ethanol gas coagulation to form hydrogen cross-linking at room temperature. Before freeze-drying, solvent exchange was carried out using *t*-BuOH. The nanofibrous chitin aerogel was carbonized at 500, 700, 900, and 1000 °C for 2 h. The nitrogen and oxygen content of chitin-based carbon

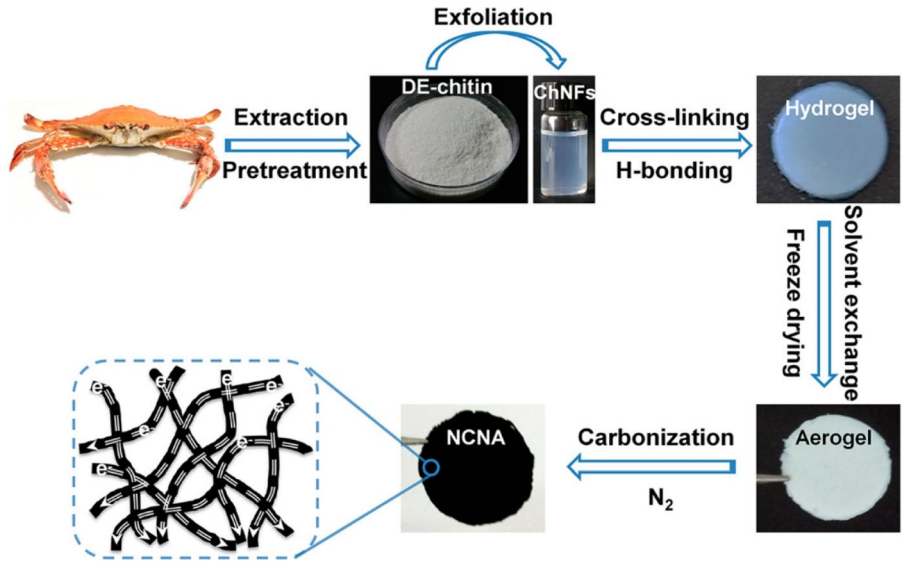

Fig. 8 Preparation steps of chitin-based carbon aerogel. Reprinted with permission from Ding et al. (2018). Copyright (2018) American Chemical Society

aerogel decreased as the carbonization temperature increased. However, when the carbonization temperature increased from 500 to 1000 °C, the surface area and pore volume substantially increased from 528 to 1597 m^2/g and from 1.5 to 3.2 cm^3/g respectively, while average pore size decreased from 5.7 to 4.1 nm, respectively. A similar decreasing trend was observed for graphitization degree as the carbonization temperature increased, Raman intensity ratio of I_D/I_G (intensity ratio of D band to G band) decreased from 1.02 to 0.89, respectively.

Hierarchal chitin-based carbon complex composites are another possible structure. For instance, nanohybrid chitin/cellulose/$NiFe_2O_4$ composite aerogel rich with nitrogen was synthesized (Liu et al. 2020c). Briefly, a homogenous composite dispersion of chitin/cellulose/$NiFe_2O_4$ synthesized in the presence of NaOH was heat treated in autoclave environment at 180 °C to form hydrogel once cooled down. After thoroughly washing with water, the chitin/cellulose/$NiFe_2O_4$ composite hydrogel was freeze-dried to obtain aerogel. Finally, at different temperatures the composite aerogel was carbonized. Before freeze-drying, the nanofibers composed of both chitin, 8 nm in diameter, and cellulose, 3–4 nm in diameter, was thought to be used as nucleation sites to homogenously growing $NiFe_2O_4$ nanoparticles with a diameter of 10 nm. However, after carbonization and freeze-drying, the nanofibrous structure along the nanoparticles became nanofiborus/nanosheets aerogel rich with nitrogen atoms. In addition, the size of nanoparticles increased dramatically to around 100 nm, which could be controlled by controlling the carbonization temperature and duration.

Protein

Protein-based carbon aerogels are rich with heteroatoms, especially nitrogen atoms, however, are brittle in nature. The brittleness has shown to be overcome by adopting protein-based composite instead. Such composites are made of protein sources, e.g. ovalbumin, soya bean flour, or silk regenerated proteins, and carbohydrates, e.g. cellulose and glucose, or graphene oxide (White et al. 2011; Yun et al. 2014a; Alatalo et al. 2016). For instance, a composite carbon aerogel was prepared from silk regenerated proteins, extracted from cocoons, and graphene oxide (Yun et al. 2014a). The composite was carbonized at 800 °C for 2 h to convert proteins to carbon and graphene oxide to rGO. Although the composite aerogel has a pore size of around 11 nm, the specific surface area, 181 m^2/g, is very modest compared with other carbon aerogels. Another example, soy bean flour, as the protein source, mixed with either glucose or cellulose were carbonized at 1000 °C to fabricate carbon aerogels

(Alatalo et al. 2016). Results showed that soy protein-glucose-based carbon aerogel has acceptable specific surface area of around 449 m^2/g and total pore volume 0.25 cm^3/g, while soy protein-cellulose-based carbon aerogel possesses higher specific surface area and larger total pore volume, 697 m^2/g and 0.38 cm^3/g, respectively, albeit its nitrogen content is lower. The difference in physical properties was attributed to the difference in the end physical structure of the composites, where glucose-based carbon aerogel resulted in aggregated nanoparticles and cellulose-based carbon aerogel resulted in fibril structure.

Others

Unconventional biowastes and biomass materials have been employed as carbon precursors to fabricate aerogels. Hydrothermal treatment accompanied with auxiliary chemical process have shown to be simple and rapid approach to fabricate biomass-based, e.g. glucose and agaric, hierarchical nanostructure carbon aerogels (Fellinger et al. 2012; Zhang et al. 2019a). For example, a hydrothermal treatment to agaric, type of mushroom fungus, solution followed by freeze-drying and carbonization chemical blowing resulted in agaric-based nanosheets carbon aerogel with high the specific surface area of 2200 m^2/g (Zhang et al. 2019a). It was argued that the blowing gas, NH_4CL, decomposed into NH_3 and HCl gases that generate mesopores in the range 5 to 10 nm and also facilitated the formation of 1.5 nm thick nanosheets carbon layers. Another recent report has utilized hydrothermally treated aloe juice, a plant source, as carbon precursor to fabricate Co_3O_4/C composite hierarchical aerogel structure with high specific surface area, 728 m^2/g (Yin et al. 2019). Figure 9 shows preparation step of aloe-based carbon composite and its surface morphology after freeze-drying, hydrothermal treatment, and carbonization. The corresponding Raman spectra and X-ray diffraction are also shown.

Unconventional carbon precursors that have been used as a starting material for aerogels include polysaccharides, waste foods, e.g. vegetables, fruits, and nuts, and biowastes, e.g. leather. Polysaccharide derivates aerogels have also successfully been utilized as carbon precursors to form hierarchical aerogel structures (El-Naggar et al. 2020; Si et al. 2016). To illustrate, resilient konjac glucomannan-based nanofibrous carbon aerogel has been designed and fabricated (Si et al. 2016). SiO_2 nanofibers have been employed as a template to support the inner honeycomb structure of the aerogel. The resultant aerogel was reported to be highly elastic with ultralarge porosity of 99.99% and ultralow density of only 0.14 mg/cm^3.

Waste foods and plant parts are excellent natural precursors for cheap and high-quality carbon aerogels. Many researchers have been investigating a wide range of biowaste organic foods, e.g. vegetables, fruits, and nuts, to fabricate high-performance electrodes in a form of 3D-structure. Cabbage waste has shown to be converted into carbon aerogels after a series of treatment, cryofreezing, freeze-drying, and carbonization (Cai et al. 2018). The partially nitrogen- and oxygen doped cabbage-based carbon aerogel have reported a high specific surface area of 536 m^2/g and an average pore size of 1.9 nm. Employing a simple approach of hydrothermal treatment, freeze-drying and carbonization, a recent study has utilized the core of two tropical fruits, namely durian and jackfruit, to fabricate carbon aerogels (Lee et al. 2020). Durian- and jackfruit-based carbon aerogels exhibited specific surface area and pore volume of around 618 m^2/g and 0.4 cm^3/g, and 511 m^2/g and 0.28 cm^3/g, respectively. Both carbon-based aerogels showed relatively high heteroatoms doping that were considered as important pseudo-capacitance performance boosters. Likewise, KOH activated hydrothermally treated pear, a fruit, has been used to fabricate highly graphitized carbon aerogel with ultrahigh specific surface area 2323 m^2/g (Myung et al. 2019). Other recent waste foods and plant parts as carbon precursors are potatoes and elm seeds (Lu et al. 2019; Guo et al. 2019).

Biowaste materials have engaged researchers' attention to synthesize biowaste-based hierarchical carbon aerogels as high-performance electrodes for energy applications. For instance, leather, a natural material, wastes were treated with KOH solution before initiating freeze-drying and carbonization processes (Liu et al. 2020d). The low-dense lather-based aerogel, 0.56 mg/cm^3, showed high specific surface area of 2523 m^2/g and heteroatoms doping. Another example, sodium lignosulphonate, a biomass substance used in food industry, as carbon precursor and mesoporous silica template as a supporting template have been used to fabricate hierarchical ordered activated with $ZnCl_2$ (Bai et al. 2020). The aerogel had a large specific surface area and pore volume of 1481 m^2/g and 2.62 cm^3/g, respectively. Likewise,

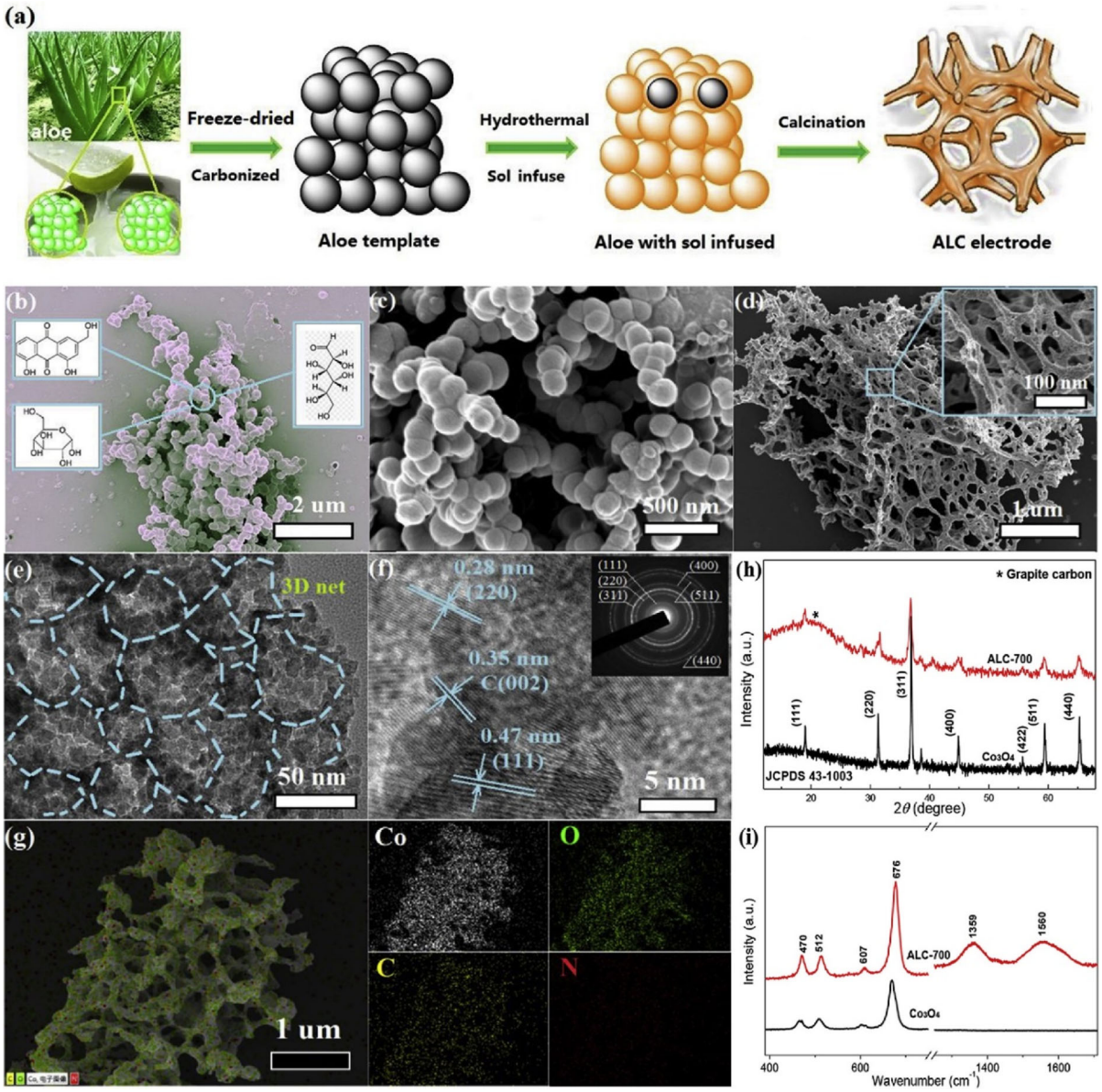

Fig. 9 **a** preparation steps of aloe-based carbon aerogel, SEM images of aloe composite after **b** freeze-drying, **c** hydrothermal treatment, and **d** carbonization at 700 °C, **e**–**g** TEM images and elemental analysis of aloe-based carbon composite aerogel, and **h**, **i** corresponding XRD pattern and Raman spectra. Reprinted with permission from Yin et al. (2019). Copyright (2019) Elsevier

wheat straw, harvesting biowaste, has been treated to fabricate lignocellulose-based 30 nm thick nanosheets carbon foam with large specific surface area and large mean pore size, 1063 m^2/g and 420 nm, respectively (Gou et al. 2020).

Bio-based nanostructured carbon materials for high-performance energy applications

Biomass and biowaste carbon precursors are abundant, environment friendly, and renewable materials. Such biomass and biowaste materials include lignin, cellulose, chitin, protein, and other unconventional biomass choices, e.g. food waste, flowers, seeds, plant

by-product wastes, etc. After carbonization, each of these materials possesses unique physical, chemical, and morphological properties qualifying it to be a high-performance electrode in energy storage devices, namely lithium-ion batteries and supercapacitors (Selvan et al. 2018; Li et al. 2018a; Zhu et al. 2020a).

The paradigm shift we are witnessing toward electric vehicles and high-performance electronic portables pushes the limit of energy storage devices every day. To meet such technological demand, new material preparation protocols have been researched and developed to reach high electrochemical performance in energy storage devices using carbon-based electrodes. Such protocols involve *doping of single atoms or heteroatoms, increasing specific surface area, and enhancing physical structure.* In the following sections, a review of the factors influencing electrochemical performance and summary of the most recent electrochemical performance of bio-based carbon electrodes in rechargeable batteries and SCs are given.

Factors influencing electrochemical performance of carbon electrodes

In energy storage devices, it has been established that N-doped (nitrogen-doped) carbon electrodes show better electrochemical performance than the same non-doped electrodes. For example, in SCs, N-doped carbon electrodes yielded lower resistance (0.23 Ω) and higher capacitance (313 $F.g^{-1}$ at 1 $A.g^{-1}$) compared with non-doped carbon electrodes that yielded higher resistance (1.32 Ω) and lower capacitance ($\sim$ 225 $F.g^{-1}$ at 1 $A.g^{-1}$) (Zhao et al. 2015a). It was also demonstrated that N-doped carbon electrodes are of hydrophilic nature (Zhai et al. 2011; Yang and Zhou 2017; Chen et al. 2017) while non-doped counterpart is of hydrophilic nature (Zhao et al. 2015a). Therefore, the enhancement in SCs using N-doped electrodes is attributed to the increased ion diffusion, improved wettability, and pseudocapacitance activity which is the result of nitrogen doping (Zhao et al. 2015a; Hou et al. 2015). Similar enhancement is seen in LIBs after nitrogen doping, which is attributed to the ability of lithium ions to be tucked and stored between the defect sites created by the presence of nitrogen functional groups (Zhang et al. 2014). Generally, N-doping can be realized by carbonizing enriched-nitrogen carbon precursors, e.g. PAN, at low temperature to maintain some of the original nitrogen content. Another important class of doping is sulfur-doping. Sulfur-doping enhances cycling stability, increases conductivity, and paves the way for more ions to be stored by providing extra reactive spots (Yun et al. 2014b; Li et al. 2015b). Additionally, oxygen- and heteroatom-doping have also shown to enhance the electrochemical performance of energy storage devices by increasing wettability, microporosity, and pseudocapacitance activity (Wu et al. 2012; Chen et al. 2014; Xu et al. 2017). For example, three-dimensional heteroatom-doping using phosphor, boron, and nitrogen atoms was shown to be an effective approach to improve electrochemical performance in SCs (Chen et al. 2014).

Another effective approach to enhance reach high electrochemical performance is by adopting materials with high specific surface area. The main virtues of high specific surface area in an electrode in energy applications are the extra space provided for ions in the electrolyte solution to be stored at higher rate, facilitation of ions diffusion, and lower electrical resistance (Yang et al. 2011; Liu et al. 2017b). It has been shown that electrodes with high specific surface area result in high-performance electrodes regardless of the initial starting materials, e.g. graphene or PAN (Zhang and Lou 2013; Zhang et al. 2013; Heo et al. 2019). Generally, for carbon-based electrodes, high specific surface area can be achieved by either physical or chemical activation or by incorporation of nanoparticles to increase roughness of the surface as is discussed in the previous section.

Physical structure is mainly related to the stability of the electrode which provides a better medium to store energy. That could be controlled by modifying the preparation protocol to involve steps promoting stable physical structure, for example, freeze-dried carbon-based aerogels allow for a stable physical structure and a control over the nanoporous structure that results in electrodes of good electrochemical stability and high-performance (Jung et al. 2015; Zhou et al. 2018). The physical structure of carbon materials could be further enhanced by allowing graphene-like nanosheets to be apart from each other so that an extra space is available for ions to be tucked in and stored. This approach was best illustrated in a recent work particularly for supercapacitors (Dai et al. 2019). It was shown that the additional spaces provided by

graphene-like nanosheets not only improved electrochemical performance but may be also was advantageous to the cycle life of the device.

High-performance bio-based nanostructured electrodes in rechargeable batteries

Efforts to utilize carbon-based materials in energy storage devices as functional electrodes have been widely noted among many research groups due to their chemical and electrochemical stability and charge storage ability (Zhu et al. 2015, 2016, 2020a; Li et al. 2018b). Conventional batteries consist of electrodes, electrolyte, and a separator. In principle, lithium ions flow in the electrolyte (e.g. lithium hexafluorophosphate dissolved in DMC or EC. See Table 7 for more details) from cathode and intercalates on anode during charging, and flow in reverse during discharging. The anode and cathode are physically separated by a porous separator to prevent short circuit control flow of ions.

Five of the most researched batteries are lithium-ion battery (LIB), lithium-oxygen battery (Li–O), lithium-sulfur battery (Li–S), sodium-ion battery (NIB), and potassium-ion battery (KIB) due to their abundance in Earth and good performance (Ji 2019). The advance of their electrochemical performance is mainly tight with the advance of the electrodes by extending the life cycle and increasing the reversible capacity. In batteries, efforts aimed at fabricating high-performance electrodes to meet the ever-increasing technological demands. For many groups, developing and testing the performance of carbon-based electrodes in batteries have been their immediate aim (Zhu et al. 2016, 2018b; Li et al. 2018a).

The most recent research has been focusing on utilizing biomass or biowaste materials that delivers high degree of oxygen and nitrogen species to allow for self-doing mechanisms after carbonization, or that delivers high specific surface area, or a combination of the two (Gao et al. 2017b). They also focused on artificially sulfur-doping the initial starting materials to allow for heteroatoms- or co-doping in order to enhance the overall performance of the battery. To demonstrate, as shown in Fig. 10, in LIBs and Li-Ss, large reversible specific capacities exceeding 500 $mAhg^{-1}$ limit with electrochemical stability over 100 cycles have been demonstrated by utilizing honeycomb-like carbon electrode derived from bagasse (Wan and Hu 2020). Such high-performance was mainly attributed to the synergetic effect of the sulfur and oxygen species hanging from the honeycomb-like structure. For both LIBs and Li-Ss, it was shown that the higher the sulfur/oxygen ratio the larger the storage capacity as long as the sulfur amount did not exceed the optimum limit because otherwise conductivity might be negatively affected. It has been shown that that bio-based carbon electrodes in Li-Ss reduce the effect of the shuttle effect (Wang et al. 2017a; Senthil and Lee 2021). A recent study focused on designing high specific surface area and pore volume for a carbon anode, derived from reed flowers, in Li–S (Wang et al. 2020c). As a result of the tailored morphology, a large reversible specific capacity of 908 $mAhg^{-1}$ with electrochemical stability over 100 cycles were achieved. It was argued that the large surface area and pore volume helped in increasing the adsorption of sulfur and polysulfide, thus minimizing dissolution of polysulfide or shuttle effect, and as a result large capacity good electrochemical stability were achieved. Other groups have also demonstrated the applicability of using the different properties of biomass-based electrodes to deliver high-performance in other storage batteries, e.g. as Li-OBs, NIBs, and KIBs, by manipulating the physical and chemical properties of those electrodes (Hao et al. 2018b; Sun et al. 2019b; Yang et al. 2020).

Efforts to develop high-performance composite biomass-based electrodes in storage batteries have also been reported (Zhang et al. 2020a; Sun et al. 2019b). Incorporating the right amount of $NiCo_2O_4$ nanoparticles/nanoneedles in carbonized pomelo peel, working as anode in LIB, increased specific surface area that in turn enhanced storage capacitance up to 474 $mAhg^{-1}$ after 120 cycles (@0.5 Ag^{-1}) (Zhang et al. 2020a). And also allowed for a stable performance over 1100 cycles at a capacitance of 363 $mAhg^{-1}$ at current density of 2 Ag^{-1}. In a separate study concerning the cathode of Li-Os, it was shown that by embedding CoFeP nanodots in a honeycomb-like anode derived from egg white rich with nitrogen and oxygen species, large storage capacitance of 1000 $mAhg^{-1}$ after 141 cycles (@0.1 Ag^{-1}) was recorded as shown in Fig. 11 (Sun et al. 2019b). Although the incorporation of CoFeP nanodots might have blocked some pores on the surface of the carbonized egg white leading to a lower specific surface area than pristine carbonized egg white, the large capacitance and the

Table 7 Electrochemical performance of biomass- and biowaste-based carbon electrodes in batteries

Carbon precursor	Nanostructure of the electrode/ Assembly state-of-the-art	Battery type	Electrolyte	Additive	Reversible specific capacity ($mAhg^{-1}$)/# of cycles/ @current density (Ag^{-1})	Capacity retention rate (%)	Coulombic efficiency	References
Bagasse	Honeycomb-like/Polymer binder	Lithium-ion	1.25 M $LiPF_6$ in a mixture of DMC[a] and EC[b] (1:1 vol%)	–	691/100/0.1	–	99.1% after 50 cycles	Wan and Hu (2020)
Lignin	Nanofiber membrane/ Binder-free	Lithium-ion	1 M $LiPF_6$ in mixture of EC &DEC[c]	Fe_2O_3	~ 715/80/ 0.05	95.1%	–	Ma et al. (2019)
Lignin	Nanofiber membrane/ Binder-free	Lithium-ion	1 M $LiPF_6$ in mixture of EC &DEC with 3 wt.% VC[c]	–	611/500/ [0.5C]	–	–	Culebras et al. (2019)
Pomelo peels	Wrinkled sheet/ Polymer binder	Lithium-ion	1 M $LiPF_6$ in a mixture of EC and DMC (1:1 vol%)	$NiCo_2O_4$	~ 500/120/ 0.05	–	97.6% after 120 cycles	Zhang et al. (2020a)
Corn straw	Nanoparticles/ Polymer binder	Lithium-ion	1 M $LiPF_6$ in a mixture of EC and DMC (1:1 vol%)	–	546/100/ [0.2C]	–	85.8% after 100 cycles	Yu et al. (2020)
Seaweed	3D connected network/ Binder-free	Lithium-ion	1 M $LiPF_6$ in a mixture of EC and DMC (1:1 vol%)	–	550/300/[1C]	–	–	Zhang et al. (2017a)
Reed flowers	Nanoporous powder/ Polymer binder	Lithium-sulfur	1 M LiTFSI in a mixture of DME[d] &DOL[e] (1:1 vol%)	–	908/100/ [0.1C]	–	99.7% after 100 cycles	Wang et al. (2020c)
Pomelo peel	Nanoporous powder/ Polymer binder	Lithium-sulfur	1 M Li2S &sublimated sulfur in a mixture of DME &DOL (1:1 vol%)	–	718/300–/ [0.2C]	–	98% after 300 cycles	Xiao et al. (2020)
Nanocellulose	3D nanofibril network/ Binder-free	Lithium-sulfur	1 M LiTFSI in a mixture of DME &DOL (1:1 vol%)	–	590/200/ [0.5C]	–	Close to 100% after 200 cycles	Chen et al. (2020a)
Egg white	3D honeycomb-like/Polymer binder	Lithium-oxygen	1 M $LiN(CF_3SO_2)_2$ in a mixture of TEGDME[f]	CoFeP	1000/141/0.1	–	–	Sun et al. (2019b)

Table 7 continued

Carbon precursor	Nanostructure of the electrode/ Assembly state-of-the-art	Battery type	Electrolyte	Additive	Reversible specific capacity ($mAhg^{-1}$)/# of cycles/ @current density (Ag^{-1})	Capacity retention rate (%)	Coulombic efficiency	References
Starch	Nanoporous skeleton/ Polymer binder	Lithium-oxygen	1 M LiTFSI in a mixture of TEGDME	IrCo	100/ ~ 210/ 0.2	77	–	Shen et al. (2019)
Pomelo peel	Microtube/ Coated on carbon paper	Lithium-oxygen	1 M LiCF3SO3 in a mixture of TEGDME	NiFe	13.8/290/0.1*	–	99.4	Jing et al. (2019)
Bagasse	Honeycomb-like/Polymer binder	Sodium-ion	1.25 M NaPF6 in a mixture of DMC &EC (1:1 vol%)	–	506/100/0.1	–	Close to 100% after 50 cycles	Wan and Hu (2020)
Bacterial cellulose	Nanofiber membrane/ Binder-free	Sodium-ion	1 M NaOTf[g] in a mixture of diglyme	–	233/100/0.2	–	–	Yang et al. (2019)
Chitin	Nanofiber/ Polymer binder	Sodium-ion	1 M $NaClO_4$ in a mixture of EC &DEC (1:1 vol%) &5 wt.% FEC[h]	–	105/8000/1	85%	Close to 100% after 8000 cycles	Hao et al. (2018b)
Spring onion peel	Parallel thin flake/ Polymer binder	Sodium-ion	1 M $NaClO_4$ in a mixture of EC &DEC (1:1 vol%) &5 wt.% FEC	–	605/2000/ 0.05	94%	–	Zhao et al. (2020)
Cotton linter pulp	Wrinkled flake cauliflower/ Polymer binder	Sodium-ion	1 M $NaClO_4$ in a mixture of EC and PC[i] (1:1 vol%) & 5 wt.% FEC		395/500/0.1	–	Close to 100% after 500 cycles	Dan et al. (2020)
Potato	Porous powder/ Polymer binder	Potassium-ion	3 M KFSI[j] in a mixture of DME	–	248/100/0.1	91.7	Close to 100% after 400 cycles	Cao et al. (2019)
Chitin	Nanofiber powder/ Polymer binder	Potassium-ion	0.8 M KPF_6 in a mixture of EC &DEC (1:1 vol%)	–	215/100/ [0.2C]	–	90% after 100 cycles	Hao et al. (2018a)
Ganoderma lucidum spore (Fungus)	Cage-like porous powder/ Polymer binder	Potassium-ion	1 M KPF_6 in a mixture of EC &DEC (1:1 vol%)	–	407/50/0.05	94.1	90% after 50 cycles	Yang et al. (2020)

Table 7 continued

Carbon precursor	Nanostructure of the electrode/ Assembly state-of-the-art	Battery type	Electrolyte	Additive	Reversible specific capacity ($mAhg^{-1}$)/# of cycles/ @current density (Ag^{-1})	Capacity retention rate (%)	Coulombic efficiency	References
Bamboo charcoal	Rod-like powder/ Polymer binder	Potassium-ion	0.8 M KPF_6 in a mixture of EC &DEC (1:1 vol%)	–	393/300/0.05	87.1	Close to 100% after 300 cycles	Tian et al. (2020)

*Capacity and current density units are in $mAhcm^{-2}$ and $mAcm^{-2}$, respectively. a refers to dimethyl carbonate, b refers to ethylene carbonate, c refers to diethyl carbonate, d refers to 1,2-dimethoxy ethane, e refers to1,3-dioxolane, f refers to tetraethylene glycoldimethyl ether, g refers to sodium triflate, h refers to fluoroethylene carbonate, i refers to propylene carbonate, and j refers to potassium bis(fluoro-slufonyl)imid

stability over 140 cycles were the result of unique physical structure (honeycomb-like) and the combined effect and activity role of Co, Fe, and P.

Most of the high-performance electrodes that are derived from some biomass precursors are assembled using polymer binders. Although polymer binders are essential additive to support the active powder in storage batteries, as a consequence, the dead-weight of the electrode increases, overall electrochemical performance drops, and the preparation time and cost increase (Zhang and Lou 2013; Shen et al. 2015; Zhang et al. 2017b). A common approach to tackle this issue is done by adopting self-standing materials such as in the case of lignin-based CNFs and bacterial cellulosic-based CNFs. Table 7 summarizes the electrochemical performance of polymer binders and binder-free electrodes derived from a wide variety of biomass and biowaste materials. Using lignin as CNFs precursor to fabricate anode for LIBs, a remarkable reversible specific capacity of around 715 $mAhg^{-1}$ with capacity retention over 95% was reported, albeit the electrochemical stability extends to only 80 cycles (Ma et al. 2019). The large capacity was the result of the incorporation of iron oxide nanoparticles which have high theoretical capacity. Self-standing bacterial cellulose-based CNFs as an anode in NIB resulted in a somewhat moderate reversible specific capacity of 233 $mAhg^{-1}$ (Yang et al. 2019). However, most self-standing biomass-based carbon electrodes lack the ability of self-doping due to the nature of the starting materials, e.g. lignin, bacterial cellulose, and cellulose acetate, that luck enough nitrogen and oxygen species after carbonization. Hence, adopting an appropriate aerogel preparation protocol as the assembly method for the biomass materials that sustain self-doping is a promising approach and also promotes a unique physical property. For example, by adopting alginate from seaweed as the starting carbon precursor, a carbon aerogel anode was fabricated for Li–S (Zhang et al. 2017a). It was shown that even at high current density of 1C the reversible specific capacity reaches 550 $mAhg^{-1}$ after 300 cycles. The adoption of nitrogen- and oxygen-enriched species biomass- and biowaste-based carbon aerogel anodes in storage batteries is still limited and more research is needed to unravel its true potential.

High-performance bio-based nanostructured electrodes in supercapacitors

SC is another important class of storage devices that can deliver high power in short period of time. Their excellent cycling stability is another outstanding feature that storage batteries lack. The main parts of a supercapacitor are electrodes, electrolyte, and a separator. As in the case with rechargeable batteries, the electrolyte provides the medium for ions to float during charging and discharging, and the separator keeps the electrodes physically apart. The electrodes are the main functional part that contributes the most

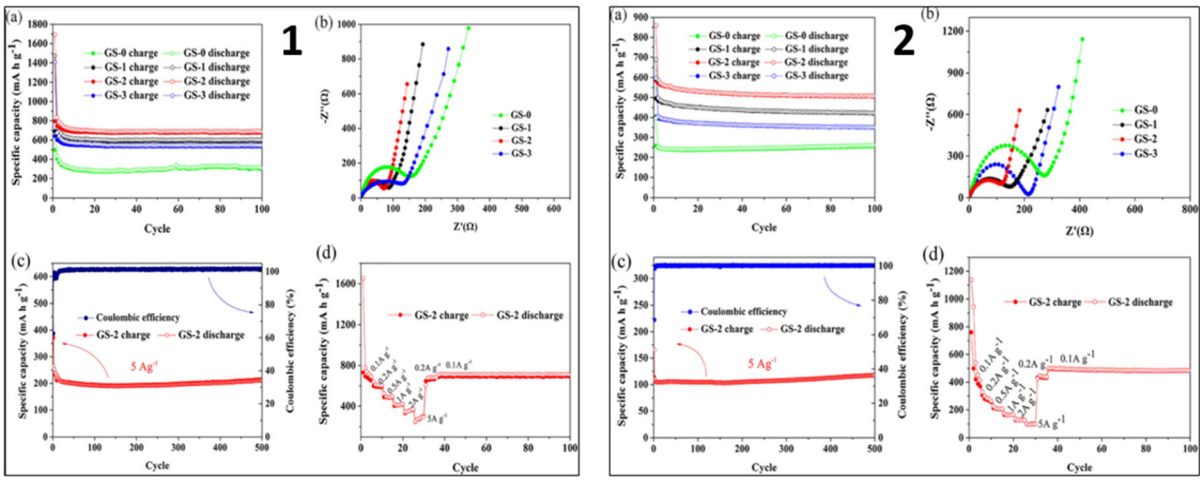

Fig. 10 Electrochemical and cycle performance of bagasse-derived electrodes at different current densities in (1) LIB and (2) in Li–S. Reprinted with permission from Wan and Hu (2020). Copyright (2020) Elsevier

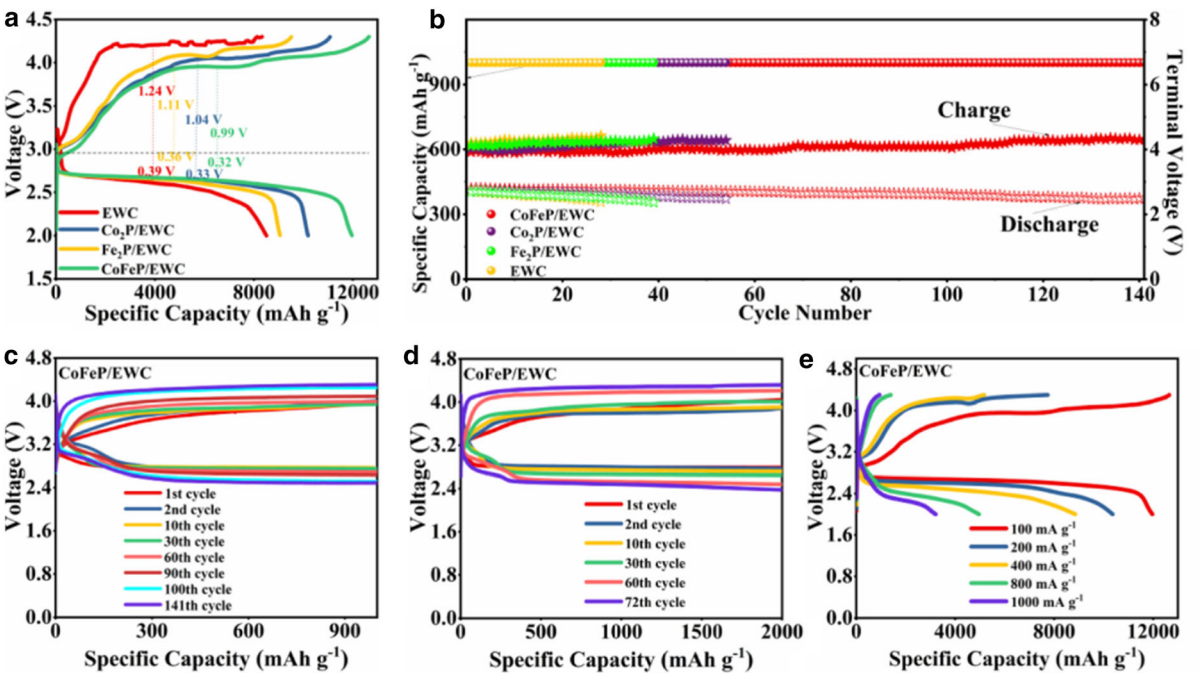

Fig. 11 Electrochemical and cycle performance of CoFeP nanodots incorporated in a honeycomb-like electrode derived from egg white at different current densities. Reprinted with permission from Sun et al. (2019b). Copyright (2018) Elsevier

to the electrochemical performance. One of the best suited electrodes is carbon-based due to their excellent physical properties and chemical stability in SCs (Merlet et al. 2012).

The recent research in SCs has been concerned about obtaining high-performance electrodes derived from renewable sources. Although the starting biomass and biowaste materials are ubiquitous, the approach of obtaining high-performance electrodes is almost the same which is fabricating electrodes with superior specific surface area, controlled physical structure, doping with different atoms, and enhanced

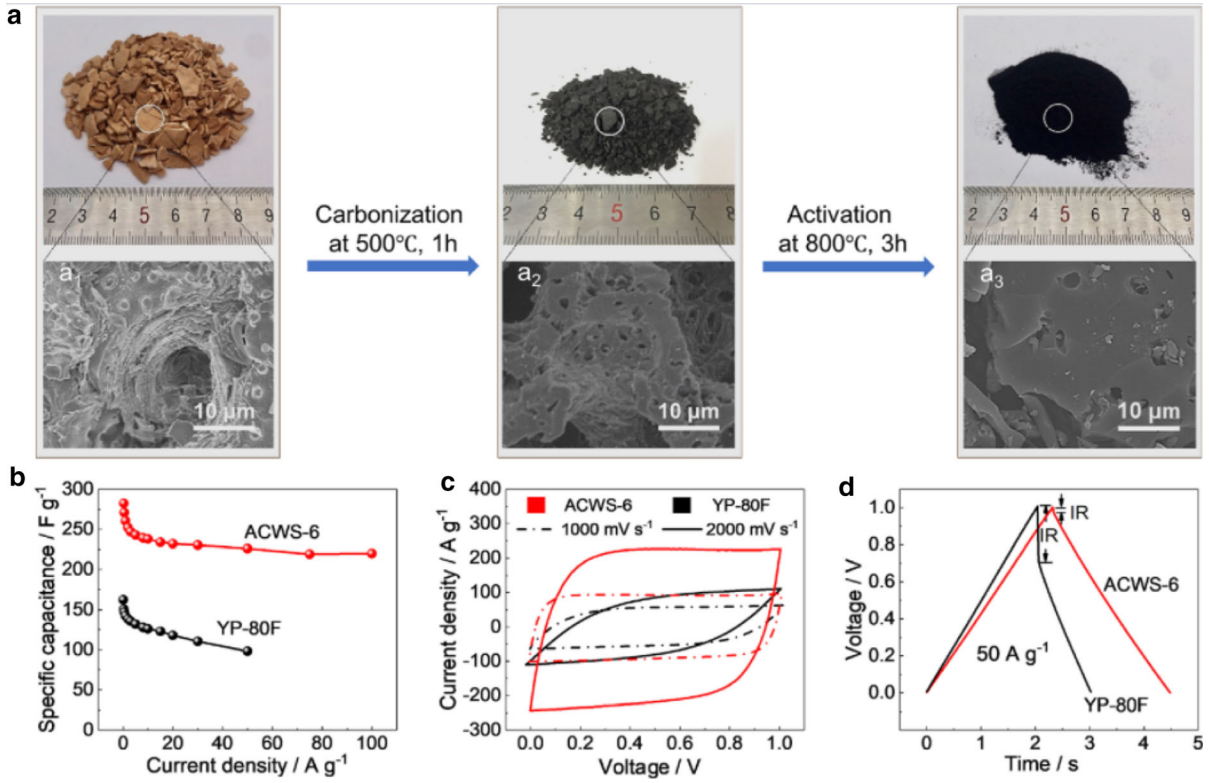

Fig. 12 Preparation steps and the electrochemical performance of the walnut shell-based electrode compared with an activated carbon counterpart. Reprinted with permission from Shang et al. (2020). Copyright (2020) Elsevier

pseudocapacitance activity by incorporating active materials. Electrodes made of activated eggshells, in a supercapacitor that its other parts (electrolyte and separator) are also made of the rest of the eggs (white, yolk, and membrane), delivered high capacitance of 421 Fg^{-1} with high power of 10 $KWkg^{-1}$ (Zhang et al. 2019b). The results were attributed to the high specific surface area and self-doped nitrogen, oxygen, and sulfur species that might have triggered pseudocapacitance activities. Utilizing walnut shell-based electrodes with ultrahigh specific surface area and tuned pore size delivered capacity of 216 Fg^{-1} with high energy density and ultrahigh power density of 48 $Whkg^{-1}$ and 100 $KWkg^{-1}$, respectively (Shang et al. 2020). This is illustrated by Fig. 12 which shows a comparison between the electrochemical performance of the walnut shell-based electrode and an activated carbon counterpart. The large surface area facilitated ion and electron transport, while the tuned pores facilitated accumulation of charges, thus larger capacitance was achieved. Other recent efforts have utilized biomass and biowaste materials such as cabbage, durian, and aloe to obtain high-performance electrodes to deliver high power density with relevantly high energy density (Cai et al. 2018; Yin et al. 2019; Lee et al. 2020). Table 8 summarizes the electrochemical performance of various bio-based carbon materials in SCs. The excellent electrochemical performance can also be explained by the inner structure that provides new paths for ion diffusions and space for storing charges, and enhanced interface between electrodes and electrolyte which is the result of nitrogen and oxygen species. In addition, the nitrogen content also increases electronic conductivity that in turn increases pseudocapacitance activities.

Unlike electrodes in batteries, binder-free electrodes in SCs are much common. The two most common approaches for a binder-free electrode are electrospun membranes and aerogels as summarized in Table 8. With such processed materials it is not only possible to obtain high-performance and self-standing materials, but also it is possible to modify the starting materials to embed additives to further enhance the performance. Incorporating graphene nanosheets in

Table 8 Electrochemical performance of biomass- and biowaste-based carbon electrodes in supercapacitors

Carbon precursor	Nanostructure of the electrode/ Assembly state-of-the-art	Electrolyte	Additive	Specific capacitance (Fg^{-1})/current density (Ag^{-1})	Energy density (Wh kg^{-1})	Power density (W kg^{-1})	Rate capability	References
Organosolv lignin	Nanofibers/ Binder-free	6 M KOH	Graphene nanosheet	267/1	9.3	493	97% after 5000 cycles	Dai et al. (2019)
N. Enzymatic hydrolysis lignin	Nanofibers/ Binder-free	6 M KOH	–	345/1	–	–	97% after 2000 cycles	Zhang et al. (2020b)
Lignin extracted from poplar sawdust	Multichannel nanofibers powder/ Polymer binder	6 M KOH	SnO_2	406/0.5	11.5	451	95% after 10,000 cycles	Cao et al. (2020)
Cellulose nanofibrils	3D nanofibril network/ Binder-free	2 M KOH	$NiCo_2S_4$	1569/0.5	53.7	184	78% after 5000 cycles	Liu et al. (2020a)
Chitin	hierarchical nanoporous structure/ Binder-free	6 M KOH	–	413/0.5	9.7	–	99.6% after 10,000 cycles	Wang et al. (2020b)
Chitin	3D nanofibril network/ Binder-free	6 M KOH	–	221/1	–	–	92% after 8000 cycles	Ding et al. (2018)
Eggshell	Graphene-like nanoporous powder/ Polymer binder	6 M KOH mixed with egg white &yolk	–	421/0.5	~ 7	~ 10,000	–	Zhang et al. (2019b)
Walnut shell	Stacked flake powder/ Polymer binder	6 M KOH	–	216/0.5	48	100,000	81% after 10,000 cycles	Shang et al. (2020)
Aloe	3D net-like network/ Binder-free	6 M KOH	Co_3O_4	1345/1	68.2	549	92.7% after 10,000 cycles	Yin et al. (2019)
Cabbage	3D nanoporous network/ Binder-free	6 M KOH	–	291/0.5	97.1	1456	96.8% after 10,000 cycles	Cai et al. (2018)
Durian	3D tunneled network/ Binder-free	0.5 M KOH	–	519/1	41.5	730	–	Lee et al. (2020)

lignin-PAN-based electrospun electrode was argued to increase specific surface area and to anchor nitrogen and sulfur species in the base material after carbonization that otherwise might have decomposed to gases (Dai et al. 2019). The composite delivered an enhanced energy density of around 9.3 Wh kg^{-1} compared to the pristine electrode's, 4.1 Wh kg^{-1}. Impressively, the incorporation of Co_3O_4 nanocrystals in aloe-based aerogel electrode improved the pseudocapacitance activity by delivering a capacitance of

1345 Fg^{-1} (@1 Ag^{-1}) with excellent cycling stability over 10,000 cycles and energy density of 68.2 $WhKg^{-1}$ (Yin et al. 2019). Other additives such as SnO_2 and $NiCo_2S_4$ have been investigated for their performance in SCs (Liu et al. 2020a; Cao et al. 2020). Even with the substantial efforts that have been made to improve the current state of SCs more research is needed to deliver higher energy density at high power density of carbon electrodes derived from biomass and biowaste resources.

Summary and perspective

Environmentally sustainable bio-based carbon precursors are excellent alternatives to precursors of petroleum chemicals origin. Bio-based carbon precursors are inexpensive due to their large abundance in nature. Moreover, bio-based carbon electrodes have excellent physical properties that permit them to perform outstandingly in energy storage applications. In this review, emerging and recent bio-based carbon precursors as high-performance electrodes in energy storage applications are classified and categorized based on their nanostructured morphologies (0D, 1D, 2D, and 3D) and natural origin. Some of these carbon precursors are lignin, cellulose, chitin, protein (e.g. egg), and other unconventional precursors (e.g. plant and food wastes). Under the four morphological categories, each of these materials is summarized and critically evaluated in terms of methodology, preparation protocols, morphology, physical properties, and doping mechanisms. In addition, the electrochemical performance of the most recent bio-based electrodes is discussed and summarized for rechargeable batteries and supercapacitors. The entirety of the review also serves as compacted guideline to design high-performance bio-based carbon electrodes for energy storage applications.

Tremendous efforts have been noted on designing and fabricating novel nanostructured bio-based electrodes with excellent morphological and physical properties that are capable of delivering high electrochemical performance in batteries and supercapacitors. Some studies focused on engineering nanoporous electrodes with specific surface area of larger than 1000 m^2/g and even exceeding 3000 m^2/g limit. Depending on the initial precursor, such physical properties are the results of the novel preparation protocols combined with some activation agents. While other studies worked on developing novel methods demonstrating the feasibility of heteroatoms- and self-doping in bio-based carbon electrodes. This is achieved either by finding methods to maintain the already existed species (e.g. nitrogen and oxygen groups) in the bone structure of the biomass material after carbonization, or by artificially importing some species by incorporating different substances. Such outstanding properties have shown to promote large capacity and ionic conductivity, increase in pseudocapacitance activity, and extend electrochemical stability. As a result, high-performance bio-based carbon electrodes have also been developed.

Despite the noted huge efforts to utilize bio-based carbon precursors as high-performance electrodes, more research focusing on further improving the current status of rechargeable batteries and supercapacitors to meet the ever-increasing future demands is imperative. To improve the status of bio-based carbon electrodes in energy applications the following challenges need to be addressed in future studies: (i) For most biomass and biowaste materials, the carbon yield is very low compared with synthetic materials. Increasing carbon yield would decrease the cost of processing which will reflect back on the total cost of the energy device. This can be approached by deploying additives that minimize the loss of carbon species during carbonization. (ii) The relation between specific surface area, pore size, and doping should be further investigated so that electrodes with optimum physical properties can be designed to obtain the best electrochemical performance possible. (iii) Due to the processing nature of some biomass and biowaste materials, the final carbonized state requires the use of organic binders to assemble it together as functional electrode. However, such approach undermines the overall performance of the electrode. To tackle this issue, developing new and simple preparation protocols to fabricate free-standing electrodes from materials that sustain self-doping are urged.

To summarize, environmentally sustainable bio-based carbon electrodes possess unique physical and chemical properties for high-performance electrochemical applications. Further research and more efforts are needed to tackle the immediate barriers to fully exploit the potential of the electrodes in energy storage applications.

References

Ago M, Okajima K, Jakes JE et al (2012) Lignin-Based Electrospun Nanofibers Reinforced with Cellulose Nanocrystals. Biomacromol 13:918–926. https://doi.org/10.1021/bm201828g

Ago M, Tardy BL, Wang L et al (2017) Supramolecular assemblies of lignin into nano- and microparticles. MRS Bull 42:371–378. https://doi.org/10.1557/mrs.2017.88

Alatalo S-M, Qiu K, Preuss K et al (2016) Soy protein directed hydrothermal synthesis of porous carbon aerogels for electrocatalytic oxygen reduction. Carbon 96:622–630. https://doi.org/10.1016/j.carbon.2015.09.108

Araujo RA, Rubira AF, Asefa T, Silva R (2016) Metal doped carbon nanoneedles and effect of carbon organization with activity for hydrogen evolution reaction (HER). Carbohydr Polym 137:719–725. https://doi.org/10.1016/j.carbpol.2015.11.036

Bai X, Wang Z, Luo J et al (2020) Hierarchical Porous Carbon with Interconnected Ordered Pores from Biowaste for High-Performance Supercapacitor Electrodes. Nanoscale Res Lett 15:88. https://doi.org/10.1186/s11671-020-03305-0

Baker DA, Gallego NC, Baker FS (2012) On the characterization and spinning of an organic-purified lignin toward the manufacture of low-cost carbon fiber. J Appl Polym Sci 124:227–234. https://doi.org/10.1002/app.33596

Brodin I, Sjöholm E, Gellerstedt G (2010) The behavior of kraft lignin during thermal treatment. J Anal Appl Pyrolysis 87:70–77. https://doi.org/10.1016/j.jaap.2009.10.005

Cai J, Niu H, Li Z et al (2015) High-Performance Supercapacitor Electrode Materials from Cellulose-Derived Carbon Nanofibers. ACS Appl Mater Interfaces 7:14946–14953. https://doi.org/10.1021/acsami.5b03757

Cai T, Wang H, Jin C et al (2018) Fabrication of nitrogen-doped porous electrically conductive carbon aerogel from waste cabbage for supercapacitors and oil/water separation. J Mater Sci Mater Electron 29:4334–4344. https://doi.org/10.1007/s10854-017-8381-5

Cao L, Kruk M (2015) Ordered arrays of hollow carbon nanospheres and nanotubules from polyacrylonitrile grafted on ordered mesoporous silicas using atom transfer radical polymerization. Polymer 72:356–360. https://doi.org/10.1016/j.polymer.2015.04.003

Cao M, Cheng W, Ni X et al (2020) Lignin-based multi-channels carbon nanofibers @ SnO2 nanocomposites for high-performance supercapacitors. Electrochim Acta 345:136172. https://doi.org/10.1016/j.electacta.2020.136172

Cao W, Zhang E, Wang J et al (2019) Potato derived biomass porous carbon as anode for potassium ion batteries. Electrochim Acta 293:364–370. https://doi.org/10.1016/j.electacta.2018.10.036

Chatterjee S, Saito T (2015) Lignin-Derived Advanced Carbon Materials. Chemsuschem 8:3941–3958. https://doi.org/10.1002/cssc.201500692

Chen C, Yu D, Zhao G et al (2016a) Three-dimensional scaffolding framework of porous carbon nanosheets derived from plant wastes for high-performance supercapacitors. Nano Energy 27:377–389. https://doi.org/10.1016/j.nanoen.2016.07.020

Chen F, Li J (2010) Synthesis and Structural Characteristics of Organic Aerogels with Different Content of Lignin. In: Adv. Mater. Res. /AMR.113–116.1837. Accessed 19 May 2020

Chen F, Xu M, Wang L, Li J (2011) Preparation and characterization of organic aerogels by the lignin - resorcinol - formaldehyde copolymer. BioResources 6:1262–1272

Chen H, Liu T, Mou J et al (2019) Free-standing N-self-doped carbon nanofiber aerogels for high-performance all-solid-state supercapacitors. Nano Energy 63:103836. https://doi.org/10.1016/j.nanoen.2019.06.032

Chen H, Wang G, Chen L et al (2018a) Three-Dimensional Honeycomb-Like Porous Carbon with Both Interconnected Hierarchical Porosity and Nitrogen Self-Doping from Cotton Seed Husk for Supercapacitor Electrode. Nanomaterials 8:412. https://doi.org/10.3390/nano8060412

Chen J, Liu Y, Liu Z et al (2020a) Carbon nanofibril composites with high sulfur loading fabricated from nanocellulose for high-performance lithium-sulfur batteries. Colloids Surf Physicochem Eng Asp 603:125249. https://doi.org/10.1016/j.colsurfa.2020.125249

Chen L-F, Huang Z-H, Liang H-W et al (2013a) Flexible all-solid-state high-power supercapacitor fabricated with nitrogen-doped carbon nanofiber electrode material derived from bacterial cellulose. Energy Environ Sci 6:3331–3338. https://doi.org/10.1039/C3EE42366B

Chen L-F, Huang Z-H, Liang H-W et al (2013b) Bacterial-Cellulose-Derived Carbon Nanofiber@MnO2 and Nitrogen-Doped Carbon Nanofiber Electrode Materials: An Asymmetric Supercapacitor with High Energy and Power Density. Adv Mater 25:4746–4752. https://doi.org/10.1002/adma.201204949

Chen L-F, Huang Z-H, Liang H-W et al (2014) Three-Dimensional Heteroatom-Doped Carbon Nanofiber Networks Derived from Bacterial Cellulose for Supercapacitors. Adv Funct Mater 24:5104–5111. https://doi.org/10.1002/adfm.201400590

Chen S, Koshy DM, Tsao Y et al (2018b) Highly Tunable and Facile Synthesis of Uniform Carbon Flower Particles. J Am Chem Soc. https://doi.org/10.1021/jacs.8b05825

Chen W, Gong M, Li K et al (2020b) Insight into KOH activation mechanism during biomass pyrolysis: Chemical reactions between O-containing groups and KOH. Appl Energy 278:115730. https://doi.org/10.1016/j.apenergy.2020.115730

Chen W, Hu C, Yang Y et al (2016b) Rapid synthesis of carbon dots by hydrothermal treatment of lignin. Mater Basel Switz. https://doi.org/10.3390/ma9030184

Chen Y, Xiao Z, Liu Y, Fan L-Z (2017) A simple strategy toward hierarchically porous graphene/nitrogen-rich carbon foams for high-performance supercapacitors. J Mater Chem A 5:24178–24184. https://doi.org/10.1039/C7TA09039K

Cheng D, Tian M, Wang B et al (2020) One-step activation of high-graphitization N-doped porous biomass carbon as advanced catalyst for vanadium redox flow battery. J Colloid Interface Sci 572:216–226. https://doi.org/10.1016/j.jcis.2020.03.069

Cherubini F (2010) The biorefinery concept: Using biomass instead of oil for producing energy and chemicals. Energy Convers Manag 51:1412–1421. https://doi.org/10.1016/j.enconman.2010.01.015

Cho HE, Seo SJ, Khil M-S, Kim H (2015) Preparation of carbon nanoweb from cellulose nanowhisker. Fibers Polym 16:271–275. https://doi.org/10.1007/s12221-015-0271-y

Cho M, Karaaslan M, Chowdhury S et al (2018) Skipping Oxidative Thermal Stabilization for Lignin-Based Carbon Nanofibers. ACS Sustain Chem Eng 6:6434–6444. https://doi.org/10.1021/acssuschemeng.8b00209

Cho M, Ko FK, Renneckar S (2019) Impact of Thermal Oxidative Stabilization on the Performance of Lignin-Based Carbon Nanofiber Mats. ACS Omega 4:5345–5355. https://doi.org/10.1021/acsomega.9b00278

Choi DI, Lee J-N, Song J et al (2013) Fabrication of polyacrylonitrile/lignin-based carbon nanofibers for high-power lithium ion battery anodes. J Solid State Electrochem 17:2471–2475. https://doi.org/10.1007/s10008-013-2112-5

Chu M, Zhai Y, Shang N et al (2020) N-doped carbon derived from the monomer of chitin for high-performance supercapacitor. Appl Surf Sci 517:146140. https://doi.org/10.1016/j.apsusc.2020.146140

Culebras M, Geaney H, Beaucamp A et al (2019) Bio-derived Carbon Nanofibres from Lignin as High-Performance Li-Ion Anode Materials. Chemsuschem 12:4516–4521. https://doi.org/10.1002/cssc.201901562

Dai Z, Ren P-G, Jin Y-L et al (2019) Nitrogen-sulphur Co-doped graphenes modified electrospun lignin/polyacrylonitrile-based carbon nanofiber as high performance supercapacitor. J Power Sources 437:226937. https://doi.org/10.1016/j.jpowsour.2019.226937

Dallmeyer I, Ko F, Kadla JF (2010) Electrospinning of Technical Lignins for the Production of Fibrous Networks. J Wood Chem Technol 30:315–329. https://doi.org/10.1080/02773813.2010.527782

Dallmeyer I, Ko F, Kadla JF (2014) Correlation of Elongational Fluid Properties to Fiber Diameter in Electrospinning of Softwood Kraft Lignin Solutions. Ind Eng Chem Res 53:2697–2705. https://doi.org/10.1021/ie403724y

Dalton N, Lynch RP, Collins MN, Culebras M (2019) Thermoelectric properties of electrospun carbon nanofibres derived from lignin. Int J Biol Macromol 121:472–479. https://doi.org/10.1016/j.ijbiomac.2018.10.051

Dan R, Chen W, Xiao Z et al (2020) N-Doped Biomass Carbon/Reduced Graphene Oxide as a High-Performance Anode for Sodium-Ion Batteries. Energy Fuels 34:3923–3930. https://doi.org/10.1021/acs.energyfuels.0c00058

Dassanayake RS, Gunathilake C, Abidi N, Jaroniec M (2018) Activated carbon derived from chitin aerogels: preparation and CO2 adsorption. Cellulose 25:1911–1920. https://doi.org/10.1007/s10570-018-1660-3

Delivand MK, Barz M, Gheewala SH (2011) Logistics cost analysis of rice straw for biomass power generation in Thailand. Energy 36:1435–1441. https://doi.org/10.1016/j.energy.2011.01.026

Demir M, Ashourirad B, Mugumya JH et al (2018) Nitrogen and oxygen dual-doped porous carbons prepared from pea protein as electrode materials for high performance supercapacitors. Int J Hydrog Energy 43:18549–18558. https://doi.org/10.1016/j.ijhydene.2018.03.220

Demiroğlu Mustafov S, Mohanty AK, Misra M, Seydibeyoğlu MÖ (2019) Fabrication of conductive Lignin/PAN carbon nanofibers with enhanced graphene for the modified electrodes. Carbon 147:262–275. https://doi.org/10.1016/j.carbon.2019.02.058

Deng L, Young RJ, Kinloch IA et al (2013) Carbon nanofibres produced from electrospun cellulose nanofibres. Carbon 58:66–75. https://doi.org/10.1016/j.carbon.2013.02.032

Deng L, Zhong W, Wang J et al (2017) The enhancement of electrochemical capacitance of biomass-carbon by pyrolysis of extracted nanofibers. Electrochim Acta 228:398–406. https://doi.org/10.1016/j.electacta.2017.01.099

Ding B, Cai J, Huang J et al (2012) Facile preparation of robust and biocompatible chitin aerogels. J Mater Chem 22:5801–5809. https://doi.org/10.1039/C2JM16032C

Ding B, Huang S, Pang K et al (2018) Nitrogen-Enriched Carbon Nanofiber Aerogels Derived from Marine Chitin for Energy Storage and Environmental Remediation. ACS Sustain Chem Eng 6:177–185. https://doi.org/10.1021/acssuschemeng.7b02164

Ding R, Wu H, Thunga M et al (2016) Processing and characterization of low-cost electrospun carbon fibers from organosolv lignin/polyacrylonitrile blends. Carbon 100:126–136. https://doi.org/10.1016/j.carbon.2015.12.078

Du B, Chen C, Sun Y et al (2020a) Unlocking the response of lignin structure by depolymerization process improved lignin-based carbon nanofibers preparation and mechanical strength. Int J Biol Macromol 156:669–680. https://doi.org/10.1016/j.ijbiomac.2020.04.105

Du B, Liu C, Wang X et al (2020b) Renewable lignin-based carbon nanofiber as Ni catalyst support for depolymerization of lignin to phenols in supercritical ethanol/water. Renew Energy 147:1331–1339. https://doi.org/10.1016/j.renene.2019.09.108

Du W, Zhang Z, Du L et al (2019) Designing synthesis of porous biomass carbon from wheat straw and the functionalizing application in flexible, all-solid-state supercapacitors. J Alloys Compd 797:1031–1040. https://doi.org/10.1016/j.jallcom.2019.05.207

Duan B, Gao X, Yao X et al (2016) Unique elastic N-doped carbon nanofibrous microspheres with hierarchical porosity derived from renewable chitin for high rate supercapacitors. Nano Energy 27:482–491. https://doi.org/10.1016/j.nanoen.2016.07.034

Echemi (2020) Polyvinyl Alcohol (PVA) Price Market Analysis - Echemi. https://www.echemi.com/productsInformation/pd20150901224-polyvinyl-alcohol.html. Accessed 6 Feb 2021

Edwards W (2020), Estimating a value for corn Stover | Ag decision maker. https://www.extension.iastate.edu/agdm/crops/html/a1-70.html. Accessed 6 Feb 2021

Eichhorn SJ (2011) Cellulose nanowhiskers: promising materials for advanced applications. Soft Matter 7:303–315. https://doi.org/10.1039/C0SM00142B

El-Naggar ME, Othman SI, Allam AA, Morsy OM (2020) Synthesis, drying process and medical application of polysaccharide-based aerogels. Int J Biol Macromol

145:1115–1128. https://doi.org/10.1016/j.ijbiomac.2019.10.037
Endo M, Kim C, Nishimura K et al (2000) Recent development of carbon materials for Li ion batteries. Carbon 38:183–197. https://doi.org/10.1016/S0008-6223(99)00141-4
Fava F, Totaro G, Diels L et al (2015) Biowaste biorefinery in Europe: opportunities and research & development needs. New Biotechnol 32:100–108. https://doi.org/10.1016/j.nbt.2013.11.003
Fei Y, Liang M, Zhou T et al (2020) Unique carbon nanofiber@Co/C aerogel derived bacterial cellulose embedded zeolitic imidazolate frameworks for high-performance electromagnetic interference shielding. Carbon 167:575–584. https://doi.org/10.1016/j.carbon.2020.06.013
Fellinger T-P, White RJ, Titirici M-M, Antonietti M (2012) Borax-Mediated Formation of Carbon Aerogels from Glucose. Adv Funct Mater 22:3254–3260. https://doi.org/10.1002/adfm.201102920
Feng Z, Chen H, Li H et al (2020) Microwave-assisted KOH activated lignite semi-coke for treatment of biologically treated wastewater from pulp and paper mill. J Environ Chem Eng 8:103924. https://doi.org/10.1016/j.jece.2020.103924
Fu R, Zheng B, Liu J et al (2003) The Fabrication and Characterization of Carbon Aerogels by Gelation and Supercritical Drying in Isopropanol. Adv Funct Mater 13:558–562. https://doi.org/10.1002/adfm.200304289
Gao L, Ma J, Li S et al (2019) 2D ultrathin carbon nanosheets with rich N/O content constructed by stripping bulk chitin for high-performance sodium ion batteries. Nanoscale 11:12626–12636. https://doi.org/10.1039/C9NR02277E
Gao S, Li X, Li L, Wei X (2017a) A versatile biomass derived carbon material for oxygen reduction reaction, supercapacitors and oil/water separation. Nano Energy 33:334–342. https://doi.org/10.1016/j.nanoen.2017.01.045
Gao Z, Zhang Y, Song N, Li X (2017b) Biomass-derived renewable carbon materials for electrochemical energy storage. Mater Res Lett 5:69–88. https://doi.org/10.1080/21663831.2016.1250834
García-Mateos FJ, Berenguer R, Valero-Romero MJ et al (2018) Phosphorus functionalization for the rapid preparation of highly nanoporous submicron-diameter carbon fibers by electrospinning of lignin solutions. J Mater Chem A 6:1219–1233. https://doi.org/10.1039/C7TA08788H
Gonugunta P, Vivekanandhan S, Mohanty AK, Misra M (2012) A Study on Synthesis and Characterization of Biobased Carbon Nanoparticles from Lignin. World J Nano Sci Eng 2:720–726. https://doi.org/10.4236/wjnse.2012.23019
Gonzalez MNG, Levi M, Turri S, Griffini G (2017) Lignin nanoparticles by ultrasonication and their incorporation in waterborne polymer nanocomposites. J Appl Polym Sci 134:45318. https://doi.org/10.1002/app.45318
Gou G, Huang F, Jiang M et al (2020) Hierarchical porous carbon electrode materials for supercapacitor developed from wheat straw cellulosic foam. Renew Energy 149:208–216. https://doi.org/10.1016/j.renene.2019.11.150
Grishechko LI, Amaral-Labat G, Szczurek A et al (2013a) Lignin–phenol–formaldehyde aerogels and cryogels. Microporous Mesoporous Mater 168:19–29. https://doi.org/10.1016/j.micromeso.2012.09.024
Grishechko LI, Amaral-Labat G, Szczurek A et al (2013b) New tannin–lignin aerogels. Ind Crops Prod 41:347–355. https://doi.org/10.1016/j.indcrop.2012.04.052
Gryglewicz G, Machnikowski J, Lorenc-Grabowska E et al (2005) Effect of pore size distribution of coal-based activated carbons on double layer capacitance. Electrochim Acta 50:1197–1206. https://doi.org/10.1016/j.electacta.2004.07.045
Guilminot E, Gavillon R, Chatenet M et al (2008) New nanostructured carbons based on porous cellulose: Elaboration, pyrolysis and use as platinum nanoparticles substrate for oxygen reduction electrocatalysis. J Power Sources 185:717–726. https://doi.org/10.1016/j.jpowsour.2008.08.030
Guo C, Hu R, Liao W et al (2017) Protein-enriched fish "biowaste" converted to three-dimensional porous carbon nano-network for advanced oxygen reduction electrocatalysis. Electrochim Acta 236:228–238. https://doi.org/10.1016/j.electacta.2017.03.169
Guo C, Li Z, Niu L et al (2016) A Nanopore-Structured Nitrogen-Doped Biocarbon Electrocatalyst for Oxygen Reduction from Two-Step Carbonization of Lemna minor Biomass. Nanoscale Res Lett 11:268. https://doi.org/10.1186/s11671-016-1489-3
Guo C, Liao W, Li Z et al (2015) Easy conversion of protein-rich enoki mushroom biomass to a nitrogen-doped carbon nanomaterial as a promising metal-free catalyst for oxygen reduction reaction. Nanoscale 7:15990–15998. https://doi.org/10.1039/C5NR03828F
Guo D, Song X, Li B et al (2019) Oxygen enriched carbon with hierarchical porous structure derived from biomass waste for high-performance symmetric supercapacitor with decent specific capacity. J Electroanal Chem 855:113349. https://doi.org/10.1016/j.jelechem.2019.113349
Haafiz MKM, Hassan A, Zakaria Z, Inuwa IM (2014) Isolation and characterization of cellulose nanowhiskers from oil palm biomass microcrystalline cellulose. Carbohydr Polym 103:119–125. https://doi.org/10.1016/j.carbpol.2013.11.055
Han J, Zhou C, Wu Y et al (2013) Self-Assembling Behavior of Cellulose Nanoparticles during Freeze-Drying: Effect of Suspension Concentration, Particle Size, Crystal Structure, and Surface Charge. Biomacromol 14:1529–1540. https://doi.org/10.1021/bm4001734
Hao R, Lan H, Kuang C et al (2018a) Superior potassium storage in chitin-derived natural nitrogen-doped carbon nanofibers. Carbon 128:224–230. https://doi.org/10.1016/j.carbon.2017.11.064
Hao R, Yang Y, Wang H et al (2018b) Direct chitin conversion to N-doped amorphous carbon nanofibers for high-performing full sodium-ion batteries. Nano Energy 45:220–228. https://doi.org/10.1016/j.nanoen.2017.12.042
Hawes GF, Yilman D, Noremberg BS, Pope MA (2019) Supercapacitors Fabricated via Laser-Induced Carbonization of Biomass-Derived Poly(furfuryl alcohol)/Graphene Oxide Composites. ACS Appl Nano Mater 2:6312–6324. https://doi.org/10.1021/acsanm.9b01284
He J, Zhang D, Wang Y et al (2020) Biomass-derived porous carbons with tailored graphitization degree and pore size

distribution for supercapacitors with ultra-high rate capability. Appl Surf Sci 515:146020. https://doi.org/10.1016/j.apsusc.2020.146020

He X, Yang CP, Zhang GL et al (2016) Supercapacitor of TiO2 nanofibers by electrospinning and KOH treatment. Mater Des 106:74–80. https://doi.org/10.1016/j.matdes.2016.05.025

Heo Y-J, Lee HI, Lee JW et al (2019) Optimization of the pore structure of PAN-based carbon fibers for enhanced supercapacitor performances via electrospinning. Compos Part B Eng 161:10–17. https://doi.org/10.1016/j.compositesb.2018.10.026

Hou J, Cao C, Idrees F, Ma X (2015) Hierarchical Porous Nitrogen-Doped Carbon Nanosheets Derived from Silk for Ultrahigh-Capacity Battery Anodes and Supercapacitors. ACS Nano 9:2556–2564. https://doi.org/10.1021/nn506394r

Hu S, Hsieh Y-L (2017) Lignin derived activated carbon particulates as an electric supercapacitor: carbonization and activation on porous structures and microstructures. RSC Adv 7:30459–30468. https://doi.org/10.1039/C7RA00103G

Hu S, Hsieh Y-L (2013) Ultrafine microporous and mesoporous activated carbon fibers from alkali lignin. J Mater Chem A 1:11279–11288. https://doi.org/10.1039/C3TA12538F

Huang Y, Lin Z, Zheng M et al (2016) Amorphous Fe2O3 nanoshells coated on carbonized bacterial cellulose nanofibers as a flexible anode for high-performance lithium ion batteries. J Power Sources 307:649–656. https://doi.org/10.1016/j.jpowsour.2016.01.026

Huang Y, Zheng M, Lin Z et al (2015) Flexible cathodes and multifunctional interlayers based on carbonized bacterial cellulose for high-performance lithium–sulfur batteries. J Mater Chem A 3:10910–10918. https://doi.org/10.1039/C5TA01515D

Huang Y, Zhu C, Yang J et al (2014) Recent advances in bacterial cellulose. Cellulose 21:1–30. https://doi.org/10.1007/s10570-013-0088-z

Hwang H-C, Woo JS, Park S-Y (2018) Flexible carbonized cellulose/single-walled carbon nanotube films with high conductivity. Carbohydr Polym 196:168–175. https://doi.org/10.1016/j.carbpol.2018.05.013

Ifuku S, Saimoto H (2012) Chitin nanofibers: preparations, modifications, and applications. Nanoscale 4:3308–3318. https://doi.org/10.1039/C2NR30383C

Im JS, Park S-J, Lee Y-S (2009) Superior prospect of chemically activated electrospun carbon fibers for hydrogen storage. Mater Res Bull 44:1871–1878. https://doi.org/10.1016/j.materresbull.2009.05.010

Ishikawa M, Sugimoto T, Kikuta M et al (2006) Pure ionic liquid electrolytes compatible with a graphitized carbon negative electrode in rechargeable lithium-ion batteries. J Power Sources 162:658–662. https://doi.org/10.1016/j.jpowsour.2006.02.077

Islam N, Li S, Ren G et al (2017) High-frequency electrochemical capacitors based on plasma pyrolyzed bacterial cellulose aerogel for current ripple filtering and pulse energy storage. Nano Energy 40:107–114. https://doi.org/10.1016/j.nanoen.2017.08.015

Jayawickramage RAP, Balkus KJ, Ferraris JP (2019) Binder free carbon nanofiber electrodes derived from polyacrylonitrile-lignin blends for high performance supercapacitors. Nanotechnology 30:355402. https://doi.org/10.1088/1361-6528/ab2274

Jayawickramage RAP, Ferraris JP (2019) High performance supercapacitors using lignin based electrospun carbon nanofiber electrodes in ionic liquid electrolytes. Nanotechnology 30:155402. https://doi.org/10.1088/1361-6528/aafe95

Jeon J-W, Zhang L, Lutkenhaus JL et al (2015) Controlling Porosity in Lignin-Derived Nanoporous Carbon for Supercapacitor Applications. Chemsuschem 8:428–432. https://doi.org/10.1002/cssc.201402621

Ji L, Wang B, Yu Y et al (2020) N, S co-doped biomass derived carbon with sheet-like microstructures for supercapacitors. Electrochim Acta 331:135348. https://doi.org/10.1016/j.electacta.2019.135348

Ji X (2019) A paradigm of storage batteries. Energy Environ Sci 12:3203–3224. https://doi.org/10.1039/C9EE02356A

Jiang Q, Qu MZ, Zhou GM et al (2002) A study of activated carbon nanotubes as electrochemical super capacitors electrode materials. Mater Lett 57:988–991. https://doi.org/10.1016/S0167-577X(02)00911-4

Jiang Y, Yan J, Wu X et al (2016) Facile synthesis of carbon nanofibers-bridged porous carbon nanosheets for high-performance supercapacitors. J Power Sources 307:190–198. https://doi.org/10.1016/j.jpowsour.2015.12.081

Jing S, Zhang Y, Chen F et al (2019) Novel and highly efficient cathodes for Li-O2 batteries: 3D self-standing NiFe@NC-functionalized N-doped carbon nanonet derived from Prussian blue analogues/biomass composites. Appl Catal B Environ 245:721–732. https://doi.org/10.1016/j.apcatb.2019.01.032

Jonoobi M, Mathew AP, Oksman K (2012) Producing low-cost cellulose nanofiber from sludge as new source of raw materials. Ind Crops Prod 40:232–238. https://doi.org/10.1016/j.indcrop.2012.03.018

Jung SM, Mafra DL, Lin C-T et al (2015) Controlled porous structures of graphene aerogels and their effect on supercapacitor performance. Nanoscale 7:4386–4393. https://doi.org/10.1039/C4NR07564A

Kadla JF, Kubo S, Gilbert RD, Venditti RA (2002) Lignin-Based Carbon Fibers. In: Hu TQ (ed) Chemical Modification, Properties, and Usage of Lignin. Springer, US, Boston, MA, pp 121–137

Khan A, Senthil RA, Pan J et al (2020) A new biomass derived rod-like porous carbon from tea-waste as inexpensive and sustainable energy material for advanced supercapacitor application. Electrochim Acta 335:135588. https://doi.org/10.1016/j.electacta.2019.135588

Kim B-J, Lee Y-S, Park S-J (2007) A study on pore-opening behaviors of graphite nanofibers by a chemical activation process. J Colloid Interface Sci 306:454–458. https://doi.org/10.1016/j.jcis.2006.10.038

Kim D-Y, Nishiyama Y, Wada M, Kuga S (2001) High-yield Carbonization of Cellulose by Sulfuric Acid Impregnation. Cellulose 8:29–33. https://doi.org/10.1023/A:1016621103245

Kopeć M, Lamson M, Yuan R et al (2019) Polyacrylonitrile-derived nanostructured carbon materials. Prog Polym Sci

92:89–134. https://doi.org/10.1016/j.progpolymsci.2019.02.003
Kuzmenko V, Naboka O, Gatenholm P, Enoksson P (2014) Ammonium chloride promoted synthesis of carbon nanofibers from electrospun cellulose acetate. Carbon 67:694–703. https://doi.org/10.1016/j.carbon.2013.10.061
Lai C, Zhou Z, Zhang L et al (2014) Free-standing and mechanically flexible mats consisting of electrospun carbon nanofibers made from a natural product of alkali lignin as binder-free electrodes for high-performance supercapacitors. J Power Sources 247:134–141. https://doi.org/10.1016/j.jpowsour.2013.08.082
Lallave M, Bedia J, Ruiz-Rosas R et al (2007) Filled and Hollow Carbon Nanofibers by Coaxial Electrospinning of Alcell Lignin without Binder Polymers. Adv Mater 19:4292–4296. https://doi.org/10.1002/adma.200700963
Lalvani SB, Hübner A, Wiltowski TS (2000) Chromium adsorption by lignin. Energy Sources 22:45–56. https://doi.org/10.1080/00908310050014207
Lazzari M, Scalarone D, Hoppe CE et al (2007) Tunable Polyacrylonitrile-Based Micellar Aggregates as a Potential Tool for the Fabrication of Carbon Nanofibers. Chem Mater 19:5818–5820. https://doi.org/10.1021/cm7019894
Le Quéré C, Jackson RB, Jones MW et al (2020) Temporary reduction in daily global CO 2 emissions during the COVID-19 forced confinement. Nat Clim Change 10:647–653. https://doi.org/10.1038/s41558-020-0797-x
Lee D-Y, An G-H, Ahn H-J (2017) High-surface-area tofu based activated porous carbon for electrical double-layer capacitors. J Ind Eng Chem 52:121–127. https://doi.org/10.1016/j.jiec.2017.03.032
Lee K, Shabnam L, Faisal SN et al (2020) Aerogel from fruit biowaste produces ultracapacitors with high energy density and stability. J Energy Storage 27:101152. https://doi.org/10.1016/j.est.2019.101152
Lee K-Y, Qian H, Tay FH et al (2013) Bacterial cellulose as source for activated nanosized carbon for electric double layer capacitors. J Mater Sci 48:367–376. https://doi.org/10.1007/s10853-012-6754-y
Lee Y-G, An G-H, Ahn H-J (2018) Protein-based carbon and platinum nanocomposites as electrocatalysts for methanol oxidation activity. J Alloys Compd 751:62–68. https://doi.org/10.1016/j.jallcom.2018.04.061
Leonard MD, Michaelides EE, Michaelides DN (2020) Energy storage needs for the substitution of fossil fuel power plants with renewables. Renew Energy 145:951–962. https://doi.org/10.1016/j.renene.2019.06.066
Lewandowski A, Zajder M, Frąckowiak E, Béguin F (2001) Supercapacitor based on activated carbon and polyethylene oxide–KOH–H2O polymer electrolyte. Electrochim Acta 46:2777–2780. https://doi.org/10.1016/S0013-4686(01)00496-0
Li Z, Xu Z, Tan X et al (2013) Mesoporous nitrogen-rich carbons derived from protein for ultra-high capacity battery anodes and supercapacitors. Energy Environ Sci 6:871–878. https://doi.org/10.1039/C2EE23599D
Li X-F, Xu Q, Fu Y, Guo Q-X (2014) Preparation and characterization of activated carbon from Kraft lignin via KOH activation. Environ Prog Sustain Energy 33:519–526. https://doi.org/10.1002/ep.11794
Li D, Lv C, Liu L et al (2015a) Egg-box structure in cobalt alginate: a new approach to multifunctional hierarchical mesoporous N-doped carbon nanofibers for efficient catalysis and energy storage. ACS Cent Sci 1:261–269. https://doi.org/10.1021/acscentsci.5b00191
Li W, Zhou M, Li H et al (2015b) A high performance sulfur-doped disordered carbon anode for sodium ion batteries. Energy Environ Sci 8:2916–2921. https://doi.org/10.1039/C5EE01985K
Li Y, Zhang H, Liu P et al (2015c) Self-supported bimodal-pore structured nitrogen-doped carbon fiber aerogel as electrocatalyst for oxygen reduction reaction. Electrochem Commun 51:6–10. https://doi.org/10.1016/j.elecom.2014.11.020
Li B, Dai F, Xiao Q et al (2016a) Activated carbon from biomass transfer for high-energy density lithium-ion supercapacitors. Adv Energy Mater 6:1600802. https://doi.org/10.1002/aenm.201600802
Li Y, Wang G, Wei T et al (2016b) Nitrogen and sulfur co-doped porous carbon nanosheets derived from willow catkin for supercapacitors. Nano Energy 19:165–175. https://doi.org/10.1016/j.nanoen.2015.10.038
Li Z, Liu J, Jiang K, Thundat T (2016c) Carbonized nanocellulose sustainably boosts the performance of activated carbon in ionic liquid supercapacitors. Nano Energy 25:161–169. https://doi.org/10.1016/j.nanoen.2016.04.036
Li S, Ren G, Hoque MNF et al (2017a) Carbonized cellulose paper as an effective interlayer in lithium-sulfur batteries. Appl Surf Sci 396:637–643. https://doi.org/10.1016/j.apsusc.2016.10.208
Li Z, Ahadi K, Jiang K et al (2017b) Freestanding hierarchical porous carbon film derived from hybrid nanocellulose for high-power supercapacitors. Nano Res 10:1847–1860. https://doi.org/10.1007/s12274-017-1573-8
Li Y, Zhu J, Shi R et al (2018a) Ultrafine and polar ZrO2-inlaid porous nitrogen-doped carbon nanofiber as efficient polysulfide absorbent for high-performance lithium-sulfur batteries with long lifespan. Chem Eng J 349:376–387. https://doi.org/10.1016/j.cej.2018.05.074
Li Y, Zhu J, Zhu P et al (2018b) Glass fiber separator coated by porous carbon nanofiber derived from immiscible PAN/PMMA for high-performance lithium-sulfur batteries. J Membr Sci 552:31–42. https://doi.org/10.1016/j.memsci.2018.01.062
Li M, Wang H, Zhu Y et al (2019a) Mo/Mo2C encapsulated in nitrogen-doped carbon nanofibers as efficiently integrated heterojunction electrocatalysts for hydrogen evolution reaction in wide pH range. Appl Surf Sci 496:143672. https://doi.org/10.1016/j.apsusc.2019.143672
Li Q, Zhu Y, Eichhorn SJ (2019b) Carbonized electrospun cellulose composite nanofibres containing silicon carbide nanoparticles. Compos Part Appl Sci Manuf 123:71–78. https://doi.org/10.1016/j.compositesa.2019.04.028
Li J, Ding Y, Gao Q et al (2020) Ultrathin and flexible biomass-derived C@CoFe nanocomposite films for efficient electromagnetic interference shielding. Compos Part B Eng 190:107935. https://doi.org/10.1016/j.compositesb.2020.107935
Liang H-W, Guan Q-F, Zhu Z et al (2012) Highly conductive and stretchable conductors fabricated from bacterial

cellulose. NPG Asia Mater 4:e19–e19. https://doi.org/10.1038/am.2012.34

Liebner F, Haimer E, Wendland M et al (2010) Aerogels from unaltered bacterial cellulose: application of scCO2 drying for the preparation of shaped, ultra-lightweight cellulosic aerogels. Macromol Biosci 10:349–352. https://doi.org/10.1002/mabi.200900371

Littlewood J, Murphy RJ, Wang L (2013) Importance of policy support and feedstock prices on economic feasibility of bioethanol production from wheat straw in the UK. Renew Sustain Energy Rev 17:291–300. https://doi.org/10.1016/j.rser.2012.10.002

Liu H, Hsieh Y-L (2002) Ultrafine fibrous cellulose membranes from electrospinning of cellulose acetate. J Polym Sci Part B Polym Phys 40:2119–2129. https://doi.org/10.1002/polb.10261

Liu H, Hsieh Y-L (2003) Surface methacrylation and graft copolymerization of ultrafine cellulose fibers. J Polym Sci Part B Polym Phys 41:953–964. https://doi.org/10.1002/polb.10400

Liu H, Yu H (2019) Ionic liquids for electrochemical energy storage devices applications. J Mater Sci Technol 35:674–686. https://doi.org/10.1016/j.jmst.2018.10.007

Liu W-J, Tian K, He Y-R et al (2014) High-yield harvest of nanofibers/mesoporous carbon composite by pyrolysis of waste biomass and its application for high durability electrochemical energy storage. Environ Sci Technol 48:13951–13959. https://doi.org/10.1021/es504184c

Liu B, Liu Y, Chen H et al (2017a) Oxygen and nitrogen co-doped porous carbon nanosheets derived from Perilla frutescens for high volumetric performance supercapacitors. J Power Sources 341:309–317. https://doi.org/10.1016/j.jpowsour.2016.12.022

Liu T, Zhang F, Song Y, Li Y (2017b) Revitalizing carbon supercapacitor electrodes with hierarchical porous structures. J Mater Chem A 5:17705–17733. https://doi.org/10.1039/C7TA05646J

Liu S, Zhao Y, Zhang B et al (2018) Nano-micro carbon spheres anchored on porous carbon derived from dual-biomass as high rate performance supercapacitor electrodes. J Power Sources 381:116–126. https://doi.org/10.1016/j.jpowsour.2018.02.014

Liu C, Wang H, Zhao X et al (2020a) Cellulose-derived carbon-based electrodes with high capacitance for advanced asymmetric supercapacitors. J Power Sources 457:228056. https://doi.org/10.1016/j.jpowsour.2020.228056

Liu H, Xie Y, Liu J et al (2020b) Laser-induced and KOH-activated 3D graphene: a flexible activated electrode fabricated via direct laser writing for in-plane micro-supercapacitors. Chem Eng J 393:124672. https://doi.org/10.1016/j.cej.2020.124672

Liu L, Hu S, Gao K (2020c) Natural nanofiber-based stacked porous nitrogen-doped carbon/NiFe2O4 nanohybrid nanosheets. Cellulose 27:1021–1031. https://doi.org/10.1007/s10570-019-02843-w

Liu Y, Zhang X, Gu X et al (2020d) One-step turning leather wastes into heteroatom doped carbon aerogel for performance enhanced capacitive deionization. Microporous Mesoporous Mater 303:110303. https://doi.org/10.1016/j.micromeso.2020.110303

Liu Z, Ciais P, Deng Z et al (2020e) Near-real-time monitoring of global CO2 emissions reveals the effects of the COVID-19 pandemic. Nat Commun 11:5172. https://doi.org/10.1038/s41467-020-18922-7

Long C, Jiang L, Wu X et al (2015) Facile synthesis of functionalized porous carbon with three-dimensional interconnected pore structure for high volumetric performance supercapacitors. Carbon 93:412–420. https://doi.org/10.1016/j.carbon.2015.05.040

Lu C, Qian X-Z, Zhu H-Y et al (2019) 3D hierarchical porous carbon derived from direct carbonization and in-situ chemical activation of potatoes toward high-performance supercapacitors. Mater Res Express 6:115615. https://doi.org/10.1088/2053-1591/ab4d36

Lu P, Hsieh Y-L (2010) Multiwalled carbon nanotube (MWCNT) reinforced cellulose fibers by electrospinning. ACS Appl Mater Interfaces 2:2413–2420. https://doi.org/10.1021/am1004128

Ľudmila H, Michal J, Andrea Š, Aleš H (2015) Lignin, potential products and their market value

Luo B, Chi M, Zhang Q et al (2019) Fabrication of lignin-based nano carbon film-copper foil composite with enhanced thermal conductivity. Nanomaterials 9:1681. https://doi.org/10.3390/nano9121681

Luo J, Genco J, Cole BJW, Fort RC (2011) Lignin recovered from the near-neutral hemicellulose extraction process as a precursor for carbon fiber. BioResources 6:4566–4593

Ma C, Li Z, Li J et al (2018) Lignin-based hierarchical porous carbon nanofiber films with superior performance in supercapacitors. Appl Surf Sci 456:568–576. https://doi.org/10.1016/j.apsusc.2018.06.189

Ma X, Elbohy H, Sigdel S et al (2016) Electrospun carbon nanofelt derived from alkali lignin for cost-effective counter electrodes of dye-sensitized solar cells. RSC Adv 6:11481–11487. https://doi.org/10.1039/C5RA23856K

Ma X, Smirnova AL, Fong H (2019) Flexible lignin-derived carbon nanofiber substrates functionalized with iron (III) oxide nanoparticles as lithium-ion battery anodes. Mater Sci Eng B 241:100–104. https://doi.org/10.1016/j.mseb.2019.02.013

Ma Z, Kotaki M, Ramakrishna S (2005) Electrospun cellulose nanofiber as affinity membrane. J Membr Sci 265:115–123. https://doi.org/10.1016/j.memsci.2005.04.044

Matsakas L, Gerber M, Yu L et al (2020) Preparation of low carbon impact lignin nanoparticles with controllable size by using different strategies for particles recovery. Ind Crops Prod 147:112243. https://doi.org/10.1016/j.indcrop.2020.112243

Matsakas L, Karnaouri A, Cwirzen A et al (2018) Formation of lignin nanoparticles by combining organosolv pretreatment of birch biomass and homogenization processes. Molecules 23:1822. https://doi.org/10.3390/molecules23071822

Mehtab T, Yasin G, Arif M et al (2019) Metal-organic frameworks for energy storage devices: batteries and supercapacitors. J Energy Storage 21:632–646. https://doi.org/10.1016/j.est.2018.12.025

Meng X, Cao Q, Jin L et al (2017) Carbon electrode materials for supercapacitors obtained by co-carbonization of coal-tar pitch and sawdust. J Mater Sci 52:760–769. https://doi.org/10.1007/s10853-016-0370-1

Meng X, Chen T, Li Y et al (2019) Assembly of carbon nanodots in graphene-based composite for flexible electro-thermal heater with ultrahigh efficiency. Nano Res 12:2498–2508. https://doi.org/10.1007/s12274-019-2476-7

Merlet C, Rotenberg B, Madden PA et al (2012) On the molecular origin of supercapacitance in nanoporous carbon electrodes. Nat Mater 11:306–310. https://doi.org/10.1038/nmat3260

Mitani S, Lee S-I, Saito K et al (2005) Activation of coal tar derived needle coke with K2CO3 into an active carbon of low surface area and its performance as unique electrode of electric double-layer capacitor. Carbon 43:2960–2967. https://doi.org/10.1016/j.carbon.2005.05.047

Moriarty P, Honnery D (2016) Can renewable energy power the future? Energy Policy 93:3–7. https://doi.org/10.1016/j.enpol.2016.02.051

Muzaffar A, Ahamed MB, Deshmukh K, Thirumalai J (2019) A review on recent advances in hybrid supercapacitors: design, fabrication and applications. Renew Sustain Energy Rev 101:123–145. https://doi.org/10.1016/j.rser.2018.10.026

Myint AA, Rhim W-K, Nam J-M et al (2018) Water-soluble, lignin-derived carbon dots with high fluorescent emissions and their applications in bioimaging. J Ind Eng Chem 66:387–395. https://doi.org/10.1016/j.jiec.2018.06.005

Myung Y, Jung S, Tung TT et al (2019) Graphene-based aerogels derived from biomass for energy storage and environmental remediation. ACS Sustain Chem Eng 7:3772–3782. https://doi.org/10.1021/acssuschemeng.8b04202

Naghdi T, Atashi M, Golmohammadi H et al (2017) Carbon quantum dots originated from chitin nanofibers as a fluorescent chemoprobe for drug sensing. J Ind Eng Chem 52:162–167. https://doi.org/10.1016/j.jiec.2017.03.039

Nguyen T-D, Shopsowitz KE, MacLachlan MJ (2014) Mesoporous nitrogen-doped carbon from nanocrystalline chitin assemblies. J Mater Chem A 2:5915–5921. https://doi.org/10.1039/C3TA15255C

Nogi M, Kurosaki F, Yano H, Takano M (2010) Preparation of nanofibrillar carbon from chitin nanofibers. Carbohydr Polym 81:919–924. https://doi.org/10.1016/j.carbpol.2010.04.006

Park B-H, Kim Y-J, Park J-S, Choi J (2011) Capacitive deionization using a carbon electrode prepared with water-soluble poly(vinyl alcohol) binder. J Ind Eng Chem 17:717–722. https://doi.org/10.1016/j.jiec.2011.05.015

Qu Y, Zhang Z, Zhang X et al (2015) Highly ordered nitrogen-rich mesoporous carbon derived from biomass waste for high-performance lithium–sulfur batteries. Carbon 84:399–408. https://doi.org/10.1016/j.carbon.2014.12.001

Rai AA, Stojanovska E, Akgul Y et al (2021) Fabrication of co-PVDF/modacrylic/SiO2 nanofibrous membrane: Composite separator for safe and high performance lithium-ion batteries. J Appl Polym Sci 138:49835. https://doi.org/10.1002/app.49835

Rai AA, Stojanovska E, Fidan G et al (2020) Structure and performance of electroblown PVDF-based nanofibrous electret filters. Polym Eng Sci 60:1186–1193. https://doi.org/10.1002/pen.25372

Rai S, Singh BK, Bhartiya P et al (2017) Lignin derived reduced fluorescence carbon dots with theranostic approaches: nano-drug-carrier and bioimaging. J Lumin 190:492–503. https://doi.org/10.1016/j.jlumin.2017.06.008

Ren G, Li S, Fan Z-X et al (2016) Ultrahigh-rate supercapacitors with large capacitance based on edge oriented graphene coated carbonized cellulous paper as flexible freestanding electrodes. J Power Sources 325:152–160. https://doi.org/10.1016/j.jpowsour.2016.06.021

Roman J, Neri W, Derré A, Poulin P (2019) Electrospun lignin-based twisted carbon nanofibers for potential microelectrodes applications. Carbon 145:556–564. https://doi.org/10.1016/j.carbon.2019.01.036

Ruiz-Rosas R, Bedia J, Lallave M et al (2010) The production of submicron diameter carbon fibers by the electrospinning of lignin. Carbon 48:696–705. https://doi.org/10.1016/j.carbon.2009.10.014

Selvan RK, Zhu P, Yan C et al (2018) Biomass-derived porous carbon modified glass fiber separator as polysulfide reservoir for Li-S batteries. J Colloid Interface Sci 513:231–239. https://doi.org/10.1016/j.jcis.2017.11.016

Senthil C, Lee CW (2021) Biomass-derived biochar materials as sustainable energy sources for electrochemical energy storage devices. Renew Sustain Energy Rev 137:110464. https://doi.org/10.1016/j.rser.2020.110464

Seo J, Park H, Shin K et al (2014) Lignin-derived macroporous carbon foams prepared by using poly(methyl methacrylate) particles as the template. Carbon 76:357–367. https://doi.org/10.1016/j.carbon.2014.04.087

Sevilla M, Fuertes AB (2010) Graphitic carbon nanostructures from cellulose. Chem Phys Lett 490:63–68. https://doi.org/10.1016/j.cplett.2010.03.011

Shang T, Xu Y, Li P et al (2020) A bio-derived sheet-like porous carbon with thin-layer pore walls for ultrahigh-power supercapacitors. Nano Energy 70:104531. https://doi.org/10.1016/j.nanoen.2020.104531

Shehnaz WuD, Guo Y et al (2018) Synergistic effect of heat treatments and KOH activation enhances the electrochemistry performance of polypyrrole nanochains (PPy-NCs). Electrochim Acta 266:151–160. https://doi.org/10.1016/j.electacta.2018.01.128

Shen J, Wu H, Sun W et al (2019) Biomass-derived hierarchically porous carbon skeletons with in situ decorated IrCo nanoparticles as high-performance cathode catalysts for Li–O2 batteries. J Mater Chem A 7:10662–10671. https://doi.org/10.1039/C9TA00543A

Shen L, Wang J, Xu G et al (2015) NiCo2S4 Nanosheets grown on nitrogen-doped carbon foams as an advanced electrode for supercapacitors. Adv Energy Mater 5:1400977. https://doi.org/10.1002/aenm.201400977

Shen Q, Zhong L (2007) Lignin-based carbon films and controllable pore size and properties. Mater Sci Eng A 445–446:731–735. https://doi.org/10.1016/j.msea.2006.09.066

Shoda M, Sugano Y (2005) Recent advances in bacterial cellulose production. Biotechnol Bioprocess Eng 10:1. https://doi.org/10.1007/BF02931175

Si M, Zhang J, He Y et al (2018) Synchronous and rapid preparation of lignin nanoparticles and carbon quantum dots from natural lignocellulose. Green Chem 20:3414–3419. https://doi.org/10.1039/C8GC00744F

Si Y, Wang X, Yan C et al (2016) Ultralight biomass-derived carbonaceous nanofibrous aerogels with superelasticity

and high pressure-sensitivity. Adv Mater 28:9512–9518. https://doi.org/10.1002/adma.201603143

Silva R, Al-Sharab J, Asefa T (2012) Edge-plane-rich nitrogen-doped carbon nanoneedles and efficient metal-free electrocatalysts. Angew Chem Int Ed 51:7171–7175. https://doi.org/10.1002/anie.201201742

Silva R, Pereira GM, Voiry D et al (2015) Co3O4 nanoparticles/cellulose nanowhiskers-derived amorphous carbon nanoneedles: sustainable materials for supercapacitors and oxygen reduction electrocatalysis. RSC Adv 5:49385–49391. https://doi.org/10.1039/C5RA08037A

Singh Gill A, Visotsky D, Mears L, Summers JD (2017) Cost estimation model for polyacrylonitrile-based carbon fiber manufacturing process. J Manuf Sci Eng. https://doi.org/10.1115/1.4034713

Son I-S, Oh Y, Yi S-H et al (2020) Facile fabrication of mesoporous carbon from mixed polymer precursor of PVDF and PTFE for high-power supercapacitors. Carbon 159:283–291. https://doi.org/10.1016/j.carbon.2019.12.049

Son WK, Youk JH, Lee TS, Park WH (2004) Electrospinning of ultrafine cellulose acetate fibers: studies of a new solvent system and deacetylation of ultrafine cellulose acetate fibers. J Polym Sci Part B Polym Phys 42:5–11. https://doi.org/10.1002/polb.10668

Stojanovska E, Kilic A (2019) Carbon nanofibers as thick electrodes for aqueous supercapacitors. J Energy Storage 26:100981. https://doi.org/10.1016/j.est.2019.100981

Sun D, Yu X, Ji X et al (2019a) Nickel/woodceramics assembled with lignin-based carbon nanosheets and multilayer graphene as supercapacitor electrode. J Alloys Compd 805:327–337. https://doi.org/10.1016/j.jallcom.2019.06.375

Sun K, Li J, Huang L et al (2019b) Biomass-derived 3D hierarchical N-doped porous carbon anchoring cobalt-iron phosphide nanodots as bifunctional electrocatalysts for LiO2 batteries. J Power Sources 412:433–441. https://doi.org/10.1016/j.jpowsour.2018.11.079

Sun L, Tian C, Li M et al (2013) From coconut shell to porous graphene-like nanosheets for high-power supercapacitors. J Mater Chem A 1:6462–6470. https://doi.org/10.1039/C3TA10897J

Tao L, Zheng Y, Zhang Y et al (2017) Liquefied walnut shell-derived carbon nanofibrous mats as highly efficient anode materials for lithium ion batteries. RSC Adv 7:27113–27120. https://doi.org/10.1039/C7RA02716H

Tian S, Guan D, Lu J et al (2020) Synthesis of the electrochemically stable sulfur-doped bamboo charcoal as the anode material of potassium-ion batteries. J Power Sources 448:227572. https://doi.org/10.1016/j.jpowsour.2019.227572

Vuorema A, Sillanpää M, Rassaei L et al (2010) Ultrathin carbon film electrodes from vacuum-carbonised cellulose nanofibril composite. Electroanalysis 22:619–624. https://doi.org/10.1002/elan.200900513

Wan H, Hu X (2020) Sulfur-doped honeycomb-like carbon with outstanding electrochemical performance as an anode material for lithium and sodium ion batteries. J Colloid Interface Sci 558:242–250. https://doi.org/10.1016/j.jcis.2019.09.124

Wan Y, Yang Z, Xiong G, Luo H (2015) A general strategy of decorating 3D carbon nanofiber aerogels derived from bacterial cellulose with nano-Fe3O4 for high-performance flexible and binder-free lithium-ion battery anodes. J Mater Chem A 3:15386–15393. https://doi.org/10.1039/C5TA03688G

Wang B, Li S, Wu X et al (2016) Biomass chitin-derived honeycomb-like nitrogen-doped carbon/graphene nanosheet networks for applications in efficient oxygen reduction and robust lithium storage. J Mater Chem A 4:11789–11799. https://doi.org/10.1039/C6TA02858F

Wang D, Peng H, Yu B et al (2020a) Biomimetic structural cellulose nanofiber aerogels with exceptional mechanical, flame-retardant and thermal-insulating properties. Chem Eng J 389:124449. https://doi.org/10.1016/j.cej.2020.124449

Wang J, Nie P, Ding B et al (2017a) Biomass derived carbon for energy storage devices. J Mater Chem A 5:2411–2428. https://doi.org/10.1039/C6TA08742F

Wang L, Schütz C, Salazar-Alvarez G, Titirici M-M (2014) Carbon aerogels from bacterial nanocellulose as anodes for lithium ion batteries. RSC Adv 4:17549–17554. https://doi.org/10.1039/C3RA47853J

Wang M, Zhang J, Yi X et al (2019a) Construction of NiMoO4 nanorods@ZIF-67 derived Co3O4 supported on cellulose based carbon aerogel for asymmetric supercapacitors. Beilstein Arch 2019:126. https://doi.org/10.3762/bxiv.2019.126.v1

Wang S-X, Yang L, Stubbs LP et al (2013) Lignin-derived fused electrospun carbon fibrous mats as high performance anode materials for lithium ion batteries. ACS Appl Mater Interfaces 5:12275–12282. https://doi.org/10.1021/am4043867

Wang Y, Liu R, Tian Y et al (2020b) Heteroatoms-doped hierarchical porous carbon derived from chitin for flexible all-solid-state symmetric supercapacitors. Chem Eng J 384:123263. https://doi.org/10.1016/j.cej.2019.123263

Wang Y, Qu Q, Gao S et al (2019b) Biomass derived carbon as binder-free electrode materials for supercapacitors. Carbon 155:706–726. https://doi.org/10.1016/j.carbon.2019.09.018

Wang Y, Yang J, Du R, Chen L (2017b) Transition metal ions enable the transition from electrospun prolamin protein fibers to nitrogen-doped freestanding carbon films for flexible supercapacitors. ACS Appl Mater Interfaces 9:23731–23740. https://doi.org/10.1021/acsami.7b05159

Wang Z, Zhang X, Liu X et al (2020c) High specific surface area bimodal porous carbon derived from biomass reed flowers for high performance lithium-sulfur batteries. J Colloid Interface Sci 569:22–33. https://doi.org/10.1016/j.jcis.2020.02.062

White RJ, Yoshizawa N, Antonietti M, Titirici M-M (2011) A sustainable synthesis of nitrogen-doped carbon aerogels. Green Chem 13:2428–2434. https://doi.org/10.1039/C1GC15349H

Wu D, Fu R, Zhang S et al (2004) Preparation of low-density carbon aerogels by ambient pressure drying. Carbon 42:2033–2039. https://doi.org/10.1016/j.carbon.2004.04.003

Wu Z-S, Winter A, Chen L et al (2012) Three-dimensional nitrogen and boron Co-doped graphene for high-

performance all-solid-state supercapacitors. Adv Mater 24:5130–5135. https://doi.org/10.1002/adma.201201948
Wu X, Jiang L, Long C, Fan Z (2015) From flour to honeycomb-like carbon foam: carbon makes room for high energy density supercapacitors. Nano Energy 13:527–536. https://doi.org/10.1016/j.nanoen.2015.03.013
Wu Z-Y, Li C, Liang H-W et al (2013) Ultralight, flexible, and fire-resistant carbon nanofiber aerogels from bacterial cellulose. Angew Chem Int Ed 52:2925–2929. https://doi.org/10.1002/anie.201209676
Xiao Q, Li G, Li M et al (2020) Biomass-derived nitrogen-doped hierarchical porous carbon as efficient sulfur host for lithium–sulfur batteries. J Energy Chem 44:61–67. https://doi.org/10.1016/j.jechem.2019.09.004
Xu X, Zhou J, Jiang L et al (2013) Porous core-shell carbon fibers derived from lignin and cellulose nanofibrils. Mater Lett 109:175–178. https://doi.org/10.1016/j.matlet.2013.07.082
Xu X, Zhou J, Jiang L et al (2014) Lignin-based carbon fibers: carbon nanotube decoration and superior thermal stability. Carbon 80:91–102. https://doi.org/10.1016/j.carbon.2014.08.042
Xu X, Zhou J, Nagaraju DH et al (2015) Flexible, highly graphitized carbon aerogels based on bacterial cellulose/lignin: catalyst-free synthesis and its application in energy storage devices. Adv Funct Mater 25:3193–3202. https://doi.org/10.1002/adfm.201500538
Xu Z, Liu Y, Chen H et al (2017) Bamboo-like, oxygen-doped carbon tubes with hierarchical pore structure derived from polymer tubes for supercapacitor applications. J Mater Sci 52:7781–7793. https://doi.org/10.1007/s10853-017-1064-z
Xu J, Zhou X, Chen M (2018a) Microwave-assisted synthesis of Cu-doped hierarchical porous carbon aerogels derived from lignin for high-performance supercapacitors. Mater Res Express 5:095002. https://doi.org/10.1088/2053-1591/aad496
Xu J, Zhou X, Chen M et al (2018b) Preparing hierarchical porous carbon aerogels based on enzymatic hydrolysis lignin through ambient drying for supercapacitor electrodes. Microporous Mesoporous Mater 265:258–265. https://doi.org/10.1016/j.micromeso.2018.02.024
Yan N, Chen X (2015) Sustainability: Don't waste seafood waste. Nat News 524:155. https://doi.org/10.1038/524155a
Yang M, Zhou Z (2017) Recent breakthroughs in supercapacitors boosted by nitrogen-rich porous carbon materials. Adv Sci 4:1600408. https://doi.org/10.1002/advs.201600408
Yang S, Feng X, Müllen K (2011) Sandwich-like, graphene-based titania nanosheets with high surface area for fast lithium storage. Adv Mater 23:3575–3579. https://doi.org/10.1002/adma.201101599
Yang BS, Kang K-Y, Jeong M-J (2017) Preparation of lignin-based carbon aerogels as biomaterials for nano-supercapacitor. J Korean Phys Soc 71:478–482. https://doi.org/10.3938/jkps.71.478
Yang J, Wang Y, Luo J, Chen L (2018a) Facile preparation of self-standing hierarchical porous nitrogen-doped carbon fibers for supercapacitors from plant protein-lignin electrospun fibers. ACS Omega 3:4647–4656. https://doi.org/10.1021/acsomega.7b01876
Yang J, Wang Y, Luo J, Chen L (2018b) Highly nitrogen-doped graphitic carbon fibers from sustainable plant protein for supercapacitor. Ind Crops Prod 121:226–235. https://doi.org/10.1016/j.indcrop.2018.05.013
Yang H, Xu R, Yu Y (2019) A facile strategy toward sodium-ion batteries with ultra-long cycle life and high initial Coulombic Efficiency: Free-standing porous carbon nanofiber film derived from bacterial cellulose. Energy Storage Mater 22:105–112. https://doi.org/10.1016/j.ensm.2019.01.003
Yang M, Dai J, He M et al (2020) Biomass-derived carbon from Ganoderma lucidum spore as a promising anode material for rapid potassium-ion storage. J Colloid Interface Sci 567:256–263. https://doi.org/10.1016/j.jcis.2020.02.023
Yiamsawas D, Beckers SJ, Lu H et al (2017) Morphology-Controlled Synthesis of Lignin Nanocarriers for Drug Delivery and Carbon Materials. ACS Biomater Sci Eng 3:2375–2383. https://doi.org/10.1021/acsbiomaterials.7b00278
Yin Q, He L, Lian J et al (2019) The synthesis of Co3O4/C composite with aloe juice as the carbon aerogel substrate for asymmetric supercapacitors. Carbon 155:147–154. https://doi.org/10.1016/j.carbon.2019.08.060
You J, Li M, Ding B et al (2017) Crab chitin-based 2D soft nanomaterials for fully biobased electric devices. Adv Mater Deerfield Beach Fla. https://doi.org/10.1002/adma.201606895
Youe W-J, Kim SJ, Lee S-M et al (2018) MnO2-deposited lignin-based carbon nanofiber mats for application as electrodes in symmetric pseudocapacitors. Int J Biol Macromol 112:943–950. https://doi.org/10.1016/j.ijbiomac.2018.02.048
Youe W-J, Lee S-M, Lee S-S et al (2016) Characterization of carbon nanofiber mats produced from electrospun lignin-g-polyacrylonitrile copolymer. Int J Biol Macromol 82:497–504. https://doi.org/10.1016/j.ijbiomac.2015.10.022
Yu K, Wang J, Wang X et al (2020) Sustainable application of biomass by-products: Corn straw-derived porous carbon nanospheres using as anode materials for lithium ion batteries. Mater Chem Phys 243:122644. https://doi.org/10.1016/j.matchemphys.2020.122644
Yu W, Lin W, Shao X et al (2014) High performance supercapacitor based on Ni3S2/carbon nanofibers and carbon nanofibers electrodes derived from bacterial cellulose. J Power Sources 272:137–143. https://doi.org/10.1016/j.jpowsour.2014.08.064
Yun YS, Cho SY, Shim J et al (2013) Microporous carbon nanoplates from regenerated silk proteins for supercapacitors. Adv Mater Deerfield Beach Fla 25:1993–1998. https://doi.org/10.1002/adma.201204692
Yun YS, Cho SY, Jin H-J (2014a) Carbon aerogels based on regenerated silk proteins and graphene oxide for supercapacitors. Macromol Res 22:509–514. https://doi.org/10.1007/s13233-014-2071-4
Yun YS, Le V-D, Kim H et al (2014b) Effects of sulfur doping on graphene-based nanosheets for use as anode materials in lithium-ion batteries. J Power Sources 262:79–85. https://doi.org/10.1016/j.jpowsour.2014.03.084
Yun SI, Kim SH, Kim DW et al (2019) Facile preparation and capacitive properties of low-cost carbon nanofibers with

ZnO derived from lignin and pitch as supercapacitor electrodes. Carbon 149:637–645. https://doi.org/10.1016/j.carbon.2019.04.105

Zakzeski J, Bruijnincx PCA, Jongerius AL, Weckhuysen BM (2010) The catalytic valorization of lignin for the production of renewable chemicals. Chem Rev 110:3552–3599. https://doi.org/10.1021/cr900354u

Zhai Y, Dou Y, Zhao D et al (2011) Carbon materials for chemical capacitive energy storage. Adv Mater 23:4828–4850. https://doi.org/10.1002/adma.201100984

Zhang LL, Zhao XS (2009) Carbon-based materials as supercapacitor electrodes. Chem Soc Rev 38:2520–2531. https://doi.org/10.1039/B813846J

Zhang G, Lou XW (2013) General solution growth of mesoporous NiCo2O4 nanosheets on various conductive substrates as high-performance electrodes for supercapacitors. Adv Mater 25:976–979. https://doi.org/10.1002/adma.201204128

Zhang L, Zhang F, Yang X et al (2013) Porous 3D graphene-based bulk materials with exceptional high surface area and excellent conductivity for supercapacitors. Sci Rep 3:1408. https://doi.org/10.1038/srep01408

Zhang B, Yu Y, Xu Z-L et al (2014) Correlation between atomic structure and electrochemical performance of anodes made from electrospun carbon nanofiber films. Adv Energy Mater 4:1301448. https://doi.org/10.1002/aenm.201301448

Zhang J, Zhang L, Yang S et al (2017a) Facile strategy to produce N-doped carbon aerogels derived from seaweed for lithium-ion battery anode. J Alloys Compd 701:256–261. https://doi.org/10.1016/j.jallcom.2017.01.082

Zhang X, Luo J, Tang P et al (2017b) A universal strategy for metal oxide anchored and binder-free carbon matrix electrode: a supercapacitor case with superior rate performance and high mass loading. Nano Energy 31:311–321. https://doi.org/10.1016/j.nanoen.2016.11.024

Zhang X, Zhao J, He X et al (2018) Mechanically robust and highly compressible electrochemical supercapacitors from nitrogen-doped carbon aerogels. Carbon 127:236–244. https://doi.org/10.1016/j.carbon.2017.10.083

Zhang H, Zhang Z, Luo J-D et al (2019a) A chemical blowing strategy to fabricate biomass-derived carbon-aerogels with graphene-like nanosheet structures for high-performance supercapacitors. Chemsuschem 12:2462–2470. https://doi.org/10.1002/cssc.201900267

Zhang Y, He J, Gao Z, Li X (2019b) Converting eggs to flexible, all-solid supercapacitors. Nano Energy 65:104045. https://doi.org/10.1016/j.nanoen.2019.104045

Zhang Y, Sun Y, Peng L et al (2019c) Se as eutectic accelerator in sulfurized polyacrylonitrile for high performance all-solid-state lithium-sulfur battery. Energy Storage Mater 21:287–296. https://doi.org/10.1016/j.ensm.2018.12.010

Zhang C, Xie Z, Yang W et al (2020a) NiCo2O4/biomass-derived carbon composites as anode for high-performance lithium ion batteries. J Power Sources 451:227761. https://doi.org/10.1016/j.jpowsour.2020.227761

Zhang W, Yang P, Luo M et al (2020b) Fast oxygen, nitrogen co-functionalization on electrospun lignin-based carbon nanofibers membrane via air plasma for energy storage application. Int J Biol Macromol 143:434–442. https://doi.org/10.1016/j.ijbiomac.2019.11.237

Zhao J, Lai H, Lyu Z et al (2015a) Hydrophilic hierarchical nitrogen-doped carbon nanocages for ultrahigh supercapacitive performance. Adv Mater 27:3541–3545. https://doi.org/10.1002/adma.201500945

Zhao Y, Liu M, Deng X et al (2015b) Nitrogen-functionalized microporous carbon nanoparticles for high performance supercapacitor electrode. Electrochim Acta 153:448–455. https://doi.org/10.1016/j.electacta.2014.11.173

Zhao G, Chen C, Yu D et al (2018a) One-step production of O-N-S co-doped three-dimensional hierarchical porous carbons for high-performance supercapacitors. Nano Energy 47:547–555. https://doi.org/10.1016/j.nanoen.2018.03.016

Zhao Y, Liu Y, Tong C et al (2018b) Flexible lignin-derived electrospun carbon nanofiber mats as a highly efficient and binder-free counter electrode for dye-sensitized solar cells. J Mater Sci 53:7637–7647. https://doi.org/10.1007/s10853-018-2059-0

Zhao G, Yu D, Zhang H et al (2020) Sulphur-doped carbon nanosheets derived from biomass as high-performance anode materials for sodium-ion batteries. Nano Energy 67:104219. https://doi.org/10.1016/j.nanoen.2019.104219

Zheng Y, Zhao W, Jia D et al (2019) Thermally-treated and acid-etched carbon fiber cloth based on pre-oxidized polyacrylonitrile as self-standing and high area-capacitance electrodes for flexible supercapacitors. Chem Eng J 364:70–78. https://doi.org/10.1016/j.cej.2019.01.076

Zhong M, Tang C, Kim EK et al (2014) Preparation of porous nanocarbons with tunable morphology and pore size from copolymer templated precursors. Mater Horiz 1:121–124. https://doi.org/10.1039/c3mh00084b

Zhou J, Zhu T, Xing W et al (2015) Activated polyaniline-based carbon nanoparticles for high performance supercapacitors. Electrochim Acta 160:152–159. https://doi.org/10.1016/j.electacta.2015.02.032

Zhou J, Bao L, Wu S et al (2017) Chitin based heteroatom-doped porous carbon as electrode materials for supercapacitors. Carbohydr Polym 173:321–329. https://doi.org/10.1016/j.carbpol.2017.06.004

Zhou Y, Hu X, Guo S et al (2018) Multi-functional graphene/carbon nanotube aerogels for its applications in supercapacitor and direct methanol fuel cell. Electrochim Acta 264:12–19. https://doi.org/10.1016/j.electacta.2018.01.009

Zhou S, Zhou L, Zhang Y et al (2019) Upgrading earth-abundant biomass into three-dimensional carbon materials for energy and environmental applications. J Mater Chem A 7:4217–4229. https://doi.org/10.1039/C8TA12159A

Zhu J, Chen C, Lu Y et al (2015) Nitrogen-doped carbon nanofibers derived from polyacrylonitrile for use as anode material in sodium-ion batteries. Carbon 94:189–195. https://doi.org/10.1016/j.carbon.2015.06.076

Zhu J, Lu Y, Chen C et al (2016) Porous one-dimensional carbon/iron oxide composite for rechargeable lithium-ion batteries with high and stable capacity. J Alloys Compd 672:79–85. https://doi.org/10.1016/j.jallcom.2016.02.160

Zhu H, Shen F, Luo W et al (2017) Low temperature carbonization of cellulose nanocrystals for high performance carbon anode of sodium-ion batteries. Nano Energy 33:37–44. https://doi.org/10.1016/j.nanoen.2017.01.021

Zhu G, Wang H, Xu H, Zhang L (2018a) Enhanced capacitive deionization by nitrogen-doped porous carbon nanofiber aerogel derived from bacterial-cellulose. J Electroanal Chem 822:81–88. https://doi.org/10.1016/j.jelechem.2018.05.024

Zhu P, Yan C, Dirican M et al (2018b) Li0.33La0.557TiO3 ceramic nanofiber-enhanced polyethylene oxide-based composite polymer electrolytes for all-solid-state lithium batteries. J Mater Chem A 6:4279–4285. https://doi.org/10.1039/C7TA10517G

Zhu J, Yan C, Zhang X et al (2020a) A sustainable platform of lignin: From bioresources to materials and their applications in rechargeable batteries and supercapacitors. Prog Energy Combust Sci 76:100788. https://doi.org/10.1016/j.pecs.2019.100788

Zhu M, Xia A, Feng Q et al (2020b) Biomass carbon materials for efficient solar steam generation prepared from carbonized enteromorpha prolifera. Energy Technol 8:1901215. https://doi.org/10.1002/ente.201901215

Zhuo H, Hu Y, Chen Z, Zhong L (2019) Cellulose carbon aerogel/PPy composites for high-performance supercapacitor. Carbohydr Polym 215:322–329. https://doi.org/10.1016/j.carbpol.2019.03.101

Zu G, Shen J, Zou L et al (2016) Nanocellulose-derived highly porous carbon aerogels for supercapacitors. Carbon 99:203–211. https://doi.org/10.1016/j.carbon.2015.11.079

Zubbri NA, Mohamed AR, Lahijani P, Mohammadi M (2021) Low temperature CO2 capture on biomass-derived KOH-activated hydrochar established through hydrothermal carbonization with water-soaking pre-treatment. J Environ Chem Eng 9:105074. https://doi.org/10.1016/j.jece.2021.105074